



University of
Stavanger

Faculty of Science and Technology

MASTER'S THESIS

Study program/Specialization: Risk Management Master's Program/ Risk Assessment and Management	Spring semester, 2020 Open / Restricted access
Writer: Maha Ibrahim Ahmed Eleryan	<i>Maha Eleryan</i> (Writer's signature)
Faculty supervisor: Jan Roar Bakke External supervisor: Geirmund Vislie (Gexcon AS)	
Thesis title: Methodology Options for Hydrogen Safety Analysis	
Credits: 30 ECTS	
Keywords: Hydrogen Hydrogen safety analysis Release modelling studies Dispersion modelling studies FLACS PHAST EFFECTS FRED	Pages: 108 + Appendices: 58 pages Stavanger, 29/07/2020

Methodology Options for Hydrogen Safety Analysis

Maha Eleryan

**Risk Management Master's Programme
Faculty of Science and Technology
University of Stavanger**



University of
Stavanger

Faculty Supervisor:
Jan Roar Bakke

Gexcon AS Supervisor:
Geirmund Vislie

**Stavanger, Norway
Spring 2020**

Abstract

The development of applications using hydrogen as a clean energy carrier has increased in recent years. Hydrogen is versatile and can be used in a wide range of applications. Hydrogen is already being widely used as a chemical feedstock for producing fertilizers and petrochemicals. Hydrogen can be used to power vehicles and generate heat and electricity. A prerequisite for commercial applications of hydrogen is to ensure that the risk associated with its production, storage, transport and use is at least not significantly higher than that of existing fuels. Hydrogen is not inherently more dangerous than other conventional fuels, but it has quite different properties, namely very low ignition energy, wide flammability range, high laminar burning velocity and high buoyancy.

Consequence analysis is a critical part of any Quantitative Risk Assessment (QRA), which is used to predict the physical effects of the accidental release of flammable materials. A wide range of consequence analysis tools exist, ranging from simple integral tools based on empirical correlations to sophisticated three-dimensional Computational Fluid Dynamics (CFD) tools. Integral tools are easy to use and require less computational time; however, they take limited account of the influence of obstacles on the flow. Whereas CFD tools are more complex and require longer computational time (typically hours or day) and more skills, but they can predict the effect of complex geometries on the flow. Despite the intrinsic differences, CFD tools and integral tools are considered to perform the same task in consequences analysis. Uncertainties are always part of any consequence analysis, especially for emerging applications. Thus, it is important to understand the underlying assumptions and inherent limitations of the available tools, as well as the expected level of accuracy in the results for different types of hazardous scenarios.

This study examines and compares the results predicted by the CFD tool (FLACS) and integral tools (FRED, PHAST and EFFECTS) which are used in hydrogen safety studies. The focus is to show where the tools predict similar results and where their results deviate strongly. It includes a description of the physical models used in FLACS, FRED, PHAST and EFFECTS for release modelling of hydrogen gas leak through an orifice from a pressurized storage tank. Release and dispersion simulations are carried out in each of FRED, EFFECTS, PHAST and FLACS for 81 hypothetical hydrogen gas release scenarios in open flat terrain. Then, sensitivity analysis is performed with variations in input parameters such as orifice size, wind speed, release direction, atmospheric stability class and surface roughness length to study their effect on the dispersion of the gas cloud. Finally, dispersion simulations are carried out in FLACS for hydrogen gas release from a dispenser in a refuelling gas station and its corresponding release scenario in open flat terrain to study the effect of obstacles on the dispersion of the gas cloud.

A comparison tool was developed using the results produced by the four tools for 72 hydrogen gas release scenarios. The comparison includes the mass flow rate, the downwind distances to lower flammability limit (LFL) and half of lower flammability limit ($\frac{1}{2}$ LFL), and the amount of flammable mass between upper and lower flammability limits. The results showed that FLACS, FRED, EFFECTS and PHAST predicted almost the same mass flow rates for hydrogen gas released at 5 bar and 25 bar; however, FLACS predicted higher mass

flow rates compared to the other tools for hydrogen gas released at 350 bar. The results of the dispersion simulations conclude that EFFECTS is not recommended for hydrogen safety studies due to the large discrepancies in the results when compared to FLACS, FRED and PHAST. FLACS predicted longer downwind distances to LFL and ½ LFL, and larger amount of flammable mass for most of the considered release scenarios; however, the results need to be compared against experimental results as it is not possible to recommend the use of one tool over the other based only on the results of this study.

Hydrogen buoyancy does not prevent the formation of a large flammable cloud. The common argument is that a release of hydrogen gas in an unconfined area will rise and disperse relatively quickly upon release; however, this is not always the case. Hydrogen buoyancy is only valid outside the part of dispersion which is controlled by the jet momentum. From the results, a higher initial pressure produces a jet with higher momentum and the buoyancy force takes longer to dominate the flow. Also, hydrogen gas releases near the ground, tend to deflect towards the ground and cling to it because of an effect known as the Coandă effect. The results showed that this effect increases with the increase in wind speed. Obstacles in the path of the gas cloud help in decreasing the jet momentum and allow the buoyancy to have more effect; however, a large flammable cloud can still be formed.

Preface

This thesis is written as a completion of Master of Science program in Risk Management at the University of Stavanger, Faculty of Science and Technology, Department of Industrial Economics, Risk Management and Planning. This work was carried out in a collaboration with Gexcon AS throughout the spring semester of 2020. Gexcon AS is a world-leading company in the field of safety and risk management and advanced dispersion, explosion and fire modelling.

Acknowledgments

Throughout the writing process of this thesis I have received support from several persons, whom I would like to thank:

- My supervisor at the University of Stavanger, Jan Roar Bakke for facilitating and introducing me to this opportunity.
- My supervisor at Gexcon, Geirmund Vislie for his guidance, advice, encouragement and feedback. I really appreciate the time he spent in reviewing and proofreading this thesis.
- Nicolas Salaün for the constructive discussion which contributed to the structure of this thesis and for his support throughout the entire process.
- Ørjan Knudsen for his guidance, continuous assistance and availability. I really appreciate the time and effort he has put into helping me.
- Josuè Quilliou for his help and feedback which provided me with new ideas.
- Hans Boot and Sonia Ruiz Pérez for their support with EFFECTS.

I am grateful to Gexcon for granting me access to their library and providing me with the necessary training, hardware and software licenses. Everyone at Gexcon made me feel welcome and treated me as part of their team.


I would also like to thank my friend Maryam Ghasemi for her support and motivation. This thesis would not have been possible without her. Finally, I would like to express my sincere gratitude to my husband and my family for their support, love and encouragement throughout my years of study.

Stavanger, July 2020
Maha Eleryan

Glossary of terms

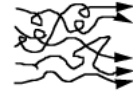
Accidental chemical release	“An unintended, or sudden release of chemical(s) from manufacturing, processing, handling, or on-site storage facilities to the air, water, or land” [4, p. xv].
Atmospheric dispersion	“Mixing and spreading of gases in air, which causes clouds to grow” [5, p. 4.11].
Atmospheric stability	“The extent to which vertical temperature gradient promote or suppress turbulence in the atmosphere” [5, p. 4.11].
Auto ignition temperature	“The minimum temperature at which a substance will self-ignite and sustain a combustion process” [6, p. 5.24].
Blast wave	“The overpressure wave traveling outward from an explosion point” [7].
Buoyancy	“The upward force that is caused by a cloud or plume in which the density is lower than the surrounding atmosphere” [5, p. 4.11].
Burning rate	“The amount of fuel consumed by the combustion process per time unit” [8, p. 23].
Burning velocity	“The velocity of the flame front with respect to the unburned gas immediately ahead of the flame” [8, p. 23].
Combustion	“Reaction process by which a flammable substance is oxidized, producing hot product gases, heat, radiation and possibly pressure waves” [9, p. 3].
Coandă effect	“The tendency of a fluid jet to flow closer to an adjacent surface due to a lower pressure region that develops between the jet flow and the surface” [10, p. 16414].
Confinement	“Obstacles such as walls and ceilings of a building, vessel, pipe, etc. that serve to limit the expansion of a dispersing or exploding vapor cloud” [4, p. xvi].

Congestion	“Small obstacles in the path of a flame front or dispersing vapour cloud that serve to deflect the flame front or cloud and to generate turbulent mixing” [4, p. xvi].
Deflagration	“A combustion wave propagating at subsonic velocity relative to the unburned gas immediately ahead of the flame” [8, p. 23].
Detonation	“A combustion wave propagating at supersonic velocity relative to the unburned gas immediately ahead of the flame” [8, p. 24].
Diffusion	“Flux of a fluid through another fluid or material due to concentration gradient” [9, p. 4].
Enthalpy	“Thermodynamic quantity that is the sum of the internal energy of system and the product of its volume multiplied by its pressure” [5, p. 2.11].
Entrainment	“The mixing of air into a vapour cloud” [4, p. xvii].
Entropy	“Thermodynamic quantity which is the measure of the amount of energy in a system not available for doing work” [5, p. 2.11].
Flame front	“Region of burning or chemical reaction (typically from fractions to several millimetres across) that separates burned and unburned regions” [9, p. 6].
Flammable mass	“The mass of fuel in a vapor cloud that is in the flammable range” [7].
Flame speed	“The velocity of the flame relative to a stationary observer” [8, p. 23].
Hazard	“An inherent chemical or physical characteristic that has the potential for causing damage to people, property, or the environment” [7].
Ideal gas	A gas consisting of molecules that do not occupy space and do not interact with one another [11].

<p>Lower Flammability Limit (LFL)</p>	<p>The “concentration of a combustible material in air below which ignition will not occur” [7].</p>
<p>Joule-Thomson process</p>	<p>“Cooling or heating that occurs when a highly compressed gas is allowed to expand in such a way the enthalpy remains constant; scientifically known as isenthalpic expansion” [9, p. 8].</p>
<p>Laminar flow</p>	<p>“Fluid particles moving along smooth paths in thin layers with one-layer gliding smoothly over an adjacent layer” [9, p. 8]</p> <div style="text-align: right;">  <p>Laminar</p> <p><i>Figure from [8, p. 25]</i></p> </div>
<p>Minimum Ignition Energy (MIE)</p>	<p>The lowest energy required “for a localized ignition source, like a spark, to successfully ignite a fuel-oxidizer mixture” [8, p. 42].</p>
<p>Permeation</p>	<p>“Flow of a fluid (gas) through another (usually solid) material by diffusion without a defect or opening of the latter” [9, p. 10].</p>
<p>Quenching gap</p>	<p>“Spark between two flat parallel-plate electrodes at which ignition of a combustible fuel/air mixture is suppressed” [9, p. 11].</p>
<p>Real gas</p>	<p>A gas consisting of molecules that occupy space and interact with one another; consequently, it does not adhere to the ideal gas law [11].</p>
<p>Risk</p>	<p>“The combination of the probability of occurrence of harm and the severity of that harm” [12, p. 13].</p>
<p>Risk management</p>	<p>“All measures and activities carried out to manage risk” [13, p. 4].</p>
<p>Shock wave</p>	<p>“Large-amplitude compression wave in which there is a rapid and great change in density, pressure and particle velocity” [9, p. 11].</p>
<p>Stoichiometric mixture</p>	<p>A mixture where “the amounts of fuel and oxygen (air) are in balance so that there is no excess of fuel or oxygen after the chemical reaction has been completed” [8, p. 40].</p>

Turbulent flow

Fluid flow which is “characterised by an irregular random fluctuation imposed on mean (time-averaged) flow velocity” [8, p. 24].



Turbulent

Figure from [8, p. 25]

Upper
Flammability
Limit (UFL)

The “concentration of a combustible material in air above which ignition will not occur” [7].

Viscosity

“Resistance of a fluid to shear motion (its internal friction)” [9, p. 13].

Nomenclature

Roman letters

a	Model constant (Abel-Noble EOS)
A	Cross-sectional area (m ²)
c	Speed of sound (m/s)
C_p	specific heat at constant pressure (J/kg K)
C_v	specific heat at constant volume (J/kg K)
C_d	Discharge coefficient
E	Internal energy (J)
g	Gibb's free energy
G	Mass flux (kg/m ² s)
h	Specific enthalpy (J/kg)
H_o	Sensible heat flux (J/m ² s)
L	Monin-Obukhov length (m)
m	Mass (kg)
\dot{m}	Mass flow rate (kg/s)
M	Mach number
n	Effective isentropic exponent
N_t	Number of time steps
P	Pressure (Pa)
P_a	Ambient pressure (Pa)
P_R	Reduced pressure
P_c	Critical pressure of the gas (Pa)

P_{crit}	Critical pressure (Pa)
R	Gas constant
s	Specific entropy (J/ kg K)
T	Temperature (K)
T_m	Melting point (K)
T_R	Reduced temperature
T_c	Critical temperature of the gas (K)
δt	The size of the time step (s)
t_{end}	Termination time (s)
t_{rel}	Release duration (s)
u	Velocity (m/s)
u_*	Friction velocity (m/s)
V	Volume (m ³)
v	Specific volume (kg/m ³)
Z	Compressibility factor
z_0	Roughness length (m)

Greek letters

γ	Isentropic ratio
ε	Dissipation of turbulent kinetic energy
ε_g	Surface roughness (m)
k	Turbulent kinetic energy
κ	Von Karman constant
ρ	Density (kg/m ³)

η	Liquid mass fraction
μ	Molecular weight
ψ	Release coefficient

Abbreviations

AFC	Alkaline Fuel Cell
AIT	Auto Ignition Temperature
ALARP	As Low As Reasonably Practicable
CCPS	Center for Chemical Process Safety
CCS	Carbon Capture and Storage
CFD	Computational Fluid Dynamics
CHP	Combined Heat and Power
CMR	Christian Michelsen Research
DDT	Deflagration to Detonation Transition
DSB	Direktoratet for Samfunnssikkerhet og Beredskap
EOS	Equation of state
FCEV	Fuel Cell Electric Vehicle
FCHEA	Fuel Cell and Hydrogen Energy Association
FLACS	Flame Acceleration Simulator
FMOLE	Mole fraction of fuel
IEA	International Energy Agency
IRENA	International Renewable Energy Agency
ISO	International Organization for Standardization
LFL	Lower Flammability Limit
MCFC	Molten Carbonate Fuel Cell

MIE	Minimum Ignition Energy
NASA	National Aeronautics and Space Administration
NORSOK	NORsk SOKkels Konkurransesepisjon
NTP	Normal Temperature and Pressure
PEM	Proton Electrolyte Membrane
PSA	Pressure Swing Absorption
QRA	Quantitative Risk Assessment
SMR	Steam Methane Reforming
SOE	Solid Oxide Electrolysis
SOFC	Solid Oxide Fuel Cell
TRL	Technology Readiness Levels
UFL	Upper Flammability Limit

Table of Contents

Abstract.....	2
Preface.....	4
Glossary of terms	5
Nomenclature.....	9
Table of Contents.....	13
List of Figures	15
List of Tables	17
1 Introduction	18
1.1 Background.....	18
1.2 Problem definition	20
1.3 Approach of the study.....	21
1.4 Limitations	22
1.5 Literature review.....	22
1.6 Structure of the thesis.....	23
2 Introduction to Hydrogen Gas	24
2.1 Hydrogen properties.....	24
2.2 Hydrogen production	25
2.3 Hydrogen applications	28
2.4 Hydrogen storage and distribution.....	30
3 Hydrogen Hazards	33
3.1 Combustion hazards.....	33
3.2 Spontaneous ignition.....	36
3.3 Asphyxiation	36
3.4 Hydrogen permeation.....	36
3.5 Hydrogen embrittlement	37
3.6 Hydrogen attack	37
4 Consequence Analysis.....	38
4.1 Release modelling.....	39
4.2 Dispersion modelling	41
4.2.1 Momentum and buoyancy effects.....	41
4.2.2 Turbulence	42

4.2.3	Wind.....	42
4.2.4	Atmospheric stability	43
4.2.5	Surface roughness	45
4.2.6	Obstacle effects	46
5	Release Modelling	47
5.1	FRED software.....	47
5.2	EFFECTS software	49
5.3	PHAST software	52
5.4	FLACS software	58
5.5	Release models summary.....	71
6	Comparative Study	73
6.1	Comparison methodology.....	73
6.2	Consequence modelling.....	74
6.3	Scenarios considered for the study	76
6.3.1	Comparative study	76
6.3.2	Sensitivity analysis.....	80
6.3.3	Hydrogen refuelling station	82
6.4	Results.....	83
6.5	Discussion.....	84
6.5.1	Release modelling.....	84
6.5.2	Dispersion modelling.....	86
7	Conclusion.....	101
8	Further Work	103
9	References	104
	Appendices.....	109

List of Figures

Figure 1.1: Comparison of explosion pressure for various Stoichiometric fuel-air mixtures in the 10 m wedge-shaped vessel [8].	19
Figure 1.2: Risk management process [21].	20
Figure 1.3: Event tree showing the sequence of events leading to hydrogen gas release [8].	21
Figure 2.1: Production pathways for hydrogen [14].	26
Figure 2.2: Fuel cell [36].	28
Figure 2.3: Technology Readiness Levels of mobility applications for hydrogen/ fuel cells [34].	30
Figure 2.4: Comparison of gravimetric energy and volumetric energy density for several fuels based on lower heating values [40].	31
Figure 4.1: Illustration of release /dispersion phenomena [2].	38
Figure 4.2: Sonic and subsonic releases [59].	40
Figure 4.3: Wind speed changes (wind gradient) with surface roughness [61].	43
Figure 4.4: Wind rose (Port of Barcelona, 2004) [59].	43
Figure 5.1: Expansion from stagnation to orifice and from orifice to ambient conditions [69].	52
Figure 5.2: Orifice model [69].	54
Figure 5.3: Zones in flow for discharge from orifice [69].	56
Figure 5.4: Schematic sketch of the under-expanded jet model used in the JET utility program [62].	59
Figure 5.5: Schematic view of the control volume for JET model momentum equation [62].	60
Figure 6.1: Hydrogen refuelling gas station.	82
Figure 6.2: Mass flow rates results for hydrogen released at pressure of 5, 25 and 350 bar and temperature of 20 °C through an orifice of 10 mm in diameter.	85
Figure 6.3: Mass flow rates results for hydrogen released at 350 bar and 20 °C through various orifice sizes (1, 3, 5, 10 mm).	85
Figure 6.4: EFFECTS concentration contours for horizontal and vertical jet releases.	86
Figure 6.5: FLACS concentration contours for hydrogen release at initial pressure of 150 and 350 bar.	89
Figure 6.6: Effect of release height – FLACS concentration contours at a release height of 2 m and 5 m.	90
Figure 6.7: Effect of release height – PHAST concentration contours at a release height of 2 m and 5 m.	91
Figure 6.8: Effect of release height – FRED concentration contours at a release height of 2 m and 5 m.	91

Figure 6.9: Downwind distances to LFL and ½ LFL at release height of 2 m and 5 m.	92
Figure 6.10: Effect of wind speed – FLACS concentration contours at release heights of 2 m and 5 m.....	93
Figure 6.11: Effect of wind speed on distance to LFL for horizontal jet release at height of 2 m and 5 m.....	93
Figure 6.12: Effect of wind speed on distance to ½ LFL for horizontal jet release at height of 2 m and 5 m.....	94
Figure 6.13: Formation of a vortex pair in a jet released in a crosswind [56].	94
Figure 6.14: Effect of wind speed – FLACS concentration contours for vertical jet releases.	95
Figure 6.15: Effect of wind speed on distance to LFL for various wind speeds (vertical jet release).	96
Figure 6.16: Effect of wind speed on distance to ½ LFL for various wind speeds (vertical jet release).	96
Figure 6.17: Effect of stability class on downwind distance to LFL.	97
Figure 6.18: Effect of stability class on downwind distance to ½ LFL.	98
Figure 6.19: Effect of roughness length on downwind distance to LFL.	99
Figure 6.20: Effect of roughness length on downwind distance to ½ LFL.	99
Figure 6.21: Effect of obstacles on the dispersion of flammable gas cloud.	100

List of Tables

Table 2.1: Definition of Technology Readiness Levels [34].	30
Table 4.1: Monin-Obukhov lengths and stability [62].	44
Table 4.2: Pasquill atmospheric stability classes [62].	45
Table 4.3: Terrain classification in terms of aerodynamical roughness length [18].	45
Table 5.1: Release models summary for FRED, EFFECTS, PHAST and FLACS.	71
Table 6.1: Release and dispersion models used in the comparative study.	74
Table 6.2: Case 1 and variations used in the comparative study.	77
Table 6.3: Case 2 and variations used in the comparative study.	77
Table 6.4: Case 3 and variations used in the comparative study.	78
Table 6.5: List of scenarios used in in the comparative study.	78
Table 6.6: Case 1 and variations used in the sensitivity analysis.	80
Table 6.7: Case 2 and variations used in the sensitivity analysis.	81
Table 6.8: Case 3 and variations used in the sensitivity analysis.	81
Table 6.9: Scenario used to study the effect of geometry.	82
Table 6.10: How results were obtained from different tools.	83
Table 6.11: Average percentage deviation in the results of the mass flow rate, comparing FLACS to FRED, EFFECTS and PHAST.	84
Table 6.12: Average percentage deviation in the distances to LFL and ½ LFL, comparing FLACS to both FRED and PHAST for horizontal jet releases (45 release scenarios).	87
Table 6.13: Average percentage deviation in the distances to LFL and ½ LFL, comparing FLACS to both FRED and PHAST for vertical jet releases (36 release scenarios).	87
Table 6.14: Average percentage deviation in the flammable mass, comparing FLACS to both FRED and PHAST (81 release scenarios).	88

1 Introduction

1.1 Background

The use of hydrogen as an energy carrier has increasingly caught interest of both public and government policy makers in recent times due to the concerns about the depletion of fossil fuels and the effect of greenhouse gas emissions on the environment [11]. In this perspective, hydrogen is considered as one of the most promising alternatives, mainly because hydrogen provides a sustainable and environmentally friendly way to produce clean energy from renewable resources. Hydrogen produces only water and heat upon combustion without any carbon dioxide emissions. But whether hydrogen is truly zero or near-zero emissions fuel, depends on how it is produced [14].

Hydrogen does not occur naturally on earth and must be extracted from its compounds such as water, natural gas and coal. Currently, hydrogen is mostly produced from fossil fuels with significant associated carbon dioxide emissions, around 830 million tons of carbon dioxide per year [15]. However, these emissions can be reduced up to 85 – 95%, if the carbon dioxide emitted during the production process is sequestered using carbon capture and storage (CCS). Hydrogen can be produced without any carbon footprint using renewable electricity, which comes from renewable energy sources such as solar and wind.

Hydrogen is versatile and can be used in a wide range of applications. Hydrogen is already being extensively used as a chemical feedstock for producing fertilizers and petrochemicals. In any future hydrogen economy, two main applications are envisioned [1]: (1) hydrogen to be used to power fuel cell electric vehicles (FCEV) and (2) hydrogen to be used in stationary fuel cells to produce heat and electricity.

However, the widespread acceptance and use of hydrogen as an alternative fuel requires significant progress in the field of hydrogen safety. Hydrogen production, storage and distribution each comes with its own inherent risks. Hydrogen is not as popular as other conventional fuels. Previous accidents involving hydrogen, such as the “Hindenburg disaster”, have tainted the reputation of hydrogen for many years and probably slowed its use as a fuel. The hydrogen-filled airship Hindenburg caught fire and crashed to the ground at its mooring mast in Lakehurst, New Jersey on May 6, 1937; 35 of the 97 people on board were killed along with a crewman on the ground. The prevailing explanation was that the fire was caused by an electric spark which most likely ignited leaking hydrogen [16].

Hydrogen is not inherently more dangerous than other conventional fuels, such as natural gas and gasoline, but its properties are quite different and must be handled with appropriate care. Hydrogen has a wider flammability limits, higher burning velocity and detonates readily. The ignition of hydrogen may result in a higher overpressure than the leakage of the same mass of any other fuel [17]. This can be shown by the results from an experiment which was carried out in the late 1980s in a wedge shaped geometry with hydrogen-air and other hydrocarbon-air mixtures [8], as shown in Figure 1.1. Hydrogen has also a very low minimum ignition energy which makes it more sensitive to ignition than other fuels. Although hydrogen has

very strong buoyancy, hydrogen release in confined areas poses a significant hazard. Hydrogen is also prone to ignite spontaneously when released from high-pressure source.

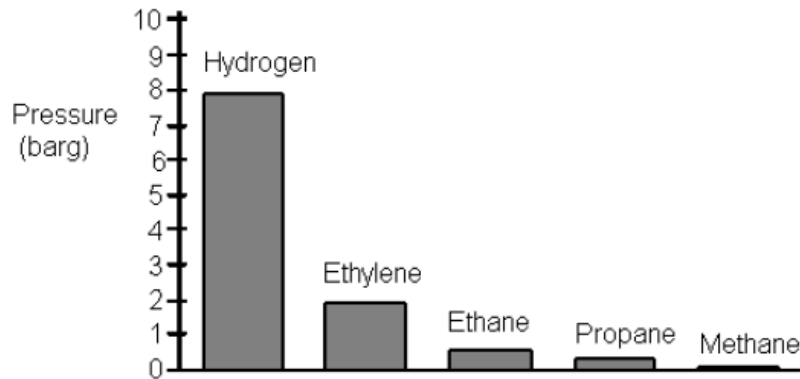


Figure 1.1: Comparison of explosion pressure for various Stoichiometric fuel-air mixtures in the 10 m wedge-shaped vessel [8].

A Quantitative Risk Assessment (QRA) is a valuable tool for determining the risk associated with the use, handling, transport and storage of hazardous materials [18]. It is used to evaluate the expected risk from potential accident scenarios, where it examines both the consequences and likelihood of potential hazardous events and expresses the results as risk to people, the environment and assets [7]. Risk assessment is a central component in an organization’s risk management. Aven defines risk management as “all measures and activities carried out to manage risk” [13, p. 4]. NORSOK Z-013 defines risk as “the combination of the probability of occurrence of harm and the severity of that harm” [12, p. 13]. The purpose of risk management is to ensure that all necessary actions and measures are developed to protect people, environment and assets from possible undesirable consequences caused by the activities performed, and to balance different concerns such as safety and costs [19].

Risk assessment provides a better understanding of potential risks and decision-making support when comparing different solutions and measures relating to risk reduction. According to ISO 31000, risk assessment consists of three sub-elements [20] – as shown in Figure 1.2:

- Risk identification – identify a list of all potential hazardous events and relevant accident scenarios that may occur associated with the defined systems. This is a critical task in risk assessment as a hazardous event that is not identified, will not be included in further analysis.
- Risk analysis – determine causes and consequences of the identified hazardous events, assess the likelihood that such events may occur, assess the uncertainty associated to them and establish the risk picture.
- Risk evaluation – compare the risk level estimated by the risk analysis with a predefined risk acceptance criterion to determine whether the risk is tolerable or risk reducing measures are required. Having identified and evaluated the risks, alternative solutions and measures should be identified and prioritized for risk reduction. The

ALARP principle emphasizes that risk should be reduced to a level ‘as low as reasonably practicable, even if the risk evaluation indicates a safety level within the defined acceptance criterion [3].

Risk assessment is followed by risk treatment, which is a process involving the selection and implementation of measures to modify risk, including measures to avoid, reduce, transfer or retain risk [19].

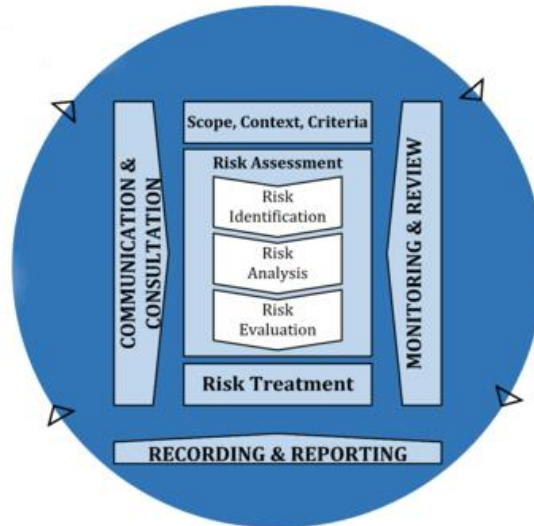


Figure 1.2: Risk management process [21].

1.2 Problem definition

The development of applications using hydrogen as a clean energy carrier has increased in recent years. A prerequisite for commercial applications of hydrogen is to ensure that the risk associated with its production, storage, transport and use is at least not significantly higher than that of existing fuel supplies [1]. Quantitative Risk Assessment (QRA) for hydrogen applications present new challenges due to the significant difference in properties of hydrogen compared to other conventional fuels, namely low ignition energy, wide flammability limits and high buoyancy [11]. Consequence analysis is a critical part of any risk assessment, which is used to predict the physical effects of the accidental release of flammable materials.

However, a wide range of consequence analysis tools exist, ranging from simple integral tools based on empirical correlations (via one-dimensional phenomenological models of varying complexity) to computational fluid dynamics (CFD) tools that account for boundary and initial conditions, and solve the governing equations for conservation of mass, momentum and energy. Integral tools are easy to use and require less computational time; however, they do not account correctly for the effects of obstacles (e.g. buildings, structures, process equipment) [22]. Geometrically complex scenarios require more rigorous calculation methods such as Computational Fluid Dynamic (CFD) codes to obtain accurate estimation of

the extent of the dispersed flammable cloud and its effects [22]. Regardless of the complexity of the consequence models, it is important to understand the underlying assumptions and inherent limitations of the available tools, as well as the expected level of accuracy in the results for different types of hazardous scenarios [3].

There are inherent uncertainties associated with most consequence analyses, especially for emerging applications. Despite the intrinsic differences, CFD tools and integral tools are considered to perform the same task in consequence analysis [2]. To this end, it is essential not only to understand the physical phenomena, such as release, dispersion, fires and explosions, but also to assess the capabilities and limitations of the different tools used in these analyses.

1.3 Approach of the study

A hydrogen accident scenario usually follows a typical sequence of events: hydrogen gas is accidentally released from a storage tank or a hydrogen system, immediate ignition could occur resulting in a jet fire, otherwise a flammable cloud is formed where the gas is mixed with air and in case of ignition a flash fire or an explosion (deflagration and/or detonation) could occur [23] – as shown in Figure 1.3.

Release and subsequent dispersion simulations are used to describe the spreading and diluting behaviour of accidental gas releases into the atmosphere. Many experts consider release and dispersion modelling studies to be the most important parts for estimating the consequences of flammable gas releases. Thus, it is important that the underlying physics of both release and dispersion phenomena is understood and modelled in the correct manner.

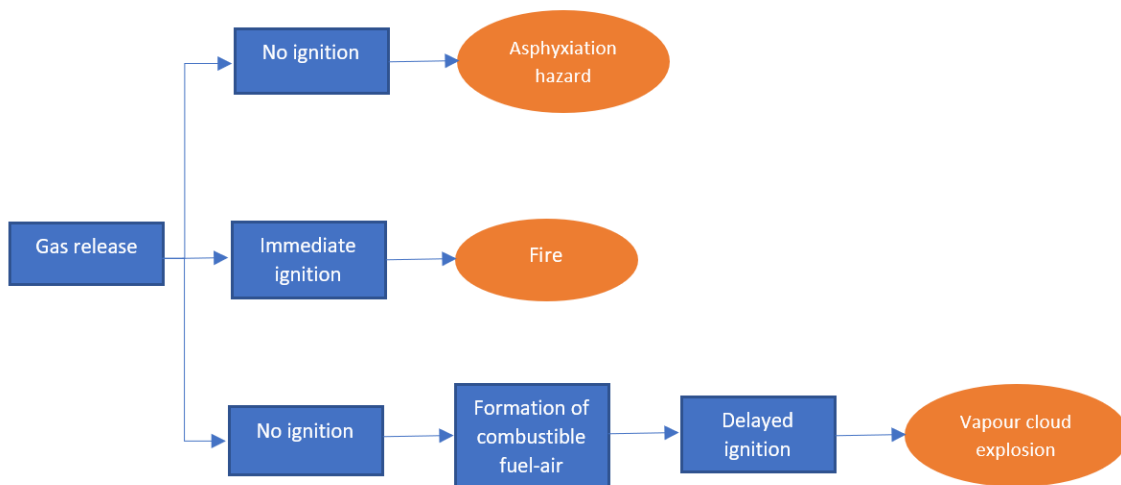


Figure 1.3: Event tree showing the sequence of events leading to hydrogen gas release [8].

This study examines and compares the results produced by integral tools and CFD tools which are used for consequence analysis in hydrogen safety studies. The focus of this study is show where the tools give similar results and where their results deviate strongly.

Four consequence analysis tools were chosen:

- FRED version 7.1.1,
- EFFECTS version 11.0.6,
- PHAST version 8.1,
- FLACS version 10.9.

The study is divided into two main parts:

- The first part describes the physical models used in the different tools for release modelling of hydrogen gas leak from a pressurized storage tank through an orifice.
- A comparative study is conducted in the second part where release and dispersion simulations are carried out for hydrogen gas releases in open flat terrain through an orifice from a pressurized tank. Mass flow rate, downwind distance to concentration levels of half of lower flammability limit (2% vol.) and lower flammability limit (4% vol.), and total flammable mass between upper and lower flammability limits (75 – 4 % vol.) are used for the comparison. A sensitivity analysis is performed to study the effect of parameters variation such as, orifice diameter, release direction, wind speed, atmospheric stability class and surface roughness length on the dispersion of the gas cloud. The effect of obstacles on the dispersion of the gas cloud is simulated in FLACS using a simple hydrogen refuelling station.

1.4 Limitations

Release and dispersion phenomena of liquid hydrogen are areas where there is a significant lack of both experimental and modelling work. There are still substantial limitations in the existing methods for consequence analysis of liquid hydrogen accidental releases. Thus, this study will focus only on hydrogen release in its gaseous form. However, a list of useful references is submitted in “Appendix E” for liquid hydrogen safety studies.

1.5 Literature review

An initial literature review was undertaken to obtain relevant published research literature comparing CFD and integral tools. Several publications and studies were found that address the difference in results of CFD and integral tools for both releases in open field and congested areas, two of which comparing FLACS and PHAST. However, none of them was for hydrogen gas releases. Also, no studies were found comparing either FRED or EFFECTS with CFD tools or comparing the integral tools (FRED, EFFECTS and PHAST).

An in-house article [24] by Gexcon, concluded that FLACS and PHAST are comparable for jet releases in unobstructed environments. However, in congested environments, PHAST is out of its validity range and deviation is expected in the results.

The article “Risk assessment of dangerous products release and dispersion: a comparison between CFD and integral models” [25], concluded that CFD codes and PHAST model (integral model) are somewhat comparable for open field releases of Sulphur dioxide (SO₂). The results of these simulations were compared with the large-scale outdoor Prairie Grass experimental data, and both CFD codes and PHAST model showed a good agreement with the field measurements. The article also described the results of simulations in congested areas, where PHAST could not distinguish the influence of obstacles.

The master’s thesis “Interpretation of geometrical effects in consequence modelling. Comparison study between the commercial consequence assessment tools FLACS and PHAST for flammable gas dispersion” [2], compares the results given by FLACS and PHAST for a set of various hazardous gas dispersion scenarios. The study concluded that FLACS and PHAST showed an overall good agreement for open field jet releases in terms of concentration decay along a centerline profile and for flammable mass. The results of FLACS and PHAST showed satisfactory results when evaluated against experimental large-scale open field trials. The study also concluded that PHAST was unable to give comparable results for releases in congested areas and that the surface roughness length cannot be used to represent real congestion that is represented in a CFD model.

In the “Comparative study on gas dispersion” jointly performed by the Directorate for Civil Protection and Emergency Planning (DSB) and Scandpower [26], a comparison between integral tools (PHAST and TRACE) and CFD tools (FLACS and KFX) has been conducted. The study concluded that both CFD and integral tools can be applied with similar accuracy for releases in unobstructed environments. However, only CFD tools should be applied for releases in congested environments.

1.6 Structure of the thesis

The study is structured as described below:

- Chapter 2 provides basic information regarding the physical and chemical properties of hydrogen, uses of hydrogen and methods used for hydrogen production, storage and distribution.
- Chapter 3 describes the potential hazards associated with gaseous hydrogen.
- Chapter 4 provides essential and basic information regarding the release and dispersion phenomena.
- Chapter 5 describes the release models used in FRED, EFFECTS, PHAST and FLACS for steady state gas releases from a storage tank through an orifice.
- Chapter 6 is dedicated for the comparison of FRED, EFFECTS, PHAST and FLACS where both release and dispersion simulations are carried out for hydrogen gas releases. It includes the description of the comparison methodology and simulation scenarios. Also, the results from the simulations and a discussion of these are presented in this chapter.
- Chapters 7 and 8 are dedicated for the final conclusions and recommendations for further work.

2 Introduction to Hydrogen Gas

2.1 Hydrogen properties

Physical properties

This section is based on information from “ISO/TR 15916:2015 standard” [9], unless stated otherwise.

Hydrogen is the most abundant element in the universe, which represents 75% by mass or 90% by volume of all matters, [27]. Hydrogen is colourless, odourless, tasteless and non-toxic at normal temperature and pressure (NTP), 20 °C and 1 atmospheric pressure. As a pure substance, hydrogen exists as a molecule, designated H₂, in which two hydrogen atoms have formed a covalent bond. Bulk hydrogen, in its gaseous form, is a mixture of ortho-hydrogen (the nuclear spin of its two atoms aligned parallel) and para-hydrogen (antiparallel) in which the temperature determines the equilibrium quantities of each form. Hydrogen exists in a gaseous form at NTP. Hydrogen is a liquid below its boiling point, -252.76 °C, and a solid below its melting point, -259.19 °C, at atmospheric pressure.

The low viscosity of hydrogen, due to its small molecular weight (2.016 g/mol), causes a comparatively high flow rate if the gas leaks through fittings, seals, or porous materials. The viscosity of gaseous hydrogen (in μPoise) is 89.48 at NTP [28].

Hydrogen has high buoyancy and greater diffusivity than other gases. Hydrogen has a density of 0.0838 kg/m³ at NTP, approximately 14 times less dense than air which makes it the lightest of all gases. If a leak occurs, hydrogen has the tendency to rise and diffuse, and form ignitable mixtures with air. In unconfined areas, these mixtures ultimately dilute to a level below the lower flammability limit (LFL). However, in (partially) confined areas, hydrogen can accumulate and stratify in regions without opening (e.g. underneath a roof) where it can reach ignition sources (e.g. ceiling lights).

Chemical properties

This section is based on information from HySafe’s “Biennial Report on Hydrogen Safety” [27] and Middha’s PhD thesis “Development, use, and validation of the CFD tool FLACS for hydrogen safety studies” [11], unless stated otherwise.

The auto-ignition temperature (AIT) for hydrogen is 858 K, which is relatively high compared to that of methane, 810 K. The minimum ignition energy (MIE) of hydrogen-air mixture is 0.017 mJ, which is much lower compared to that of methane, 0.274 mJ. This makes hydrogen far more sensitive to ignition so that even a very small spark as those produced by wearing certain types of clothing are enough to ignite a hydrogen-air mixture. The minimum ignition energy tends to be near the stoichiometric hydrogen-air mixture, which contains 29.5% vol. of hydrogen. The ignition energy of hydrogen is similar to that of

methane at the lower flammability limit (LFL). In addition, sparks from electrical equipment (order of joules) or electrostatic sparks (order of tens millijoules) have greater energies than that required to ignite most hydrocarbons [29].

The flammability range of hydrogen is between 4 – 75% vol. in air (at NTP), and up to 95% vol. in oxygen. Hydrogen has a very wide flammability limits compared to that of natural gas 5 – 15% vol. in air. The premixed flame temperature of a stoichiometric hydrogen-air mixture is 2403K. It is difficult to quench a hydrogen flames [28]. The quenching gap in air is the “spark gap between two flat parallel-plate electrodes at which ignition of a combustible fuel/air mixture is suppressed” [9, p. 11]. Faster burning gases have smaller quenching gaps. The quenching gap for a stoichiometric hydrogen-air mixture at NTP is 0.64 mm. The burning velocity of stoichiometric hydrogen-air mixture is 2.55 m/s reaching a maximum of 3.2 m/s at a concentration of 40.1% vol., which would even increase to 11.75 m/s in pure oxygen. These values are higher compared to other hydrocarbon fuel-air mixtures, due to the fast chemical kinetics and high diffusivity of hydrogen. Consequently, there is a higher possibility for transition from deflagration to detonation causing much severe damage.

The detonability range of hydrogen is between 18 – 59% vol. in air; however, lower detonability limit as low as 11 vol% was observed in some experiments. The detonation cell size is a measure of the reactivity of the mixture which serves as an indicator for deflagration to detonation transition (DDT). The smaller the cell size, the more reactive is the mixture. Hydrogen-air mixture is highly reactive with a detonation cell size of 10 – 15 mm, whereas the cell size of methane-air mixture is as large as 330 mm (least detonation sensitivity).

2.2 Hydrogen production

This section is based on information from the report “Hydrogen: a renewable energy perspective” by the International Renewable Energy Agency (IRENA) [30], unless stated otherwise.

Although hydrogen is an abundant element in the universe, it does not exist naturally and must be extracted from other compounds, such as natural gas, coal and water. Hydrogen is considered as a “clean” energy carrier, but it is only as clean as the feedstock and method used to produce it. Most hydrogen is currently produced from steam methane reforming (SMR) and coal gasification, which produce carbon dioxide as a by-product. This type of hydrogen is often called “grey hydrogen”. Hydrogen produced from steam methane reforming (SMR) has an emissions intensity of around 285 grams of carbon dioxide per kilowatt-hour (kWh) and coal gasification around 675 grams of carbon dioxide per kilowatt-hour [31]. Carbon dioxide emitted during the production of grey hydrogen can be sequestered using carbon capture and storage (CCS) with reduction efficiency of 85 – 95%. In this case, hydrogen is often called “blue hydrogen”. Water electrolysis is a promising option for hydrogen production from renewable resources. Electrolysis is the process of using electricity to split water into hydrogen and oxygen. This type of hydrogen is often called “green hydrogen”, if electricity used during this process comes from renewable energy sources, such as solar or wind.

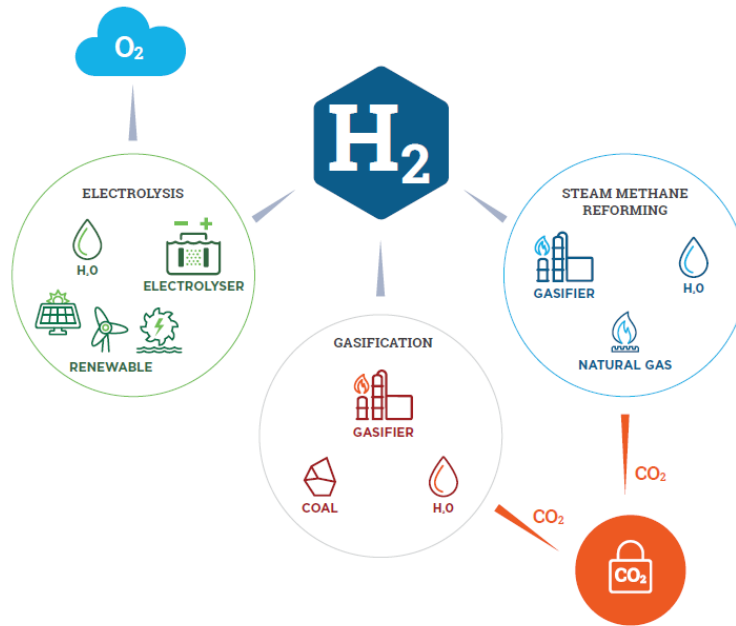


Figure 2.1: Production pathways for hydrogen [14].

Hydrogen production from steam methane reforming, gasification of coal and water electrolysis are briefly discussed in the following sections.

Steam Methane Reforming (SMR)

This section is based on information from the website of the “U.S. Department of Energy's Office of Energy Efficiency and Renewable Energy (EERE)” [32], unless stated otherwise.

Steam Methane Reforming is currently the most widely used method for producing hydrogen, estimated to be 68% of the world’s hydrogen production. High-temperature steam (700°C – 1000°C) is used to produce hydrogen from natural gas. In steam-methane reforming, methane reacts with steam under pressure of 3 – 25 bar in the presence of a catalyst to produce a synthesis gas, consisting of hydrogen, carbon monoxide and a small amount of carbon dioxide. Steam reforming is endothermic reaction, which means that the reaction requires the introduction of heat. Subsequently, the carbon monoxide and steam are reacted using a catalyst to produce carbon dioxide and more hydrogen in so-called water-gas shift reaction. The carbon dioxide and hydrogen gas streams are further separated using a pressure swing absorption (PSA) process

Steam-methane reforming reaction.

$$\text{CH}_4 + \text{H}_2\text{O} (+ \text{heat}) \rightarrow \text{CO} + 3\text{H}_2$$

Water-gas shift reaction

$$\text{CO} + \text{H}_2\text{O} \rightarrow \text{CO}_2 + \text{H}_2 (+ \text{small amount of heat})$$

Coal gasification

This section is based on information from the website of the “U.S. Department of Energy's Office of Energy Efficiency and Renewable Energy (EERE)” [33], unless stated otherwise.

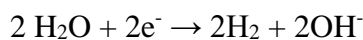
Hydrogen is produced by first reacting coal with oxygen and steam to form synthesis gas, consisting of hydrogen and carbon monoxide. This reaction is endothermic, which requires the input of heat, similar to the steam methane reforming. The process then involves a water-gas shift reaction, where the carbon monoxide and steam are reacted to produce carbon dioxide and hydrogen. The carbon dioxide and hydrogen gas streams are further separated using a pressure swing absorption (PSA) process.

Electrolysis

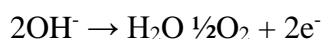
This section is based on information from “Shell hydrogen study” [34], unless stated otherwise.

Electrolysis is the process of using electricity to split water into hydrogen and oxygen. This reaction takes place in a unit called an electrolyser, which consists of a DC source and two noble-metal-coated electrodes separated by an electrolyte. Electrolysers are differentiated by the electrolyte materials and the temperature at which they operate: low temperature electrolysis, including alkaline electrolysis and proton electrolyte membrane (PEM) electrolysis; and high temperature electrolysis, including solid oxide electrolysis (SOE). Alkaline electrolysis is the market leader which has been used in hydrogen production for over 100 years, while PEM electrolysis has been used since the 1960s [35]. SOE is still at an advanced R&D stage and is not yet commercially available.

Alkaline electrolysis operates at temperature around 60 – 80 °C and has an energy efficiency of 65 – 82% providing hydrogen with very high purity. In an alkaline electrolyser, the cathode loses electrons to the aqueous solution. The water is dissociated, leading to the formation of hydrogen (H₂) and hydroxide ions (OH⁻).



The charged hydroxide then moves toward the anode where the electrons are absorbed, and the hydroxide ions are oxidized to form water and oxygen.



2.3 Hydrogen applications

This section is based on information from “Shell hydrogen study” [34] and the website of the “Fuel Cell and Hydrogen Energy Association (FCHEA)” [36], unless stated otherwise.

Hydrogen is versatile that can be used in a wide range of applications, including industrial applications and energy applications. Today hydrogen is mostly used in many industrial applications, such as the production of ammonia production, methanol production and removing sulphur from fuels in oil refining.

The use of hydrogen for energy purposes occurs mainly in fuel cells. A fuel cell is a device that uses hydrogen and oxygen to generate electricity by an electrochemical process. A fuel consists of an anode, a cathode and an electrolyte membrane, as shown in Figure 2.2. Hydrogen enters the fuel cell at the anode while oxygen enters at the cathode. Activated by a catalyst, hydrogen atom split into protons and electrons, which move to the cathode in two different paths. The electrons pass through an external circuit, generating a flow of electricity. The protons move to the cathode through the electrolyte membrane, where they are combined with oxygen and the electrons to produce water and heat. Fuel cells are categorized primarily by the type of electrolyte and the temperature at which the cell is operated. There are four main types of fuel cell, the alkaline fuel cell (AFC), the proton exchange membrane (PEM) fuel cell, the solid oxide fuel cell (SOFC) and the molten carbonate fuel cell (MCFC).

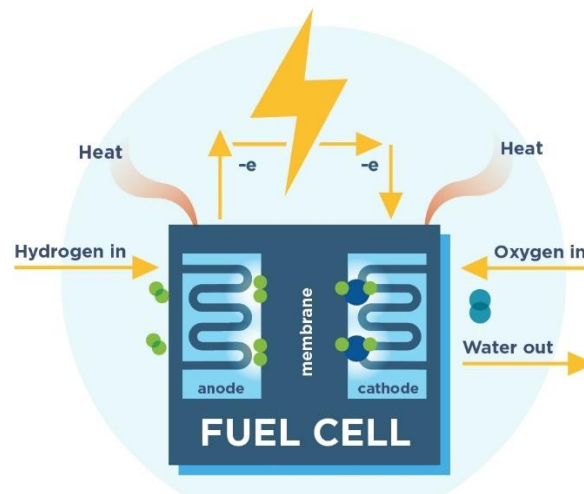


Figure 2.2: Fuel cell [36].

Stationary energy applications

This section is based on information from “Shell hydrogen study” [34], unless stated otherwise.

Stationary fuel cells can be used to produce electricity in off-grid areas and for emergency backup power to ensure continuous operation of highly sensitive technical systems, such as telecommunications networks and data centers. Many companies around the United States are

using stationary fuel cells for primary and backup power including Adobe, Apple, AT&T, Sprint, eBay, Google, Honda, Microsoft and Walmart [37]. According to the Fuel Cell and Hydrogen Energy Association (FCHEA), as of January 2020, there are more than 550 megawatts (MW) of stationary fuel cells installed in the United States providing clean, reliable, distributed power to customers across the country [37]. In Singapore, hydrogen fuel cells are used to generate electricity for a building at the SP Group's training center, which is the first zero-emission building in Southeast Asia powered by green hydrogen [38].

In addition to the generated electricity, the heat that is produced by the fuel cell can be used to cover parts of residential and industry heating demands. The process is referred to as "Combined Heat and Power" (CHP), which can provide high efficiency up to 95%. As of the end of 2018, there are 225,000 residential fuel cell CHP systems installed globally [39].

Mobility applications

This section is based on information from "Shell hydrogen study" [34], unless stated otherwise.

Hydrogen can power fuel cell electric vehicles (FCEV) including cars, buses, trucks and trains. During the past decade, fuel cells emerged as a potential replacement for the conventional internal combustion engines. Fuel cells have higher efficiency compared with the internal combustion engines and produce zero carbon dioxide emissions (tail-pipe emissions are only water). Fuel cell electric vehicles predominately use proton exchange membrane (PEM) fuel cells. Hydrogen powered vehicles have faster refuelling time and can travel longer distances compared to battery electric vehicles. However, they require a network of refuelling stations, similar to what exists for petrol and diesel.

The Shell Hydrogen Study [34] has analyzed the maturity of hydrogen-powered vehicles, according to the Technology Readiness Levels (TRL), which is a measurement system developed by NASA to assess the maturity level of a particular technology. The TRL scale goes from TRL 1 to TRL 9. The study focuses only on levels starting from TRL 5 as prototypes have been tested for almost all the vehicles considered. Table 2.1 defines the Technology Readiness Level used. A technology established in the market requires at least a proven functionality in the field of use (= TRL 8). Fuel cell industrial trucks, such as forklifts, are almost fully mature and already at the early stage of commercial use. Passenger cars have reached a series of production, while buses are close behind. Figure 2.3 shows the Technology Readiness Levels of mobility applications for fuel cells.

According to the International Energy Agency (IEA) [15], 381 hydrogen refuelling stations are in operation and around 11,200 hydrogen fuel cell passenger cars are already on the road globally. Toyota, Hyundai and Honda now produce hydrogen fuel cell passenger cars [39]. The Hydrogen Council envisions 3000 refuelling stations globally by 2025, which would be sufficient to provide hydrogen for about 2 million FCEVs [39].

Table 2.1: Definition of Technology Readiness Levels [34].

Level	Description
TRL 5	Experimental setup in operational environment – key technology elements tested in a relevant environment.
TRL 6	Prototype in operational environment – technical feasibility demonstrated in the area of application.
TRL 7	Prototype in use – demonstration almost to scale in the operational environment.
TRL 8	Qualified system with proof of functional capability in area of use – product.
TRL 9	Qualified system with proof of successful use – product.

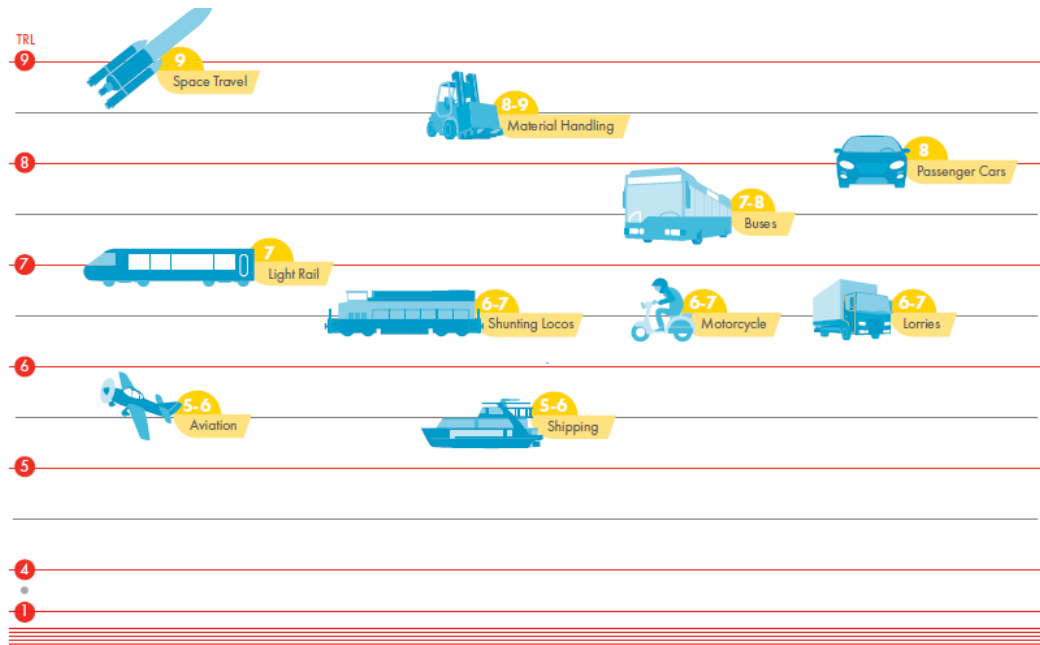


Figure 2.3: Technology Readiness Levels of mobility applications for hydrogen/ fuel cells [34].

2.4 Hydrogen storage and distribution

The storage of hydrogen is a key enabling technology for the use of hydrogen as an energy carrier. Hydrogen has the highest gravimetric energy density 120 MJ/kg, nearly three times that of gasoline, 44MJ/kg [40]. However, the volumetric energy density of hydrogen is comparatively low. The volumetric energy density of hydrogen at NTP is 0.01 MJ/l while that of gasoline is 32MJ/l [40]. Thus, for hydrogen storage to be economically feasible, its density must be increased. Hydrogen can be stored as a compressed gas in pressure tanks, or as a liquid in cryogenic tanks. Hydrogen can also be stored on the surface of solids (by adsorption) or within solids (by absorption). In this section, only hydrogen storage and distribution in its gaseous form will be discussed.

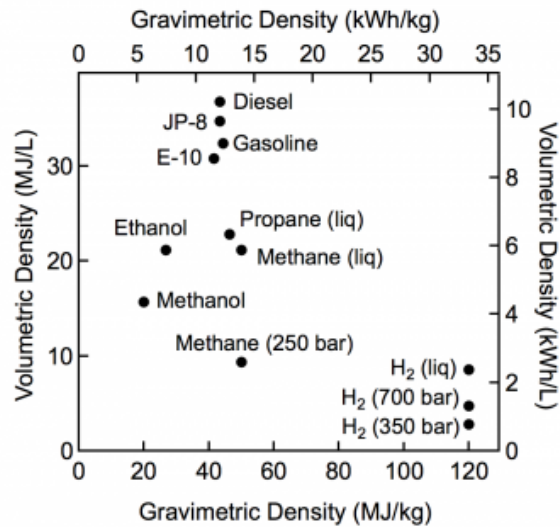


Figure 2.4: Comparison of gravimetric energy and volumetric energy density for several fuels based on lower heating values [40].

Hydrogen storage

This section is based on information from the journal article “The role of hydrogen and fuel cells in the global energy system” by Staffell et al. [39], unless stated otherwise.

Hydrogen is promoted as a medium for storage of electricity, which can be used for long-term or seasonal demands. This requires large scale hydrogen storage in order to balance out the intermittency in electricity generation from wind and solar power. Underground storage in salt caverns are considered most suitable for large scale hydrogen storage. Underground storage of natural gas has been used for many years, where natural gas is stored in bulk to balance seasonal supply/demand fluctuations or for crisis preparedness [34].

Compressed hydrogen with storage pressures of 350 bar or 700 bar is used for hydrogen storage tanks on-board of fuel cell electric vehicle (FCEV), depending on the type of vehicle (light duty or heavy duty). When hydrogen is compressed to 350 bar, the volumetric energy density increases to 2.9 MJ/l; while when compressed to 700 bar the volumetric energy density increases to is 4.8 MJ/l [34]. As a hydrogen fuel cell electric vehicle, Toyota Mirai has a driving range of 500 km with on-board storage tank capacity of 5 kg. The storage tank has a volume of around 120 litres at 700 bar storage pressure which takes it takes 5 minutes to refuel the tank [41]. On-board hydrogen storage tanks are made of light-weight carbon fiber composites (Type IV), with inner line made of high molecular weight polymer that serves as hydrogen gas permeation barrier and outer shell for impact and damage resistance [42].

It is important that the storage tanks at the refuelling stations have enough capacities to meet customers demand. A simple hydrogen refuelling station consists of storage tanks, hydrogen compressors, a precooling system and a hydrogen dispenser which dispenses hydrogen to pressures of 350 bar or 700 bar depending on the type of vehicle. If hydrogen is produced locally, it will be fed directly into the refuelling station while if it is produced in a centralized production facility, it has to be delivered to the refuelling station using tube trailers. Then

hydrogen is compressed to high pressures, up to 950 bar, and then stored in buffer tanks until needed.

Hydrogen distribution

This section is based on information from the journal article “the role of hydrogen and fuel cells in the global energy system” by Staffell et al. [39], unless stated otherwise.

There are typically two possibilities for hydrogen gas distribution depending on the size of demand and the transportation distance. Small quantities of hydrogen can be transported as a compressed gas in tube trailers. Large trailers are available to transport hydrogen from the centralized production facilities to the refuelling stations which has 1000 kg hydrogen capacity at a pressure of 500 bar.

Pipelines are considered as the most efficient method for transporting large quantities of gaseous hydrogen over short distances. Approximately 3000 km high-pressure hydrogen pipelines are currently operating in Europe and North America for industrial processes.

3 Hydrogen Hazards

According to CCPS, hazard is defined as “an inherent chemical or physical characteristic that has the potential for causing damage to people, property, or the environment” [7]. Hazard identification process involves identifying of all potential hazardous events that may occur associated with the defined systems [43]. It is the first and most critical task in the risk assessment as what has not been identified will not be evaluated and hence cannot be mitigated or avoided. Hydrogen is not inherently more dangerous than other conventional fuels; however, it has different properties and must be handled with appropriate care to avoid the realization of a hazard.

3.1 Combustion hazards

This section is based on information from “ISO/TR 15916:2015 standard”[9], unless stated otherwise.

While the fast diffusion of hydrogen may dilute a cloud of released gas, this should not be taken as granted. Under most conditions, the effects of fluid dynamics (such as wind, momentum, or buoyancy controlled flow) will dominate the diffusion process. In the case of a buoyancy-controlled flow, the resulting fluid dynamics will form a rising turbulent plume that will dominate the molecular diffusion. Likewise, hydrogen released from a high-pressure storage vessel, where the pressure in the vessel is greater than 2 bar and the flow is sonic, will result in a jet. The jet will be momentum-controlled due to the high exit velocity of the gas and the fluid dynamics will dominate the molecular diffusion and buoyancy effects of the hydrogen. However, at some distance from the exit, the gas velocity is reduced (due to the air entrainment) to a level at which the buoyancy force is dominant.

For hydrogen to combust, two additional elements need to be present: an oxidizer and a source of ignition. Hydrogen combustion occurs in three different physical processes, as:

- A non-premixed flame (jet fire),
- A premixed flame propagating as a deflagration wave (a subsonic process),
- A premixed flame coupled with a shock wave propagating as a detonation wave (a supersonic process).

Non-premixed combustion process

This section is based on information from “ISO/TR 15916:2015 standard”[9], unless stated otherwise.

An immediate ignition of high-pressure hydrogen release will result in a jet fire, with flame length of 10 m to 15 m. Due to heat-absorbing water vapour produced during the combustion of hydrogen and the absence of carbon combustion reaction, hydrogen fire has significantly

less radiant heat than hydrocarbon fires [44]. This radiation is just outside the visible range near the ultraviolet (UV) spectrum, most of the emissions is around 311 nm. Roughly, hydrogen is considered to dissipate approximately 15% of the energy in radiant emissions compared to 40% for hydrocarbons [45]. Unlike other hydrocarbons, hydrogen burns with a pale blue flame that is almost invisible in daylight. Thus, hydrogen flame will be dangerous in the sense that it is almost impossible to see with the naked eye and personnel near a hydrogen flame may not sense the proximity of the flame. Direct contact with combusting hydrogen can cause severe burns as the flame temperature is in the same order of that of hydrocarbons (approximately 2000 °C) [45]. However, hydrogen is considered less dangerous, as the low emissivity of hydrogen flame reduces the heat transfer by radiation to the surroundings. The potential for smoke inhalation damage is judged to be low.

Premixed combustion process

This section is based on information from Bjerketvedt et al. “Gas explosion handbook” [8], the “Yellow Book” [5] and “ISO/TR 15916:2015 standard” [9], unless stated otherwise.

A gas explosion is defined as a process where combustion of a premixed flammable mixture is causing rapid increase of pressure. For gas explosions, there are two different mechanisms of flame propagation through a flammable mixture: a deflagration and a detonation. A deflagration is defined as “a combustion wave propagating at subsonic velocity relative to the unburned mixture immediately ahead of the flame” [8, p. 23]. A deflagration is the most common mechanism of flame propagation in an accidental gas explosion. The flame speed of deflagrations ranges from a few m/s up to 500 - 1000 m/s, resulting in overpressures from a few mbar to several bar. A detonation is defined as “a combustion wave propagating at supersonic velocity relative to the unburned mixture immediately ahead of the flame” [8, p. 24]. A detonation wave can propagate at a velocity of 1500 - 2000 m/s and the maximum pressure produced is typically 15 to 20 bar. The damaging effects of explosions are mostly due to the overpressure (blast wave) which can cause significant injury to people and damage to equipment and facilities.

When a flammable cloud of hydrogen-air mixture is ignited, the flame will start to propagate away from the ignition location with a laminar burning velocity in the order of 2 - 3 m/s (which is about 10 times faster than of hydrocarbons flames). The laminar burning velocity is defined as “the velocity of the flame front with respect to the unburned mixture immediately ahead of the flame” [8, p. 23]. It is an important parameter as it provides information about the reactivity of a fuel and the expected consequences in case of an explosion relatively to other fuels. The visible flame propagation velocity for hydrogen-air mixture is significantly higher than the laminar burning velocity. This can be caused by the expansion of hot combustion products behind the flame which adds a convection velocity to the flame propagation velocity.

This can be explained by considering the flame propagation in a tube filled with premixed mixture which is open at one end and closed at the other. If the ignition occurs at the open end, the flame speed will not be affected by the expansion of hot combustion products which will be vent directly through the open end. In this case, the flame propagates at the laminar burning velocity. However, if the ignition occurs at the closed end, the flame starts to

accelerate as the flame is pushed more rapidly into the unburned mixture by the expansion of the hot combustion products. In this case, the actual flame speed will be equal the laminar burning velocity multiplied by the expansion ratio. The expansion ratio is defined as “the ratio between the densities of the unburnt mixture and the combustion products” [5, p. 5.16].

The presence of obstacles in the flow can accelerate the flame further due to the turbulence generated by the interaction of the flow field with obstacles ahead of the flame. Turbulence wrinkles the flame front and increases the flame surface area, thereby causes higher burning rate and consequently its speed. The presence of confinement and congestion can accelerate the flame to hundreds of meters per second with an attendant formation of considerable overpressures, reaching several barg. Explosions of hydrogen-air mixture are often initiated as a fast deflagration with flame speed in the order of several hundred meters per second. The maximum propagation velocity of a deflagration wave in a turbulent flow field is limited to the speed of sound in the unburnt gas mixture, which is 975 m/s for a stoichiometric hydrogen-air mixture at NTP. Deflagration of hydrogen-air mixture can produce pressures as high as 8 times the initial pressures, even more in special geometries, depending on the flame speed.

Turbulence and various flame front instabilities, due to confinement and congestion, can even accelerate the flame up to a greater level leading to deflagration to detonation transition (DDT). Detonation differs from deflagration in that there is a leading shock wave which is coupled with the combustion wave. Detonation of hydrogen-air mixtures can produce pressures as much as 20 times the initial pressure and 50 times the initial pressure with reflection.

The detonation wave front does not consist of a single uniform shock wave but possesses multiple transverse waves generating a cell structure with a characteristic length scale that is the denotation cell size. The size of the detonation cell is used as a measure of the fuel-air mixture sensitivity to detonation. The cell size depends on the mixture composition; more reactive mixtures have smaller cell sizes. The cell size is also a measure for the minimum geometrical dimensions allowing a detonation to propagate. The detonation cell size of a stoichiometric hydrogen-air mixture is of the order of 10 – 15 mm.

The direct initiation of a detonation requires a hydrogen-air mixture closer to the stoichiometric ratio composition and significantly higher ignition energy than is needed for deflagration. Detonation is a self-sustained combustion mechanism, which means that it does not require confinement and congestion to propagate at high speed.

3.2 Spontaneous ignition

This section is based on information from the JRC reference report “Prioritization of research and development for modelling the safe production, storage, delivery and use of hydrogen” [23] and Middha’s PhD thesis “Development, use, and validation of the CFD tool FLACS for hydrogen safety studies” [11], unless stated otherwise.

The possibility of spontaneous ignition (ignition for no apparent reason) of accidental hydrogen release from high-pressure systems is well known and several explanation have been proposed by Astbury and Hawksworth [46]. One of these explanations is the reverse Joule-Thompson effect during isenthalpic expansion through valves. At ambient temperature, the temperature of hydrogen will increase, rather than decrease, upon expansion to the atmospheric pressure which may lead to ignition.

Another explanation is “diffusion ignition”, sudden release of hydrogen from a high-pressure source can produces a shock wave which causes the temperature of hydrogen-air mixture to rise leading to ignition. It has been also observed that the downstream geometry following the release from a high-pressure source has an impact on whether the ignition will occur. This phenomenon has been investigated in several experimental and numerical studies by Dryer et al. [47], Golub et al. [48]–[51], Mogi et al. [52], Xu et al. [53] and Yamada et al. [54].

3.3 Asphyxiation

Hydrogen leaks cannot be detected by human senses and can cause asphyxiation in confined areas if reached sufficient concentration levels. Hydrogen can produce suffocation by diluting the oxygen concentration level in air below the level necessary to sustain life [55].

3.4 Hydrogen permeation

This section is based on information from “ISO/TR 15916:2015 standard” [9], unless stated otherwise.

Hydrogen as the smallest molecule has a high tendency for diffusion and permeation through confining walls. Thus, hydrogen vessels and piping systems require good seals and welded joints are preferred where leaks cannot be tolerated. The permeation rate varies for the different types of materials. For metals such as steel, the permeation rate is considered negligible with insignificant quantities permeating over very long period. Some caution should be observed with polymer materials which have high permeability. This can pose significant hazard if the gas flow entered a small unventilated volume as large amount of hydrogen can accumulate in high spots and reach ignition sources (e.g. ceiling lights). However, usually the permeation process is slow enough so that ignitable mixtures are not developed.

3.5 Hydrogen embrittlement

This section is based on information from “ISO/TR 15916:2015 standard”[9], unless stated otherwise.

Hydrogen can cause embrittlement to many metallic materials, which occurs when hydrogen permeate into the lattice structure of the material. Hydrogen embrittlement can cause a significant degradation in the mechanical properties of metals, which can lead in catastrophic failure of containment structures. Hydrogen embrittlement is influenced by a large number of variables such as the temperature and pressure of the environment; the purity, concentration and exposure time of the hydrogen; and the stress state, physical and mechanical properties, microstructure, surface conditions and the nature of any crack front in the material.

3.6 Hydrogen attack

This section is based on information from “ISO/TR 15916:2015 standard” [9], unless stated otherwise.

Many low-alloyed structural steels can suffer from hydrogen attack when exposed hydrogen at high temperatures (above 200 °C). It is a non-reversible degradation of the steel microstructure, which is caused by the chemical reaction between diffusing hydrogen and the carbon in the steel producing methane. The severity of hydrogen attack increases with the increase in temperature and pressure.

4 Consequence Analysis

An accidental release of hazardous material will typically result in several physical effects (such as fires, explosions or toxic exposure) that could cause serious damage to the people, environment and infrastructure. A wide range of consequence modelling tools exists to predict the physical effects of such accidental release of flammable and/or toxic materials. Effective use of these tools requires good knowledge of the physical phenomena involved.

In this chapter, basic knowledge is provided for release and dispersion phenomena of accidental gas releases. DeVuall et al. [56] describes the evolution of a release/dispersion scenario by three regions:

- An isolated source region, where release rate estimates are nearly independent of environmental conditions.
- A coupled source/dispersion region, where both source and environmental parameters are important in estimating the concentration field. The initial plume velocity and density as well as the ambient wind field affect the path of the gas cloud and the dilution rate.
- A final region, where the ambient wind and weather dominate the dispersion process. The concentration of the released gas is low, and the gas is dispersed as a passive pollutant by the ambient turbulence.

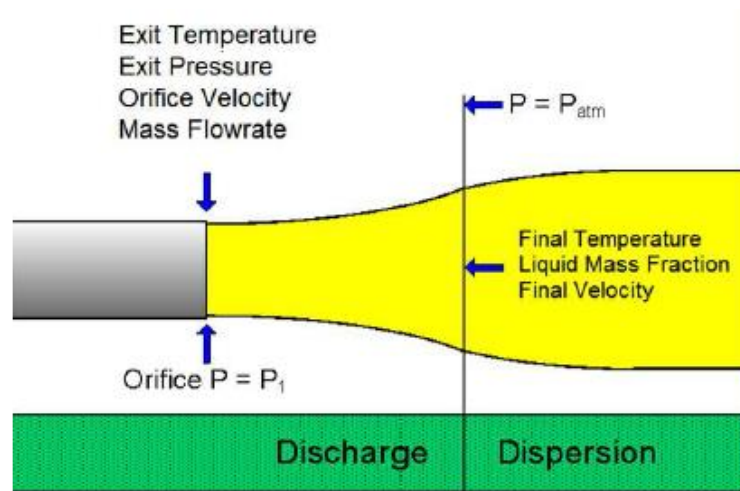


Figure 4.1: Illustration of release /dispersion phenomena [2].

4.1 Release modelling

This section is based on information from the “Yellow Book” [5], unless stated otherwise.

Release modelling is the first and most critical step for accurate estimation of downwind air concentrations resulting from an accidental gas release [57]. It is used to describe the evolution of the flow from the stagnation conditions to the orifice conditions and subsequently to the ambient conditions.

The key parameters required by the release models are:

- The physical properties of the gas.
- The thermodynamic state of the gas in storage (stagnation conditions), such as initial pressure and temperature.
- The geometry of the release source (size of the orifice).

The release models provide quantitative information about the source term, such as:

- The mass flow rate and duration of the release.
- The thermodynamic state of the released gas, such as pressure and temperature.
- Velocity of the released gas at the boundaries of the source region.

For gas releases, it is important to know the density as a function of pressure and temperature. For ideal gas, the equation of state is given by:

$$P = \rho \frac{RT}{\mu} \quad (1)$$

Where P is the absolute pressure, ρ is the gas density, T is the absolute temperature, R is a gas constant and μ is the molecular weight.

An ideal gas is a gas consisting of molecules which do not occupy space and they do not attract or repel each other [11]. In reality, gas molecules do occupy space and they interact with one another depending on the molecules structure. Thus, real gases do not adhere to the ideal gas law. Real gases deviate from ideal behaviour, mostly when subjected to high pressures or cryogenic (low) temperatures [58]. In such cases, the equation of state for real gas is given by:

$$P = Z\rho \frac{RT}{\mu} \quad (2)$$

Where Z is a compressibility factor which is a function of the so-called reduced temperature and pressure, $Z = f(P_R, T_R)$, with, $P_R = \frac{P}{P_c}$ and $T_R = \frac{T}{T_c}$.

When a gas exits through an orifice, there are two possible situations: sonic flow or subsonic flow. Sonic flow occurs when the downstream pressure (pressure at the orifice outlet) is low enough that the gas velocity at the orifice reaches its maximum possible velocity which is its local speed of sound. Further decrease of the downstream pressure will not cause any increase in the gas velocity. This depends on the critical pressure, P_{crit} ,

$$P_{crit} = \left(\frac{2}{\gamma + 1} \right)^{\frac{\gamma}{\gamma - 1}} \quad (3)$$

Where γ is the isentropic ratio, $\gamma = \frac{c_p}{c_v}$.

If the pressure ratio $\left(\frac{P_0}{P_a} \right)$ is below the critical pressure, then the flow is sonic, and the gas exit the orifice at its local speed of sound. Otherwise, the flow is subsonic, and the gas will exit the orifice at a speed lower than its local speed of sound. Where P_0 is the pressure inside containment and P_a is the ambient pressure.

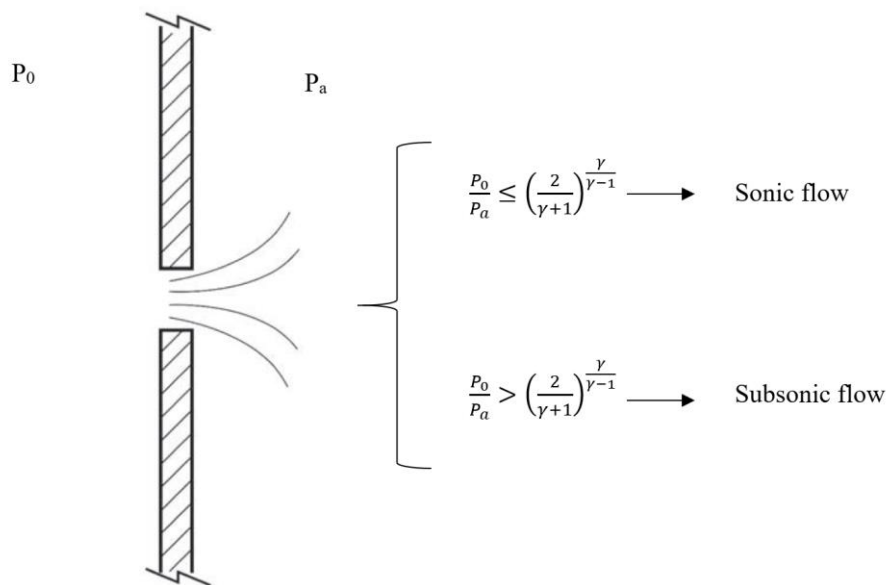


Figure 4.2: Sonic and subsonic releases [59].

4.2 Dispersion modelling

Dispersion is the dilution of the gas cloud by mixing with air [60]. Dispersion models are used to predict how the gas will be spread in the ambient atmosphere.

The output of these dispersion models are [57]:

- Distances to certain concentration levels at ground level, typically Lower flammability level (LFL) and upper flammability level (UFL).
- Contour plots of these concentrations.
- Flammable mass within certain concentration bounds.

Apart from the physical properties of the released gas, and the release conditions (pressure, temperature, and velocity), the dispersion is dependent on both the meteorological conditions (direction and speed of wind and the atmospheric stability) and the topographical conditions.

The following sections describe the main factors affecting the dispersion.

4.2.1 Momentum and buoyancy effects

This section is based on information from Mannan's "Lees' loss prevention in the process industries: hazard identification, assessment and control" [61], unless stated otherwise.

The dispersion of released material is determined by its momentum and buoyancy. If momentum forces predominate, the fluid forms a jet, while if buoyancy forces predominate, it forms a plume.

For high momentum releases (described as a momentum jet), the dispersion in the initial phase will be dominated by the jet momentum, due to the high difference between the jet velocity and the local wind speed. As the jet velocity reduces, due to air entrainment, the jet/plume becomes dominated by buoyancy. For low momentum release, the dispersion will be dominated by buoyancy and atmospheric turbulence.

The released gas may have positive, neutral, or negative buoyancy:

- When the gas has a positive buoyancy, it means that its density is lighter than air and will rise upwards. Lighter density could be due to low molecular weight or high temperature of the gas (hot gas).
- When the gas has a neutral buoyancy, it means that its density is close to the density of air.
- When a gas has a negative buoyancy, it means that its density is higher than the density of air and will fall towards the ground level. Higher density could be due to high molecular weight or low temperature of the gas (cold gas).

4.2.2 Turbulence

This section is based on information from the “Yellow Book” [5], unless stated otherwise.

The lower part of the atmosphere in which the releases take place is called the mixed layer, with a height that varies between 200 – 2000 m. Turbulence is the dominant mechanism in the mixing and diluting of gas releases in the mixed layer.

There are two types of turbulence:

- Mechanical turbulence, which is generated by the resistance of the earth’s surface on the wind. This resistance causes the wind to be sheared and creates turbulence, due to the flow instabilities and a downward turbulent flux of momentum to compensate the resistance force. The wind shear depends on the upper wind speed and the surface roughness.
- Thermal turbulence, which is generated due to heating of the earth’s surface (mainly by the sun). Hot patches of air near the earth’s surface start to rise which causes an upward turbulent flux of heat.

Turbulence generates irregular movements of air known as eddies, which can range in size from several hundreds of meters diameter down to few millimeters. Turbulent eddies smaller than the size of the cloud will uniformly disperse the material and increase the cloud size. Turbulent eddies much larger than the cloud size will only move the cloud without changing its size and geometry. Eddies with the same size as the cloud will change its geometry and increase its contour.

4.2.3 Wind

This section is based on information from Mannan’s “Lees’ loss prevention in the process industries: hazard identification, assessment and control” [61] and Casal’s “Evaluation of the effects and consequences of major accidents in industrial plants” [59], unless stated otherwise.

Wind is air in motion, which is caused by the Coriolis forces (which result from the rotating earth) and the differences in atmospheric pressure (which result from the uneven heating of earth’s surface). Wind forms when air moves from areas of higher pressure to areas of lower pressure.

Wind speed changes with height. Atmospheric turbulence, generated by the drag which the earth’s surface exerted on the wind, reduces the wind speed near the surface. This drag has a straightforward frictional component but also an aerodynamic component caused by the complex flow around obstacles such as trees, rocks, buildings, etc. [60]. Thus, the wind speed gradient is strongly influenced by the roughness of the earth’s surface. In Figure 4.3, the same wind speed is reached at a higher elevation in urban areas than that for a planar terrain. The wind has an entrainment effect which leads to the dispersion of a gas cloud. Thus, the effect of wind will be different for releases at the ground level compared to releases at elevated height.

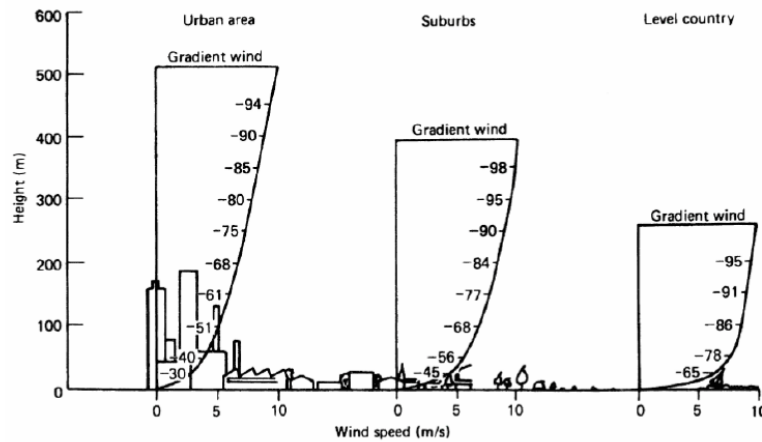


Figure 4.3: Wind speed changes (wind gradient) with surface roughness [61].

The information on the wind for a given location is provided by a wind rose, which is a graphical representation of the frequency of the winds according to their direction and speed, as shown in Figure 4.4.

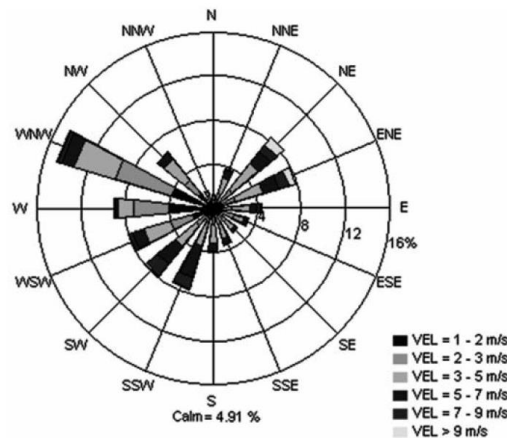


Figure 4.4: Wind rose (Port of Barcelona, 2004) [59]

4.2.4 Atmospheric stability

The section is based on information from the “Yellow Book” [5], unless stated otherwise.

Atmospheric stability describes the tendency for vertical mixing in the atmosphere and therefore, for turbulence generation by natural forces [4]. The temperature of the air decreases with altitude in the troposphere. If an air parcel rises through the atmosphere, it will expand as the pressure decreases with altitude. If this process is assumed to be adiabatic (no heat exchange with the surrounding air), the temperature of the air parcel will decrease.

The atmospheric stability can be divided into three categories, showing the tendency of the air parcel to move vertically based on the temperature difference between the air parcel and its surroundings,

- **Stable:** when the rising air parcel has lower temperature than its surroundings, it is forced downward. During stable condition, the heat flux is downwards (this occurs as the surface is cooled at night by heat radiation to the sky).
- **Unstable:** when the rising air parcel has high temperature than its surroundings, it will continue rising upwards. During unstable condition, there is a heat flux from the surface upwards (this occurs as the surface is heated by the sun).
- **Neutral:** when the rising air parcel has the same temperature as its surroundings (no forces due to density differences are applied on the air parcel).

Turbulence enhances the dispersion of the gas cloud in the atmosphere. High turbulence intensity is found during unstable atmospheric conditions where more vertical mixing is expected, while stable atmospheric conditions hinders the development of turbulence [59]. The stability of the mixed layer is determined by the ratio of turbulence generated by the temperature gradient and the turbulence generated mechanically by wind shear at the surface. This ratio is expressed by the Monin-Obukhov length, which is defined as:

$$L = - \frac{\rho_a c_p T_a u_*^3}{\kappa g H_o} \quad (4)$$

Where H_o is the sensible heat flux from the surface and u_* is the friction velocity. Table 4.1 provide interpretation of the Monin-Obukhov length with respect to atmospheric stability.

Table 4.1: Monin-Obukhov lengths and stability [62].

Monin-Obukhov length (L)	Stability
Small negative, $-100 \text{ m} < L < 0$	Very unstable
Large negative, $-10^5 < L < -100$	Unstable
Very Large, $ L > 10^5$	Neutral
Large positive, $10 < L < 10^5$	Stable
Small positive, $0 < L < 10$	Very stable

Atmospheric stability can be classified using qualitative schemes, such as Pasquill scheme, which is a method of categorizing the amount of atmospheric turbulence present by assigns letters from A (unstable) through D (neutral) to F (stable). Table 4.2 provides the six stability classes as defined by Pasquill.

Table 4.2: Pasquill atmospheric stability classes [62].

Stability class	Description
A	Very unstable
B	Unstable
C	Slightly unstable
D	Neutral
E	Slightly stable
F	Stable

4.2.5 Surface roughness

This section is based on information from DeVuall et al. “Understanding atmospheric dispersion of accidental releases” [56], Woodward’s “Estimating the flammable mass of a vapor cloud” [4] and the “Purple Book” [18], unless stated otherwise.

The effect of the surface roughness on the wind speed gradient is shown in Figure 4.3. An aerodynamic roughness length z_0 is used to characterize the influence of surface features (existence of trees, buildings, etc.) on the wind flow and the atmospheric turbulence. Higher values of roughness length produce higher turbulence and consequently faster dilution and mixing of the gas cloud.

The roughness length can range from less than a millimeter for ice and mud flats to several meters in an urban area. The roughness length is used for obstacles that are relatively small to the height of the gas cloud. Large obstacles (such as skyscrapers and mountains) have large effect on the dispersion of the gas cloud and in that case the use of an average roughness length is not valid anymore. The roughness length is approximately 10% of the obstacle height. Table 4.3 provides terrain classification in terms of the aerodynamic roughness length z_0 . The roughness length z_0 and the average height ε_g of the surface irregularities are related approximately by [62]: $z_0 = \frac{\varepsilon_g}{30}$.

Table 4.3: Terrain classification in terms of aerodynamical roughness length [18],

- (1) x is a typical upwind obstacle distance and h is the height corresponding to major obstacles.
- (2) These values are rough indications. The use of an aerodynamic roughness length, z_0 , does not account for the effects of large obstacles

Class	Terrain description	z_0 (m)
1	Open water, fetch at least 5 km	0.0002
2	Mud flats, snow; no vegetation, no obstacles	0.005
3	Open flat terrain; grass, few isolated obstacles	0.03
4	Low crops; occasional large obstacles, $x/h > 20$ ⁽¹⁾	0.10
5	High crops, scattered obstacles, $15 < x/h < 20$ ⁽¹⁾	0.25
6	Parkland, bushes, numerous obstacles, $x/h < 15$ ⁽¹⁾	0.5
7	Regular large obstacle coverage (suburb, forest)	(1.0) ⁽²⁾
8	City center with high-and-low-rise buildings	(3.0) ⁽²⁾

4.2.6 Obstacle effects

This section is based on information from the “Yellow Book” [5], unless stated otherwise.

The presence of obstacles in the path of the gas cloud can significantly influence its flow and dispersion. There is a recirculation zone behind the obstacle which may extend to about ten times the obstacle height. In the wake downwind of the obstacle, turbulent eddies exist due to the disturbance of the obstacle to the wind flow. Turbulence induced by obstacles enhances the dispersion of the gas cloud.

5 Release Modelling

A wide range of consequence modelling tools exists which are used to predict the physical effects of the accidental release of flammable and/or toxic materials. They use various modelling techniques, ranging from simple integral (one-dimensional phenomenological) models to sophisticated three-dimensional Computational Fluid Dynamics (CFD) codes.

Integral models use differential equations which have been correlated with empirical coefficients (based on experimental data and observations). Integral models are easy to use and require less computational time; however, they take limited account of the influence of physical obstructions and terrain. Surface roughness parameter is usually used to represent the effect of buildings and trees in the area of the release, which in most cases only a crude approximation [63]. Thus, in most cases, the results of such models tend to overestimate the impacts in the far field and underestimate the impacts in the near field [63].

Computational fluid dynamics (CFD) is a branch of fluid mechanics that uses numerical methods and algorithms to solve and analyse problems that involve fluid flow [62]. Computers are used to perform the required calculations to simulate the interaction of liquids and gases with surfaces defined by given boundary conditions [2]. CFD simulations are more complex and require longer computational time (typically hours or days), but they take into account the effect of complex geometries, which is a key advantage compared to integral models.

This chapter provides a description of the physical models used in FRED, EFFECTS, PHAST and FLACS for release modelling of hydrogen gas leak through an orifice from a pressurized storage tank.

5.1 FRED software

This section is based on information from the website of Gexcon AS [64] and “FRED’s technical guide” [60], unless stated otherwise.

Shell FRED is a consequence modelling tool which includes validated Fire, Release, Explosion and Dispersion models that predict consequences of accidental and design releases of products from process, storage, transport and distribution operations. It is a 2D empirical tool that models ideal facilities (no terrain, no obstructions, etc.). It is simple to use and gives fast predictions.

FRED has been continuously developed and validated by Shell since the 1980s and has been extensively used by oil, gas and petrochemical companies, engineering contractors, insurers and regulators throughout the world. The integrated models rely on an extensive and unique program of large-scale experiments, combined with validated scientific research, that assure the reliability and consistency of the results.

FRED contains several release models which can be used for modelling specific major hazard releases. The two main models are:

- The GENREL (GENERALised RELEase) model which is incorporated into the Pressurised Release scenario. The model is used for steady state releases.
- The TARS (Transient Adiabatic Release Scenario) model which is used within the Unified Scenario. The model is used form transient (time-varying) releases.

In this study, only the GENREL model will be described and for more information about TARS model, please refer to FRED's technical guide.

Generalized Release (GENREL) model

The model calculates the steady-state mass flow rate of a fluid through an orifice or a pipe given the pressure, temperature and composition of the fluid prior to the release. The model uses the standard equations for the gas discharge through an orifice for sonic and subsonic flows.

If the flow is sonic, the mass flow rate through the orifice is calculated by,

$$\dot{m} = C_d A \frac{P_0}{\sqrt{\frac{R}{\mu} T_0}} \sqrt{\gamma \left(\frac{2}{\gamma + 1} \right)^{\frac{\gamma+1}{\gamma-1}}} \quad (5)$$

Where P_0 is the initial pressure and T_0 is the initial temperature inside the vessel.

For subsonic flow, the mass flow rate is calculated by,

$$\dot{m} = C_d A \psi \frac{P_0}{\sqrt{\frac{R}{\mu} T_0}} \sqrt{\gamma \left(\frac{2}{\gamma + 1} \right)^{\frac{\gamma+1}{\gamma-1}}} \quad (6)$$

Where,

$$\psi = \left(\frac{P_a}{P_0} \right)^{\frac{1}{\gamma}} \sqrt{1 - \left(\frac{P_a}{P_0} \right)^{\frac{\gamma-1}{\gamma}}} \sqrt{\left(\frac{2}{\gamma-1} \right) \left(\frac{\gamma+1}{2} \right)^{\frac{\gamma+1}{\gamma-1}}}$$

5.2 EFFECTS software

This section is based on information from Vinnem's "Offshore risk assessment: principles, modelling and applications of QRA studies" [43] and the website of Gexcon AS [65], unless stated otherwise.

EFFECTS is an affordable and easy-to-use software which includes release, dispersion, fire and explosion models for the calculation of physical effects and consequences of the (accidental) release hazardous materials. EFFECTS software has been developed by TNO since the 1980s and is one of the leading tools world-wide for the consequence analysis using integral modelling. TNO and Gexcon AS have started a joint venture to further develop and market the software since the end of 2018.

Models in EFFECTS are based on the TNO's Coloured Books which are used around the world as valuable standard reference materials in safety studies,

- The "Yellow Book" provides solid, scientific information, and is internationally recognized as the standard reference work for consequence analysis [5].
- The "Green Book" describes the relationship between physical phenomena (heat radiation, explosion over-pressure, toxic doses) and the resulting damage [66].

The release of gas through an orifice in a vessel can be described using two coupled independent sub-models [5]:

- A sub model "vessel dynamics" which describes the dynamic behaviour of the gas stored in the vessel.
- A sub model "outflow" which estimates the mass flow rate and the conditions of the released gas as a function of the conditions in the vessel.

Dynamics of compressed gas stored in a vessel

This section is based on information from the "Yellow Book" [5] and "EFFECTS' user and reference manual" [67], unless stated otherwise.

The vessel dynamics model aims at estimating the decrease of pressure and temperature in the vessel caused by the gas outflow. Due to the release of gas, the remaining gas in the vessel will expand, causing a decrease of gas temperature (cooling) and pressure (depressurization).

The model is in a form of iterative numerical procedure in which the gas release from the vessel is described in small steps. These steps should be small enough to consider the conditions in the vessel to be constant during one time-step.

The numerical procedure is performed as the following:

- 1- Set the initial condition and termination condition of the numerical procedure. The initial condition of the vessel (stagnation state) is given by, the initial storage pressure P_0 , the initial storage temperature T_0 and the initial gas density ρ_0 , meaning $i=0$.
- 2- Set the size of the time step δt , which is given by:

$$\delta t = \frac{t_{\text{end}}}{N_t} \quad (7)$$

The larger the number of steps N_t , the higher the accuracy of the model but the more time is required for the calculation. Typically, $N_t = 50$ is appropriate for most calculations.

- 3- Starting every step at time t_i in the iteration with a condition in the vessel given by P_i , T_i , ρ_i , the following procedure is carried out to calculate the condition in the vessel at the end of the small time-step δt , which is given by P_{i+1} , T_{i+1} , ρ_{i+1} .

The release rate \dot{m}_i is given by a generalized function f ,

$$\dot{m}_i = f(P_i, T_i, \rho_i) \quad (8)$$

Due to the gas release in period δt , the gas density in the vessel decreases (assuming constant volume). The reduction in density is given by:

$$\delta \rho = -\frac{\dot{m}_i}{V} \delta t \quad (9)$$

Due to the decrease of the gas density, the gas will expand (assuming isentropic flow), and the gas temperature will decrease. The reduction in temperature is given by:

$$\delta T = \frac{P_i}{(\rho_i^2 C_v)} \delta \rho \quad (10)$$

Thus, the new condition of the vessel at time t_{i+1} is given by: P_{i+1} , T_{i+1} , ρ_{i+1} .

$$t_{i+1} = t + \delta t \quad (11)$$

$$\rho_{i+1} = \rho_i + \delta\rho \quad (12)$$

$$T_{i+1} = T_i + \delta T \quad (13)$$

The change in density and temperature of the gas forces the pressure to adapt to the new conditions. According to the equation of state of (real) gases,

$$P_{i+1} = \frac{Z\rho_{i+1}RT_{i+1}}{\mu} \quad (14)$$

4- The iterative numerical procedure should be repeated as long as the following conditions are still valid,

$$t_i < t_{\text{end}} \quad P_i > P_a \quad T_i > T_m$$

Where, ‘i’ is the current step.

Gas release through an orifice:

This section is based on information from the “Yellow Book” [5] and “EFFECTS’ user and reference manual” [67], unless stated otherwise.

The modelling of the gas release through orifices estimates the mass flow rate as a function of pressure drop over the orifice. By assuming isentropic (adiabatic and reversible) flow, the mass flow rate of the gas release through an orifice is estimated by,

$$\dot{m} = C_d A \psi \sqrt{\rho_0 P_0 \gamma \left(\frac{2}{\gamma + 1}\right)^{\frac{\gamma+1}{\gamma-1}}} \quad (15)$$

Where P_0 is the initial pressure inside the vessel and ρ_0 is the density of gas. The factor ψ^2 , depends on whether the gas release is sonic or not. For sonic release, $\psi^2 = 1$. While for subsonic release,

$$\psi^2 = \left(\frac{2}{\gamma - 1}\right) \left(\frac{\gamma + 1}{2}\right)^{\frac{\gamma+1}{\gamma-1}} \left(\frac{P_a}{P_0}\right)^{\frac{2}{\gamma}} \left(1 - \left(\frac{P_a}{P_0}\right)^{\frac{\gamma-1}{\gamma}}\right)$$

5.3 PHAST software

This section is based on information from the website of DNV GL [68] and “PHAST’s technical reference” [69], unless stated otherwise.

PHAST (Process Hazard Analysis Software Tool) is an integral tool developed by Det Norske Veritas (DNV), which determines the consequences of accidental releases of hazardous materials. PHAST examines the progress of a potential incident from the initial release to far-field dispersion analysis, including modelling of pool spreading and evaporation, and flammable and toxic effects. It has been continuously developed by experts for over 30 years. The integrated models are constantly validated and verified.

PHAST includes both steady-state (DISC model) and time-varying (TVDI model) discharge models for the release of toxic/flammable materials from an orifice in a vessel. These models first calculate the expansion from the initial storage conditions to the orifice and subsequently impose the ATEX model to calculate the expansion from the orifice conditions to the final conditions at the atmospheric pressure. The ATEX post-expansion conditions are then used as the source term for the dispersion model.

In this study, only the DISC model and ATEX model will be described and for further information about the TVDI model, please refer to PHAST’s technical reference.

Figure 5.1 illustrates the subsequent zones in the flow in case of a release from an orifice:

- (st) stagnation point.
- (o) upstream orifice (nozzle entrance; area A_o , velocity u_o , pressure P_o).
- (vc) downstream orifice (nozzle throat; vena contracta area A_{vc} , velocity u_{vc} , pressure P_{vc} , temperature T_{vc}).
- (f) end of atmospheric expansion zone (area A_f , velocity u_f , pressure $P_f =$ ambient pressure, temperature T_f).

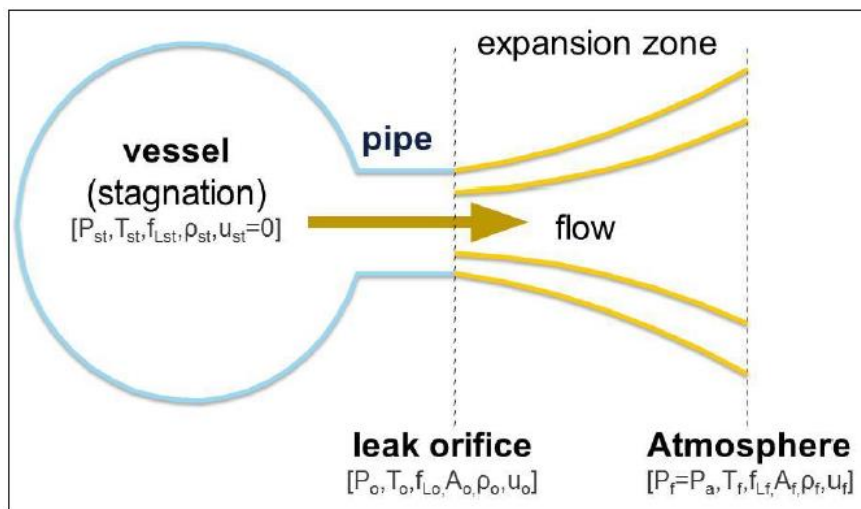


Figure 5.1: Expansion from stagnation to orifice and from orifice to ambient conditions [69].

DISC model/ Orifice model

This section is based on information from “PHAST’s technical reference” [69], unless stated otherwise.

The DISC model is a collection of instantaneous and continuous discharge models, including orifice model, pipe model, instantaneous model and vent from vapor space model. In this study, only the orifice model will be described and for further information about the other models, please refer to PHAST’s technical reference.

The orifice model is a continuous (not-time varying) model which simulates the release from a small orifice in a vessel. It calculates the initial release rate, typically the worst-case, and the duration associated with this release rate. The chemical stored in the vessel could be gas/vapour, liquid or two-phase.

The outputs of the model are:

- Release rate, \dot{m} (kg/s).
- Release duration, t_{rel} (s).
- Orifice pressure, P_o (Pa).
- Orifice temperature, T_o (K).
- Orifice mass liquid fraction, η_{Lo} .
- Orifice velocity, u_o (m/s).
- Discharge coefficient, C_d .

Conservation of entropy and energy are applied in the orifice model for the initial expansion from storage to the orifice conditions. The following equations are used to determine the orifice conditions.

By conservation of energy, assuming initially the material is stagnant:

$$h(P_{st}, T_{st}, \eta_{st}) = h(P_o, T_o, \eta_o) + \frac{u_o^2}{2} \quad (16)$$

By conservation of entropy (isentropic expansion to the orifice):

$$s(P_{st}, T_{st}, \eta_{st}) = s(P_o, T_o, \eta_o) \quad (17)$$

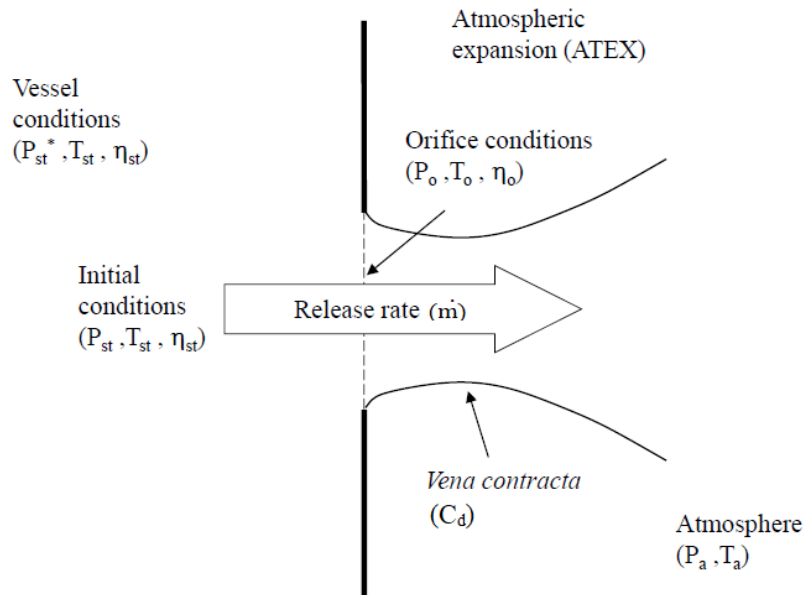


Figure 5.2: Orifice model [69].

The orifice pressure P_o is equal to the ambient pressure in case of subsonic release, and is determined from the critical pressure in case of sonic release,

$$P_o = \max [P_a, P_{crit}] \quad (18)$$

P_{crit} is the critical pressure at the orifice and is defined as the pressure at which the mass flux, G_o , through the orifice is maximized,

$$G_o = \frac{u_o}{v_o} \quad (19)$$

The specific volume is calculated as,

$$v_o = \frac{\eta_o}{\rho_{Lo}} + \frac{(1 - \eta_o)}{\rho_{Vo}} \quad (20)$$

The mass flow rate, \dot{m}^* (kg/s) is then,

$$\dot{m}^* = A_o G_o \quad (21)$$

This represents an idealized mass flow rate, and the frictional effects of the convergent flow at the orifice (represented by the vena contracta) has to be taken into account. This is done by reducing the orifice cross-sectional area ($A_{vc} < A_o$), the ratio of this reduction is the discharge coefficient, C_d .

$$A_{vc} = C_d A_o \quad (22)$$

Thus, the mass flow rate, \dot{m} is given by,

$$\dot{m} = A_{vc} G_o \quad (23)$$

Finally, the duration of the release, t_{rel} , is given by,

$$t_{rel} = \frac{m_{st}}{\dot{m}} \quad (24)$$

The sequence of steps used to determine the orifice conditions is:

1. For a given P_o , the temperature and liquid fraction are determined from the isentropic expansion equation (17).
2. Calculate orifice velocity u_o from the conservation of energy equation (16).
3. Calculate the mass flux from equation (19).
4. The orifice pressure P_o is iterated until the mass flux is maximized and P_o is set according to equation (18).
5. Calculate the mass flow rate from equation (23).
6. Calculate the release duration from equation (24).

ATEX model

This section is based on information from PHAST's technical reference [69], unless stated otherwise.

The ATEX model calculates the expansion from the vena-contracta conditions to the final post-expansion conditions, where the final conditions are imposed at a planar surface as shown in Figure 5.3.

The input to the ATEX model is:

- Orifice or pipe exit diameter d_o .
- Vena-contracta temperature T_{vc} and pressure P_{vc} .
- Exit velocity u_o or mass flow rate \dot{m} .

The final conditions are given by 5 unknown post-expansion data: area A_f , velocity u_f , temperature T_f or liquid fraction f_{Lf} , density ρ_f and specific enthalpy h_f . Along the expansion zone one-dimensional homogeneous flow is assumed in thermal equilibrium with zero air entrainment.

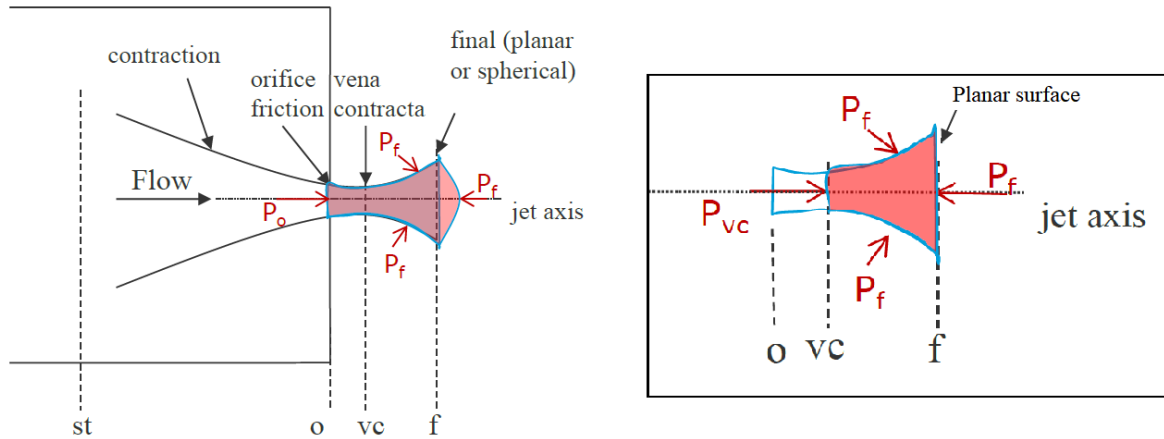


Figure 5.3: Zones in flow for discharge from orifice [69].

ATEX contains two models for the expansion from the conditions in the exit plane down to the atmospheric, which are ‘conservation of momentum model’ and ‘isentropic model’. For gas releases, the conservation of momentum model is normally selected since the isentropic model results in larger final post-expansion velocities and hence smaller temperatures. Thus, in this study, only the conservation of momentum model will be described and for further information about the isentropic model, please refer to PHAST’s technical reference.

The ATEX conservation of momentum model imposes three conservation equations (conservation of mass, momentum and energy) and two equations of state for density and enthalpy to determine the five unknown variables.

Mass conservation,

$$\rho_f A_f u_f = \rho_{vc} A_{vc} u_{vc} \quad (25)$$

Momentum conservation,

$$\rho_f A_f u_f^2 = \rho_{vc} A_{vc} u_{vc}^2 + (P_{vc} - P_f) A_{vc} \quad (26)$$

Energy conservation,

$$\rho_f A_f u_f \left[h_f + \frac{1}{2} u_f^2 \right] = \rho_{vc} A_{vc} u_{vc} \left[h(P_{vc}, T_{vc}; f_{Lvc}) + \frac{1}{2} u_{vc}^2 \right] \quad (27)$$

Density equation of state,

$$\rho_f = \rho_f(P_a, T_f; f_{Lf}) \quad (28)$$

Enthalpy equation of state,

$$h_f = h(P_a, T_f; f_{Lf}) = f_{Lf} h_L(P_a, T_f) + (1 - f_{Lf}) h_v(P_a, T_f) \quad (29)$$

The post-expansion data can be determined as follows:

1. The post-expansion mass flow rate, \dot{m}_f , is calculated from equation (25),

$$\dot{m}_f = \rho_{vc} A_{vc} u_{vc} \quad (30)$$

2. Calculate the post-expansion speed, u_f , from equation (26),

$$u_f = u_{vc} + \frac{P_{vc} - P_a}{\rho_{vc} u_{vc}} \quad (31)$$

3. Calculate post-expansion specific enthalpy, h_f , from equation (27),

$$h_f = h_{vc} + \frac{1}{2} [u_f^2 - u_{vc}^2] \quad (32)$$

4. Calculate the post-expansion temperature, T_f , from equation (29), in case of gas release $f_{Lf} = 0$.
5. Calculate the post-expansion density, ρ_f , from equation (28).
6. Calculate the post-expansion jet area,

$$A_f = \frac{\dot{m}_f}{(u_f \rho_f)} \quad (33)$$

5.4 FLACS software

This section is based on information from “FLACS user’s manual” [62] and Middha’s PhD thesis “Development, use, and validation of the CFD tool FLACS for hydrogen safety studies” [11], unless stated otherwise.

FLACS (Flame ACcelerator Simulator) is a leading computational fluid dynamics (CFD) code for ventilation, dispersion, explosion and fire simulations in complex process areas. Its sophisticated and user-friendly nature allows users to accurately model the exact geometry of any process facility, determining its effect on the complex interaction of flow, turbulence, chemical reaction and combustion. FLACS has been developed by Christian Michelsen Institute (CMI), Christian Michelsen Research (CMR) and currently Gexcon AS since 1980s.

FLACS solves the compressible conservation equations for mass, momentum, enthalpy and mass fraction of species on a 3-D Cartesian grid using a finite volume method. FLACS uses k- ϵ model for modelling the convection, diffusion, production and dissipation of turbulence (see Launder and Spalding [70]). One of the key advantages of FLACS compared to other commercial CFD codes is the use of the distributed porosity concept for representing complex geometries, taking into account the influence of obstacles such as equipment, piping, explosion panels and walls. Today, FLACS is widely accepted as an industry standard for CFD explosion modelling and one of the best-validated tools for modelling flammable and toxic releases in the technical safety context.

The JET utility program in FLACS uses a pseudo-source model, also called notional-nozzle model proposed by Birch et al. [71], to calculate the status of an under-expanded jet (in terms of temperature, velocity, diameter and density) at the conditions where the jet pressure is atmospheric.

JET utility program

This section is based on information from “FLACS user’s manual” [62], unless stated otherwise.

The single planar shock model in the JET utility program is based on a one-dimensional model for the release of an ideal gas from a pressurized reservoir through a nozzle into an open atmosphere. From a high-pressure reservoir (stagnation point), there is isentropic flow through the nozzle (at position 1 as shown in Figure 5.4). This is followed by a single normal shock wave, which is located at the interface between positions 2 and 3, as shown in Figure 5.4. Between the nozzle and the shock, the expansion is modelled as an adiabatic process for a compressible gas (conservation of mass, momentum and energy are employed). The thermodynamic change across the shock front is not isentropic; here the Rankine–Hugoniot relations are utilized. The pressure downstream of the shock front (at position 3 as shown in Figure 5.4) is equal to the ambient pressure, and the flow subsonic from position 3. The model does not consider air entrainment in the region up to the hypothetical nozzle at position 3, downstream of the shock front. The output reported by the JET utility program is the

conditions at position 3 (and the area and the subsonic velocity of the expanded jet after the shock).

A schematic of the jet model is shown below in Figure 5.4:

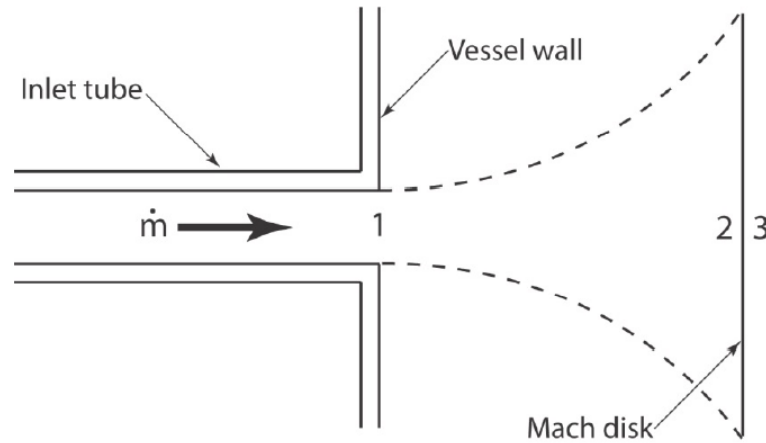


Figure 5.4: Schematic sketch of the under-expanded jet model used in the JET utility program [62], defining the states where analytical models are applied; sonic conditions are assumed at the jet exit at position 1, the normal shock is located at the interface between positions 2 and 3; from position 3 the flow is subsonic.

A large reservoir of high-pressure gas at stagnant conditions with pressure P_0 and temperature T_0 is assumed to be present upstream of what is shown in Figure 5.4. The gas flows from the reservoir into the inlet tube with mass flow rate \dot{m} and exits from the tube under sonic conditions to the ambient condition at position 1.

The conditions at the jet exit are determined assuming an isentropic expansion from the reservoir conditions to the jet exit:

$$\frac{P_1}{P_0} = \left(\frac{2}{\gamma + 1} \right)^{\frac{\gamma}{\gamma - 1}} \quad (34)$$

$$\frac{T_1}{T_0} = \frac{2}{\gamma + 1} \quad (35)$$

$$\rho_1 = \frac{P_1 M}{RT_1} \quad (36)$$

$$u_1 = c_1 = \sqrt{\gamma RT_1} \quad (37)$$

$$\dot{m} = \rho_1 u_1 A_1 \quad (38)$$

The quantities P_0 , T_0 , A_1 and the gas (hence M and γ) are assumed to be given. Assuming adiabatic expansion between positions 1 and 2, a one-dimensional momentum balance (ignoring entrainment and viscosity) is applied to the control volume shown in the Figure 5.5.

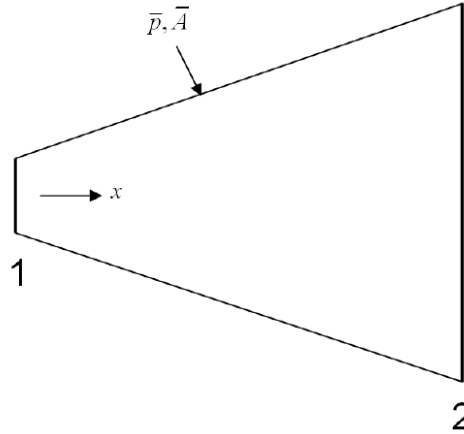


Figure 5.5: Schematic view of the control volume for JET model momentum equation [62].

The momentum balance can be written as:

$$\rho_2 u_2^2 A_2 - \rho_1 u_1^2 A_1 = P_1 A_1 - P_2 A_2 + \bar{P} \bar{A}_x \quad (39)$$

Let $\bar{P} = \alpha P_1 + (1 - \alpha) P_2$ and let $\bar{A}_x = \Delta A = A_2 - A_1$; then the equation can be written as,

$$\rho_2 u_2^2 A_2 - \rho_1 u_1^2 A_1 = (P_1 - P_2) [\alpha A_2 + (1 - \alpha) A_1] \quad (40)$$

And with the aid of the continuity equation solving for u_2 gives:

$$u_2 = u_1 \left\{ 1 + \frac{(P_1 - P_2)}{\rho_1 u_1^2} \left[\alpha \frac{A_2}{A_1} + (1 - \alpha) \right] \right\} \quad (41)$$

Setting $\alpha = 0$ in the above equation; yields the expression used by the Jet utility program for the velocity at position 2.

Normal shock relations, conservation of mass, ideal gas equation and equality of A_2 and A_3 are used to relate states 2 and 3:

$$M_3^2 = \frac{M_2^2 + \frac{2}{\gamma - 1}}{\frac{2\gamma}{\gamma - 1} M_2^2 - 1} = \frac{u_3^2}{c_3^2} = \frac{u_3^2}{\gamma R T_3} \quad (42)$$

$$P_3 = P_2 \left(\frac{2\gamma}{\gamma + 1} M_2^2 - \frac{\gamma - 1}{\lambda + 1} \right) \quad (43)$$

$$T_3 = T_2 \frac{\left(1 + \frac{\gamma - 1}{2} M_2^2 \right)}{\left(1 + \frac{\gamma - 1}{2} M_3^2 \right)} \quad (44)$$

The adiabatic energy equation between station 1 and 2 gives:

$$T_2 = T_1 + \frac{(u_1^2 - u_2^2)}{2C_p} \quad (45)$$

From the equation of state and conservation of mass, A_2 can be determined, giving the Mach disk diameter for the Jet model.

The JET hydrogen real gas model

This section is based on the model developed in Middha's PhD thesis "Development, use, and validation of the CFD tool FLACS for hydrogen safety studies"[11], unless stated otherwise.

The model above is based on the ideal gas law, which can be accurately used to describe the behaviour of real gases at pressures up to approximately 100-150 barg at ambient temperatures. At higher pressures, the results become increasingly inaccurate, as the deviation in the density of hydrogen is very significant at pressures which are commonly used for the storage of hydrogen (350 bar or 700 bar). Another version of the JET utility program was developed to include the real gas effect. The model uses the Abel-Noble equation of state (EOS), which can predict the density at higher pressures to a reasonable accuracy.

The Abel-Noble EOS is given by:

$$Z = \frac{P}{\rho R T} = \frac{1}{1 - \frac{\rho}{a}} = 1 + \frac{P}{a R T} \quad (46)$$

The first step is to modify the thermodynamic equations for modelling hydrogen releases from high pressure sources. Denoting the “effective” isentropic exponent as n ($n = \gamma$ for ideal gas, where $\gamma = \frac{C_p}{C_v}$).

The effective isentropic exponent is given by [72]:

$$n = \frac{\gamma \left[Z + T \left(\frac{\partial Z}{\partial T} \right)_\rho \right]}{Z + T \left(\frac{\partial Z}{\partial T} \right)_p} \quad (47)$$

For the Abel-Noble EOS,

$$Z = 1 + \frac{P}{aRT} \Rightarrow \left(\frac{\partial Z}{\partial T} \right)_p = -\frac{P}{aRT^2} \quad (48)$$

Also,

$$Z = \frac{a}{a - \rho} \Rightarrow \left(\frac{\partial Z}{\partial T} \right)_\rho = 0$$

Therefore,

$$n = \frac{\gamma[Z + 0]}{Z - T \frac{P}{aRT^2}} = \frac{\gamma Z}{1} = \gamma Z \quad (49)$$

The speed of sound for a real gas is given by:

$$c = \sqrt{ZnRT} = Z\sqrt{\gamma RT} = Zc_{\text{ideal}} \quad (50)$$

The flow velocity through a nozzle (throat) for an ideal gas as function of the pressure is given by:

$$u = c_{\text{ideal}} \left[\frac{2}{\gamma - 1} \left(1 - \frac{P}{P_0} \right)^{\frac{\gamma-1}{\gamma}} \right]^{\frac{1}{2}} \quad (51)$$

Where P_0 is the pressure inside the reservoir. The corresponding equation for a real gas is given by:

$$u = c_{\text{real}} \left[\frac{2}{n-1} \left(1 - \frac{P}{P_0} \right)^{\frac{n-1}{n}} \right]^{\frac{1}{2}} \quad (52)$$

The enthalpy change is given by:

$$dh = C_p dT + \left[v - T \left(\frac{\partial v}{\partial T} \right)_P \right] dP \quad (53)$$

Where v is the specific volume, $v = \frac{1}{\rho}$.

For a real gas,

$$\left(\frac{\partial v}{\partial T} \right)_P = \left(\frac{\partial \left(\frac{ZRT}{P} \right)}{\partial T} \right)_P = \frac{RT}{P} \left(\frac{\partial Z}{\partial T} \right)_P + \frac{ZR}{P} = \frac{v}{Z} \left(\frac{\partial Z}{\partial T} \right)_P + \frac{v}{T}$$

Using the relation above and equation (53), we get:

$$dh = C_p dT - \left[\frac{Tv}{Z} \left(\frac{\partial Z}{\partial T} \right)_P \right] dP \quad (54)$$

The Gibb's free energy is given by:

$$g = h - Ts$$

Therefore,

$$dg = dh - Tds - sdT$$

Also,

$$dg = vdP - sdT$$

$$\Rightarrow Tds = dh - vdP = dh - \frac{dP}{\rho} \quad (55)$$

For isentropic flow, $ds = 0$. Using equations (54) and (55), we get:

$$Tds = C_p dT - \frac{dP}{\rho} \left[\frac{T}{Z} \left(\frac{\partial Z}{\partial T} \right)_P + 1 \right] = 0$$

And since $\frac{P}{\rho} = ZRT$, using this relation in the equation above gives,

$$0 = C_p dT - \frac{dP}{P} ZRT \left[\frac{T}{Z} \left(\frac{\partial Z}{\partial T} \right)_P + 1 \right]$$

Therefore,

$$\frac{dT}{T} = \frac{dP}{P} \frac{R}{C_p} \left[T \left(\frac{\partial Z}{\partial T} \right)_P + Z \right] \quad (56)$$

Also,

$$dE = Tds - Pdv = C_v dT + \left[T \left(\frac{\partial P}{\partial T} \right)_v - P \right] dv$$

Using the isentropic flow condition ($ds = 0$) again, we get:

$$C_v dT = -T \left(\frac{\partial P}{\partial T} \right)_v dv = \frac{T}{\rho^2} \left(\frac{\partial P}{\partial T} \right)_\rho d\rho \quad (57)$$

For a real gas,

$$\left(\frac{\partial P}{\partial T}\right)_\rho = \rho Z R + \rho R T \left(\frac{\partial Z}{\partial T}\right)_\rho \quad (58)$$

Using equations (57) and (58), we get:

$$\frac{dT}{T} = \frac{R}{C_v} \frac{d\rho}{\rho} \left[Z + T \left(\frac{\partial Z}{\partial T}\right)_\rho \right] \quad (59)$$

Using equations (56) and (59), we get:

$$\frac{d\rho}{\rho} \frac{R}{C_v} \left[Z + T \left(\frac{\partial Z}{\partial T}\right)_\rho \right] = \frac{dP}{P} \frac{R}{C_p} \left[T \left(\frac{\partial Z}{\partial T}\right)_P + Z \right]$$

$$\frac{d\rho}{\rho} = \frac{dP}{P} \frac{C_v}{C_p} \frac{\left[Z + T \left(\frac{\partial Z}{\partial T}\right)_\rho \right]}{\left[Z + T \left(\frac{\partial Z}{\partial T}\right)_P \right]} \quad (60)$$

Using equations (49) and (60), we get:

$$\frac{d\rho}{\rho} = \frac{1}{n} \frac{dP}{P} \quad (61)$$

Equation (61) can be used to determine the relation between the change of pressure and density under isentropic conditions. For an ideal gas, the well-known relationship states that, $\frac{\rho}{\rho_0} = \left(\frac{P}{P_0}\right)^{\frac{1}{\gamma}}$. Using the definitions connected to the Abel-Noble EOS given by equations (46) and (49), we have for the real gas case:

$$\frac{d\rho}{\rho} = \frac{1}{\gamma Z} \frac{dP}{P} = \frac{a - \rho}{\gamma a} \frac{dP}{P}$$

$$\Rightarrow \frac{d\rho}{\rho(a - \rho)} = \frac{1}{\gamma a} \frac{dP}{P}$$

By integrating, we get:

$$\frac{\rho}{\rho_0} \frac{a - \rho_0}{a - \rho} = \left(\frac{P}{P_0} \right)^{\frac{1}{\gamma}} \quad (62)$$

Other relevant thermodynamic quantities need also to be evaluated for the chosen EOS, such as the difference in the constant pressure and constant volume heat capacities. This is given by:

$$C_p - C_v = \frac{-T \left(\frac{\partial P}{\partial T} \right)_v^2}{\left(\frac{\partial P}{\partial v} \right)_T} \quad (63)$$

And since $P = \frac{ZRT}{v}$, therefore,

$$\left(\frac{\partial P}{\partial T} \right)_v = \frac{ZR}{v} + \frac{RT}{v} \left(\frac{\partial Z}{\partial T} \right)_v \quad (64)$$

For the Abel-Noble EOS,

$$Z = \frac{va}{va - 1} \Rightarrow \left(\frac{\partial Z}{\partial T} \right)_v = 0 \quad (65)$$

Substituting equation (65) into equation (64), we get:

$$\left(\frac{\partial P}{\partial T} \right)_v = \frac{ZR}{v} \quad (66)$$

Also,

$$\left(\frac{\partial P}{\partial v} \right)_T = -\frac{ZRT}{v^2} + \frac{RT}{v} \left(\frac{\partial Z}{\partial v} \right)_T \quad (67)$$

For the Abel-Noble EOS,

$$Z = \frac{va}{va - 1} \Rightarrow \left(\frac{\partial Z}{\partial v}\right)_T = -\frac{a}{(va - 1)^2} \quad (68)$$

Substituting equation (68) into equation (67), we get:

$$\left(\frac{\partial P}{\partial v}\right)_T = -\frac{ZRT}{v^2} + \frac{RT}{v} \left[-\frac{a}{(va - 1)^2}\right] = -\frac{RTa}{v} \frac{va}{(va - 1)^2} = -\frac{RT}{v^2} Z^2 \quad (69)$$

By using equations (63), (66) and (69), we get:

$$C_p - C_v = T \frac{Z^2 R^2}{v^2} \frac{v^2}{RTZ^2} = R \quad (70)$$

Therefore, the result is the same as that for an ideal gas.

Next, the conservation of energy is considered. This is given by:

$$\frac{du^2}{2} + \frac{dP}{\rho} + Tds = 0 \quad (\text{for isentropic flow, } ds=0) \quad (71)$$

By integrating and using the fact the velocity, u , is zero in the reservoir (stagnation point), we get:

$$\frac{u^2}{2} = \int_{P_0}^P \frac{dP}{\rho} \quad (72)$$

From equation (62), $\frac{\rho}{\rho_0} \frac{a - \rho_0}{a - \rho} = \left(\frac{P}{P_0}\right)^{\frac{1}{\gamma}}$ and by setting $\frac{\rho_0}{a - \rho_0} = B$, thus, $\frac{\rho}{a - \rho} = B \left(\frac{P}{P_0}\right)^{\frac{1}{\gamma}}$.

From this, the density can be calculated as,

$$\rho = \frac{aB \left(\frac{P}{P_0}\right)^{\frac{1}{\gamma}}}{1 + B \left(\frac{P}{P_0}\right)^{\frac{1}{\gamma}}} \Rightarrow \frac{1}{\rho} = \frac{1}{a} \left(1 + \frac{1}{B} \left(\frac{P}{P_0}\right)^{-\frac{1}{\gamma}}\right) \quad (73)$$

Substituting equation (73) into equation (72), we get:

$$\frac{u^2}{2} = -\frac{P_0}{a} \int_1^{\frac{P}{P_0}} \left[1 + \frac{1}{B} \left(\frac{P}{P_0} \right)^{-\frac{1}{\gamma}} \right] d \left(\frac{P}{P_0} \right)$$

$$\frac{u^2}{2} = \frac{P_0}{a} \left[\left(1 - \frac{P}{P_0} \right) + \frac{1}{B} \frac{\gamma}{\gamma - 1} \left(1 - \left(\frac{P}{P_0} \right)^{\frac{\gamma-1}{\gamma}} \right) \right] \quad (74)$$

At the throat, the Mach number $M = 1$. Using equations (46), (49) and (50), we get:

$$u^2 = C_{\text{real}}^2 = \gamma Z^2 RT = \gamma \frac{P}{\rho} \frac{a}{a - \rho} \quad (75)$$

Using equation (73), equation (75) can be expressed in terms of pressure only because the terms involving the density can be expressed as:

$$\frac{1}{\rho} \frac{a}{a - \rho} = \frac{1}{a} \left[2 + B \left(\frac{P}{P_0} \right)^{\frac{1}{\gamma}} + \frac{1}{B} \left(\frac{P}{P_0} \right)^{-\frac{1}{\gamma}} \right] \quad (76)$$

Combining equations (74) and (76), a relation is obtained that needs to be solved for $\left(\frac{P}{P_0} \right)$ in order to get the pressure at the throat (and hence the other properties),

$$\frac{\gamma P}{2 P_0} \left[2 + B \left(\frac{P}{P_0} \right)^{\frac{1}{\gamma}} + \frac{1}{B} \left(\frac{P}{P_0} \right)^{-\frac{1}{\gamma}} \right] = \left(1 - \frac{P}{P_0} \right) + \frac{1}{B} \frac{\gamma}{\gamma - 1} \left(1 - \left(\frac{P}{P_0} \right)^{\frac{\gamma-1}{\gamma}} \right) \quad (77)$$

Next, we need to represent the normal shock equations for the real gas model. The normal shock equations are generally given by:

$$\rho_1 u_1 = \rho_2 u_2 \quad \text{Mass conservation}$$

$$P_1 + \rho_1 u_1^2 = P_2 + \rho_2 u_2^2 \quad \text{Momentum conservation}$$

$$h_1 + \frac{u_1^2}{2} = h_2 + \frac{u_2^2}{2} \quad \text{Energy conservation}$$

For a real gas,

$$\rho u^2 = \frac{P}{ZRT} \frac{u^2}{\gamma RT Z^2} \gamma RT Z^2 = \gamma Z P M^2 \quad (78)$$

Since $M^2 = \frac{u^2}{\gamma RT Z^2}$, substituting into equation (78):

$$\rho u^2 = \gamma Z P M^2$$

Therefore, the momentum conservation equation can be written as:

$$P_1(1 + \gamma Z_1 M_1^2) = P_2(1 + \gamma Z_2 M_2^2)$$

Or,

$$\frac{P_2}{P_1} = \frac{(1 + \gamma Z_1 M_1^2)}{(1 + \gamma Z_2 M_2^2)} \quad (79)$$

Similarly, the mass conservation equation can be written as:

$$\begin{aligned} \rho_1 u_1 = \rho_2 u_2 &\Rightarrow \rho_1^2 u_1^2 = \rho_2^2 u_2^2 \Rightarrow \frac{P_1^2}{Z_1^2 R T_1^2 \gamma} = \frac{P_2^2}{Z_2^2 R T_2^2 \gamma} \\ &\Rightarrow \frac{P_1^2}{T_1^2} M_1^2 = \frac{P_2^2}{T_2^2} M_2^2 \end{aligned}$$

Hence,

$$\frac{T_2}{T_1} = \left(\frac{P_2}{P_1}\right)^2 \left(\frac{M_2}{M_1}\right)^2 \quad (80)$$

Next, we need to represent the energy conservation equation in terms of the Abel-Noble EOS. Substituting equation (48) into equation (54), we get:

$$\left(\frac{\partial Z}{\partial T}\right)_p = -\frac{P}{aRT^2} \Rightarrow \frac{T_V}{Z} \left(\frac{\partial Z}{\partial T}\right)_p = \frac{P_V}{ZRT} \frac{1}{a} = \frac{1}{a}$$

Therefore, equation (54) can be written as:

$$dh = C_p dT - \frac{1}{a} dP \quad (81)$$

Hence, the energy conservation equation can be written as:

$$\begin{aligned} C_p T_1 - \frac{1}{a} P_1 + \frac{u_1^2}{2} &= C_p T_2 - \frac{1}{a} P_2 + \frac{u_2^2}{2} \\ \Rightarrow C_p T_1 - \frac{1}{a} P_1 + M_1^2 \frac{\gamma R Z_1^2 T_1}{2} &= C_p T_2 - \frac{1}{a} P_2 + M_2^2 \frac{\gamma R Z_2^2 T_2}{2} \end{aligned}$$

Combining and simplifying, we get:

$$T_1 \left(1 + \frac{\gamma - 1}{2} M_1^2 Z_1^2\right) + \frac{\gamma - 1}{a\gamma R} (P_2 - P_1) = T_2 \left(1 + \frac{\gamma - 1}{2} M_2^2 Z_2^2\right) \quad (82)$$

Equations (79), (80) and (82) represent the normal shock equations for the current EOS. These equations are solved numerically using the Newton-Raphson technique to arrive at the Mach number after the shock and hence the values of all other parameters.

5.5 Release models summary

Table 5.1 provides a summary of the release models described in this chapter.

Table 5.1: Release models summary for FRED, EFFECTS, PHAST and FLACS.

Software	Type of model	Release model
FRED	Integral model	<p><u>Model name:</u> Generalized Release (GENREL) model.</p> <p>The release of gas through an orifice in a vessel is modelled in FRED using the GENREL (GENERALISED RELEASE) model which is incorporated into the Pressurized Release scenario. The model calculates the steady state mass flow rate using two generalized equations for sonic flow and subsonic flow.</p>
EFFECTS	Integral model	<p><u>Model name:</u> Gas Release From Vessel</p> <p>The release model in EFFECTS is based on the Yellow Book. A quasi-stationary of gas flow from a vessel through an orifice is described using two coupled independent sub-models:</p> <ul style="list-style-type: none"> • A sub model “vessel dynamics” which describes the dynamic behaviour of the gas stored in the vessel. The changes of pressure, temperature and mass content in the vessel caused by the gas release are estimated using iterative numerical procedure in which the gas release from the vessel is described in small steps, assuming the conditions in the vessel to be constant during one time-step. • A sub model “outflow” which estimates the mass flow rate and the conditions of the released gas as a function of the conditions in the vessel. Assuming isentropic flow, the model uses well-known relations for calculating steady state mass flow rate for both sonic and subsonic releases.

Table 5.1: Release models summary for FRED, EFFECTS, PHAST and FLACS – Continued.

Software	Type of model	Release model
PHAST	Integral model	<p><u>Model name:</u> DISC/ATEX model.</p> <p>The release model in PHAST calculates both the expansion from the initial storage conditions to the orifice conditions (DISC model), as well as the subsequent expansion from orifice conditions to atmospheric conditions (ATEX model).</p> <p>The DISC model is a collection of instantaneous and continuous discharge models. The orifice model is used for a continuous (not-time varying) gas release from a small orifice in a vessel. The model applies conservation of entropy and energy for the initial expansion from storage to the orifice conditions. The ATEX conservation of momentum model imposes three conservation equations (conservation of mass, momentum and energy) and two equations of state for density and enthalpy to determine the post-expansion data.</p>
FLACS	CFD model	<p><u>Model name:</u> JET utility program (a pseudo-source model, also called notional-nozzle model).</p> <p>FLACS JET utility program is based on a one-dimensional model for the release of an ideal gas from a pressurized reservoir through a nozzle into an open atmosphere. From a high-pressure reservoir (stagnation point), there is isentropic flow through the nozzle, followed by a single normal shock wave. Between the nozzle and the shock, the expansion is modelled as an adiabatic process for a compressible gas (conservation of mass, momentum and energy are employed). The thermodynamic change across the shock front is not isentropic; here the Rankine–Hugoniot relations are utilized. The pressure downstream of the shock front is equal to the ambient pressure, and the flow subsonic. This is based on the notional nozzle model proposed by Birch et al.</p> <p>Another version of the JET utility program was developed to include the real gas properties. The model uses the Abel-Noble equation of state (EOS).</p>

6 Comparative Study

6.1 Comparison methodology

The comparative study is conducted using both integral tools (FRED, EFFECTS and PHAST) and CFD tool (FLACS). The focus of this study is to show where the tools predict similar results and where their results deviate strongly. Both release and dispersion simulations are carried out. The comparison includes the mass flow rate, the downwind distances to gas concentrations corresponding to lower flammability limit (LFL) and half of lower flammability limit (1/2 LFL) and the amount of flammable mass between the upper flammability limit (UFL) and lower flammability limit (LFL).

A premixed fuel-air mixture will only burn if the fuel concentration lies within the upper and lower flammability limits. Below the lower flammability limit (LFL) the fuel-air mixture is too “lean” to burn, while above the upper flammability limit (UFL) the mixture is too “rich” to burn [6]. The amount of flammable mass is defined as “the mass of fuel in a vapour cloud that is in the flammable range” [4, p. xvii]. Calculating the flammable mass is important as it may give an indication of the maximum explosion overpressure generated if the gas cloud is ignited [2].

It is recognized that there are significant differences between integral and CFD tools. Integral tools, such as FRED, EFFECTS and PHAST, cannot predict the effects of physical obstructions and terrain on the flow. Surface roughness length is usually used to represent the effect of buildings and trees in the area of the release, which in most cases only a crude approximation [63]. However, CFD tools, such as FLACS, can predict the effects of complex geometries and take into account the influence of obstacles on the dispersion of the gas cloud. For this reason, simulations will be carried out in open flat terrain where the results are expected to be relatively similar, as stated by several articles [24]–[26]. The simulations were performed from the user’s perspective with the attempt to provide similar inputs to the different tools as much as possible.

The study is conducted using several hypothetical hydrogen gas release scenarios which is stored under pressure. Variation of release conditions (such as storage pressure, orifice size and release direction), meteorological conditions (such as wind speed and atmospheric stability class) and topographical conditions (surface roughness length) will be studied. All leaks are simulated as continuous releases at constant rates and are assumed to last until the gas cloud reaches steady state.

The comparative study is divided into three parts which will be described further in the coming sections:

- The first part is dedicated for the comparison of the results predicted by FRED, EFFECTS, PHAST and FLACS using large-scale hydrogen gas release scenarios. The aim is to improve the fundamental knowledge in describing explosible hazard

from possible hydrogen gas leakage, which will be formalized in a toolbox and be used in early phase engineering stages of new development projects.

- The second part is dedicated for a sensitivity analysis where the variation of release conditions, meteorological conditions and topographical conditions are studied to evaluate their effect on the hazardous distances and flammable mass predicted by the different tools.
- The effect of geometry on the dispersion of the hydrogen gas cloud is studied in the third part. Both obstructed and its corresponding unobstructed release scenarios are simulated in FLACS.

6.2 Consequence modelling

Consequence modelling is used to model the effect of various scenarios of accidental hydrogen gas release. It is carried out in several steps; once the accident scenarios are defined, release models are selected to describe the evolution of the flow from the stagnation conditions to the orifice conditions and subsequently to the ambient conditions. A dispersion model is subsequently used to predict how the gas will be spread in the ambient atmosphere. Table 6.1 presents the models used for release and dispersion modelling in the different tools for this study.

Table 6.1: Release and dispersion models used in the comparative study.

Tool	Models
FRED	<p>This section is based on information from “FRED’s technical guide”[60], unless stated otherwise.</p> <p>For release modelling, the “Generalized Release (GENREL)” model is used, as described in section 5.1.</p> <p>For dispersion modelling, the “AEROPLUME” model is used which is part of the HGSYSTEM suite of programs. AEROPLUME is a jet dispersion model which can describe either gaseous jets or two-phase releases. It can predict the dispersion of buoyant as well as heavy gases. AEROPLUME is intended to predict the dispersion in near field. For dispersion in the far-field, AEROPLUME invokes “PGPLUME” model (a standard Gaussian dispersion model) to finish its calculations.</p> <p>Full models description can be found in “HGSYSTEM 3.0: technical reference manual and user's guide” by Post [73].</p>

Table 6.1: Release and dispersion models used in the comparative study – Continued.

Tool	Models
EFFECTS	<p>This section is based on information from “EFFECTS’ user and reference manual” [67], unless stated otherwise.</p> <p>For release modelling, the “gas release from vessel” model is used, as described in section 5.2.</p> <p>For dispersion modelling, first the “turbulent free jet” model is used as an offset and starting conditions for dispersion, calculating the diameter of the expanded jet and the limit of momentum distance. Then the “dense gas dispersion” model is used to finish the dispersion calculations, which is based the SLAB-code from Lawrence Livermore National laboratory. The model is mainly for heavy gases, but it can take into account density differences for lighter than air chemicals as well.</p> <p>Full models description can be found in the “Yellow Book” [5].</p>
PHAST	<p>This section is based on information from “PHAST’s technical reference” [69], unless stated otherwise.</p> <p>For release modelling, both “DISC” model and “ATEX” model are used to calculate the expansion from the initial storage conditions to the orifice conditions, as well as the subsequent expansion from orifice conditions to atmospheric conditions, as described in section 5.3.</p> <p>For dispersion modelling, the “Unified Dispersion Model (UDM)” is used. The UDM models the dispersion following a ground-level or elevated two-phase unpressurized or pressurized release. It allows for continuous, instantaneous, constant finite-duration and general time-varying releases. It includes a unified model for jet, heavy and passive two-phase dispersion including possible droplet rainout, pool spreading and re-evaporation.</p> <p>Full models description can be found in “PHAST’s technical reference” [69].</p>

Table 6.1: Release and dispersion models used in the comparative study – Continued.

Tool	Models
FLACS	<p>This section is based on information from “FLACS user’s manual” [62], unless stated otherwise.</p> <p>FLACS solves the compressible Navier-Stokes equations on a 3D Cartesian grid using a finite volume method. The conservation equations of mass, impulse, enthalpy, turbulence and mass fraction of species are closed by invoking the ideal gas equation of state. FLACS uses a standard k-ε model for turbulence (see Launder and Spalding [70]). The FLACS code uses a “distributed porosity concept” which enables the detailed representation of complex geometries on relatively coarse computational meshes. Large objects and walls are represented on-grid, whereas smaller objects are represented using sub-grid. The pre-processor Porcalc reads the grid and geometry files and assigns volume and area porosities to each rectangular grid cell.</p> <p>The single planar shock model in the JET utility program, as described in section 5.4, is used for release modelling. The model is based on a one-dimensional model for the release of an ideal gas from a pressurized reservoir through a nozzle into an open atmosphere. It can be accurately used to describe the behaviour of real gases at pressures up to approximately 100-150 barg at ambient temperatures. At higher pressures, the results become increasingly inaccurate. Thus, a real gas model (using Abel-Noble EOS), as described in section 5.4, is used for hydrogen releases from high-pressure systems to obtain more accurate results.</p> <p>For further details, please refer to “FLACS user’s manual” [62].</p>

6.3 Scenarios considered for the study

6.3.1 Comparative study

The comparative study is carried out using large-scale hydrogen gas release scenarios. The results from these release scenarios are then used to develop a comparison tool. Hydrogen gas is hypothetically released from a pressurized storage tank through an orifice on its side. Three cases are used with different storage pressure (5 bar, 25 bar and 350 bar) at a temperature of 20°C. The orifice diameter and release direction are varied. To study the impact of hydrogen buoyancy and ground surface on the hydrogen cloud, the leak source is positioned at a height of 2 m above the ground. For boundary conditions, this study uses a windy scenario with

Pasquill atmospheric stability class D, while the wind speed is varied. Wind direction is at 270°, in the positive x-axis direction. The ground is assumed to be an open flat terrain with few obstacles, with roughness length of 0.03 m. Tables 6.2, 6.3 and 6.4 present the cases that were chosen with the different variations. Table 6.5 presents the 72 scenarios that were simulated in each of FRED, EFFECTS, PHAST and FLACS.

Table 6.2: Case1 and variations used in the comparative study.

<p><u>Case 1:</u></p> <ul style="list-style-type: none"> • Initial storage pressure: 5 bar • Initial temperature: 20 °C • Ambient temperature: 20 °C • Ambient pressure: 1 bar <ul style="list-style-type: none"> • Release height: 2 m • Wind direction: 270° (+ x direction) • Atmospheric stability class: D – neutral • Surface roughness length: 0.03 m <p><u>Variations:</u></p> <ul style="list-style-type: none"> • Orifice diameter: 3 mm, 5 mm, 10 mm, 50 mm • Release direction: horizontal (+x direction), vertical (+z direction) • Wind speed: 2 m/s, 5 m/s, 8 m/s 	
--	--

Table 6.3: Case 2 and variations used in the comparative study.

<p><u>Case 2:</u></p> <ul style="list-style-type: none"> • Initial storage pressure: 25 bar • Initial temperature: 20 °C • Ambient temperature: 20 °C • Ambient pressure: 1 bar <ul style="list-style-type: none"> • Release height: 2 m • Wind direction: 270° (+ x direction) • Atmospheric stability class: D – neutral • Surface roughness length: 0.03 m <p><u>Variations:</u></p> <ul style="list-style-type: none"> • Orifice diameter: 3 mm, 5 mm, 10 mm, 50 mm • Release direction: horizontal (+x direction), vertical (+z direction) • Wind speed: 2 m/s, 5 m/s, 8 m/s 	
---	--

Table 6.4: Case 3 and variations used in the comparative study.

<p><u>Case 3:</u></p> <ul style="list-style-type: none"> • Initial storage pressure: 350 bar • Initial temperature: 20 °C • Ambient temperature: 20 °C • Ambient pressure: 1 bar 		<ul style="list-style-type: none"> • Release height: 2 m • Wind direction: 270° (+ x direction) • Atmospheric stability class: D – neutral • Surface roughness length: 0.03 m
<p><u>Variations:</u></p> <ul style="list-style-type: none"> • Orifice diameter: 1 mm, 3 mm, 5 mm, 10 mm • Release direction: horizontal (+x direction), vertical (+z direction) • Wind speed: 2 m/s, 5 m/s, 8 m/s 		

Table 6.5: List of scenarios used in in the comparative study.

Scenario Number	Pressure (bar)	Orifice Diameter (mm)	Release Direction	Wind speed (m/s)	Wind Direction
1	5	3	Horizontal jet	2	Along release direction
2	5	3	Horizontal jet	5	Along release direction
3	5	3	Horizontal jet	8	Along release direction
4	5	5	Horizontal jet	2	Along release direction
5	5	5	Horizontal jet	5	Along release direction
6	5	5	Horizontal jet	8	Along release direction
7	5	10	Horizontal jet	2	Along release direction
8	5	10	Horizontal jet	5	Along release direction
9	5	10	Horizontal jet	8	Along release direction
10	5	50	Horizontal jet	2	Along release direction
11	5	50	Horizontal jet	5	Along release direction
12	5	50	Horizontal jet	8	Along release direction
13	5	3	Vertical jet	2	Normal to release direction
14	5	3	Vertical jet	5	Normal to release direction
15	5	3	Vertical jet	8	Normal to release direction
16	5	5	Vertical jet	2	Normal to release direction
17	5	5	Vertical jet	5	Normal to release direction
18	5	5	Vertical jet	8	Normal to release direction
19	5	10	Vertical jet	2	Normal to release direction
20	5	10	Vertical jet	5	Normal to release direction
21	5	10	Vertical jet	8	Normal to release direction
22	5	50	Vertical jet	2	Normal to release direction

Table 6.5: List of scenarios used in the comparative study – Continued.

Scenario Number	Pressure (bar)	Orifice Diameter (mm)	Release Direction	Wind speed (m/s)	Wind Direction
23	5	50	Vertical jet	5	Normal to release direction
24	5	50	Vertical jet	8	Normal to release direction
25	25	3	Horizontal jet	2	Along release direction
26	25	3	Horizontal jet	5	Along release direction
27	25	3	Horizontal jet	8	Along release direction
28	25	5	Horizontal jet	2	Along release direction
29	25	5	Horizontal jet	5	Along release direction
30	25	5	Horizontal jet	8	Along release direction
31	25	10	Horizontal jet	2	Along release direction
32	25	10	Horizontal jet	5	Along release direction
33	25	10	Horizontal jet	8	Along release direction
34	25	50	Horizontal jet	2	Along release direction
35	25	50	Horizontal jet	5	Along release direction
36	25	50	Horizontal jet	8	Along release direction
37	25	3	Vertical jet	2	Normal to release direction
38	25	3	Vertical jet	5	Normal to release direction
39	25	3	Vertical jet	8	Normal to release direction
40	25	5	Vertical jet	2	Normal to release direction
41	25	5	Vertical jet	5	Normal to release direction
42	25	5	Vertical jet	8	Normal to release direction
43	25	10	Vertical jet	2	Normal to release direction
44	25	10	Vertical jet	5	Normal to release direction
45	25	10	Vertical jet	8	Normal to release direction
46	25	50	Vertical jet	2	Normal to release direction
47	25	50	Vertical jet	5	Normal to release direction
48	25	50	Vertical jet	8	Normal to release direction
49	350	1	Horizontal jet	2	Along release direction
50	350	1	Horizontal jet	5	Along release direction
51	350	1	Horizontal jet	8	Along release direction
52	350	3	Horizontal jet	2	Along release direction
53	350	3	Horizontal jet	5	Along release direction
54	350	3	Horizontal jet	8	Along release direction
55	350	5	Horizontal jet	2	Along release direction
56	350	5	Horizontal jet	5	Along release direction
57	350	5	Horizontal jet	8	Along release direction
58	350	10	Horizontal jet	2	Along release direction
59	350	10	Horizontal jet	5	Along release direction
60	350	10	Horizontal jet	8	Along release direction
61	350	1	Vertical jet	2	Normal to release direction
62	350	1	Vertical jet	5	Normal to release direction

Table 6.5: List of scenarios used in the comparative study – Continued.

Scenario Number	Pressure (bar)	Orifice Diameter (mm)	Release Direction	Wind speed (m/s)	Wind Direction
63	350	1	Vertical jet	8	Normal to release direction
64	350	3	Vertical jet	2	Normal to release direction
65	350	3	Vertical jet	5	Normal to release direction
66	350	3	Vertical jet	8	Normal to release direction
67	350	5	Vertical jet	2	Normal to release direction
68	350	5	Vertical jet	5	Normal to release direction
69	350	5	Vertical jet	8	Normal to release direction
70	350	10	Vertical jet	2	Normal to release direction
71	350	10	Vertical jet	5	Normal to release direction
72	350	10	Vertical jet	8	Normal to release direction

6.3.2 Sensitivity analysis

A sensitivity analysis is carried out to study the effect of orifice diameter, release direction, wind speed, atmospheric stability class and surface roughness length on mass flow rate, downwind distances to LFL and ½ LFL, and flammable mass. Tables 6.6, 6.7 and 6.8 present the defined three base cases and the different variations. For each variation of one parameter, all other parameters are kept as the base case values.

Table 6.6: Case 1 and variations used in the sensitivity analysis.

<p><u>Base case 1:</u></p> <ul style="list-style-type: none"> • Initial storage pressure: 5 bar • Initial temperature: 20 °C • Orifice diameter: 10 mm • Ambient temperature: 20 °C • Ambient pressure: 1 bar • Release height: 2 m <p style="margin-left: 20px;">• Release direction: horizontal (+x direction)</p> <p style="margin-left: 20px;">• Wind speed: 2 m/s</p> <p style="margin-left: 20px;">• Wind direction: 270° (+ x direction)</p> <p style="margin-left: 20px;">• Atmospheric stability class: D – neutral</p> <p style="margin-left: 20px;">• Surface roughness length: 0.03 m</p> <p><u>Variations:</u></p> <ul style="list-style-type: none"> • Orifice diameter: 3 mm, 5 mm, 10 mm, 50 mm • Release direction: horizontal (+x direction), vertical (+z direction) • Wind speed: 2 m/s, 5 m/s, 8 m/s • Atmospheric stability class: D – neutral, F – stable • Surface roughness length: 0.005 m, 0.03 m, 0.1 m
--

Table 6.7: Case 2 and variations used in the sensitivity analysis.

<p><u>Base case 2:</u></p> <ul style="list-style-type: none"> • Initial storage pressure: 25 bar • Initial temperature: 20 °C • Orifice diameter: 10 mm • Ambient temperature: 20 °C • Ambient pressure: 1 bar • Release height: 2 m 		<ul style="list-style-type: none"> • Release direction: horizontal (+x direction) • Wind speed: 2 m/s • Wind direction: 270° (+ x direction) • Atmospheric stability class: D – neutral • Surface roughness length: 0.03 m
<p><u>Variations:</u></p> <ul style="list-style-type: none"> • Orifice diameter: 3 mm, 5 mm, 10 mm, 50 mm • Release direction: horizontal (+x direction), vertical (+z direction) • Wind speed: 2 m/s, 5 m/s, 8 m/s • Atmospheric stability class: D – neutral, F – stable • Surface roughness length: 0.005 m, 0.03 m, 0.1 m 		

Table 6.8: Case 3 and variations used in the sensitivity analysis.

<p><u>Base case 3:</u></p> <ul style="list-style-type: none"> • Initial storage pressure: 350 bar • Initial temperature: 20 °C • Orifice diameter: 5 mm • Ambient temperature: 20 °C • Ambient pressure: 1 bar • Release height: 2 m 		<ul style="list-style-type: none"> • Release direction: horizontal (+x direction) • Wind speed: 2 m/s • Wind direction: 270° (+ x direction) • Atmospheric stability class: D – neutral • Surface roughness length: 0.03 m
<p><u>Variations:</u></p> <ul style="list-style-type: none"> • Orifice diameter: 1 mm, 3 mm, 5 mm, 10 mm • Release direction: horizontal (+x direction), vertical (+z direction) • Wind speed: 2 m/s, 5 m/s, 8 m/s • Atmospheric stability class: D – neutral, F – stable • Surface roughness length: 0.005 m, 0.03 m, 0.1 m 		

6.3.3 Hydrogen refuelling station

The effect of obstacles on the gas cloud dispersion is simulated in FLACS using a hydrogen refuelling station, which contains a compressor, a high-pressure storage tank, precooling system and a dispenser, as shown in Figure 6.1. Hydrogen is hypothetically released from the dispenser through an orifice at an initial pressure of 350 bar and a temperature of 20 °C. The size of the orifice is 3 mm in diameter with the leak positioned at a height of 0.9 m above the ground in the positive x-axis direction. The release conditions give a mass flow rate of 1.2391 g/s. For boundary conditions, Pasquill atmospheric stability class D, wind speed of 2 m/s and surface roughness length of 0.03 m are used. Wind direction is at 270°, in the same direction as that of the leak. Both obstructed release scenario, represented by refuelling gas station, and its corresponding release scenario in an open flat terrain are simulated. Table 6.9 describes the release scenario to be simulated in FLACS.

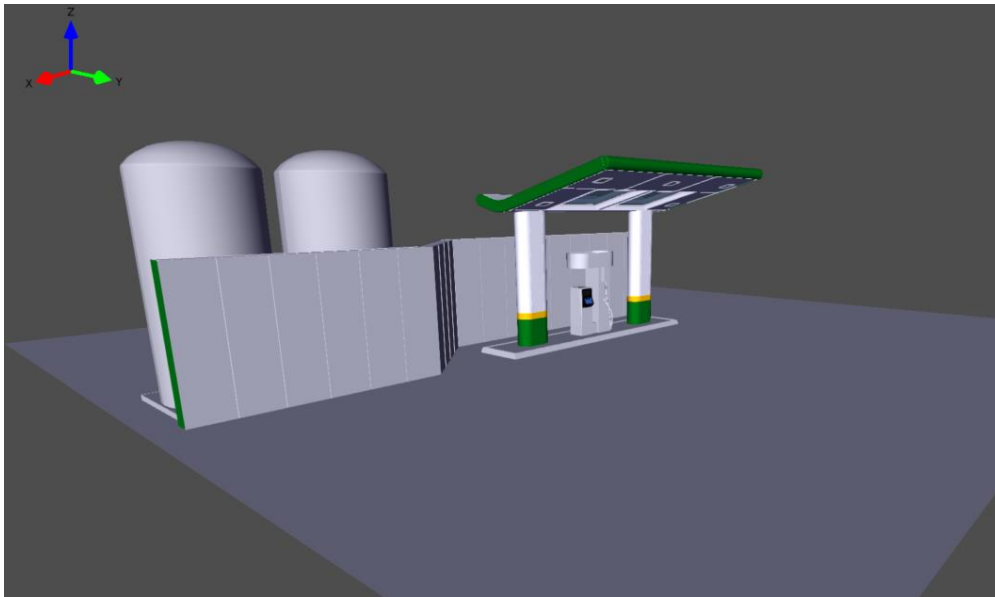


Figure 6.1: Hydrogen refuelling gas station.

Table 6.9: Scenario used to study the effect of geometry.

Refuelling gas station scenario:

- | | |
|--|--|
| <ul style="list-style-type: none"> • Initial storage pressure: 350 bar • Initial temperature: 20 °C • Orifice diameter: 3 mm • Ambient temperature: 20 °C • Ambient pressure: 1 bar | <ul style="list-style-type: none"> • Release height: 0.9 m • Release direction: horizontal (+x direction) • Wind speed: 2 m/s • Wind direction: 270° (+ x direction) • Atmospheric stability class: D – neutral • Surface roughness length: 0.03 m |
|--|--|

6.4 Results

All results were documented in appendices:

- Appendix A – contains a link to the comparison tool.
- Appendix B – contains the results of the comparative study.
- Appendix C – contains the results of the sensitivity study.
- Appendix D – contains the results of dispersion simulations for hydrogen gas release in a refuelling gas station and open flat terrain.

Table 6.10 shows how the results were obtained from the different tools.

Table 6.10: How results were obtained from different tools.

Tool	Outputs
FRED	<ul style="list-style-type: none"> • The mass flow rate was obtained from release summary report. • The downwind distances to LFL and ½ LFL were obtained from the dispersion summary report. • The amount of flammable mass between UFL and LFL was obtained from the dispersion summary report.
EFFECTS	<ul style="list-style-type: none"> • The mass flow rate was obtained from release summary report. • The downwind distances to LFL and ½ LFL were obtained from the graph for the side view of the cloud. • The amount of flammable mass between UFL and LFL was not calculated by EFFECTS.
PHAST	<ul style="list-style-type: none"> • The mass flow rate was obtained from the discharge report. • The downwind distances to LFL and ½ LFL were obtained from the graph for the side view of the cloud. • The amount of flammable mass between UFL and LFL was obtained from the explosion report.
FLACS	<ul style="list-style-type: none"> • The mass flow rate was obtained from cl.xxxxxx.N001. • The downwind distances to LFL and ½ LFL were obtained from the postprocessor Flowvis using the 2D cut plane for FMOLE-3D (mole fraction of fuel) variable. • The amount of flammable mass between UFL and LFL was obtained from the rtxxxxxx.FUEL file.

6.5 Discussion

6.5.1 Release modelling

The mass flow rate was calculated in each of FRED, EFFECTS, PHAST and FLACS for 12 hydrogen gas release scenarios. FLACS, FRED, EFFECTS and PHAST predicted almost the same mass flow rates for hydrogen gas releases at initial pressures of 5 bar and 25 bar. For hydrogen release at initial pressure of 350 bar, FLACS predicted the highest mass flow rate compared to the other tools. Table 6.11 gives the average percentage deviation in the calculated mass flow rates, comparing FLACS to FRED, EFFECTS and PHAST. For detailed results, please refer to “Appendix B”.

Table 6.11: Average percentage deviation in the results of the mass flow rate, comparing FLACS to FRED, EFFECTS and PHAST.

Initial storage pressure (bar)	Average percentage deviation between FLACS and FRED	Average percentage deviation between FLACS and EFFECTS	Average percentage deviation between FLACS and PHAST
5	0%	0%	0%
25	0%	1%	0%
350	8%	9%	5%

Another version of the JET utility program, described in section 5.4, was developed in FLACS to account for the non-ideal behaviour of hydrogen release at high pressures. This model was used for hydrogen gas releases at 350 bar. The mass flow rates predicted by the model using the Abel-Noble EOS were 0.2% higher than that predicted by the model using ideal gas EOS. For detailed results, please refer to “Appendix B”.

The calculated mass flow rates depend on the physical properties of the gas, the thermodynamic state of the gas in storage such as initial pressure and temperature, and the orifice cross-sectional area. In this study, both initial storage pressure and orifice diameter were varied to analyse their effect on the results predicted by the different tools.

Effect of initial storage pressure

An increase in initial storage pressure is expected to increase the mass flow rate. This was observed in the results predicted by FLACS, FRED, EFECTS and PHAST. This is can be shown in Figure 6.2, where the mass flow rates are given for hydrogen gas release through an orifice diameter of 10 mm from storage tank at different values of initial pressure 5 bar, 25 bar and 350 bar.

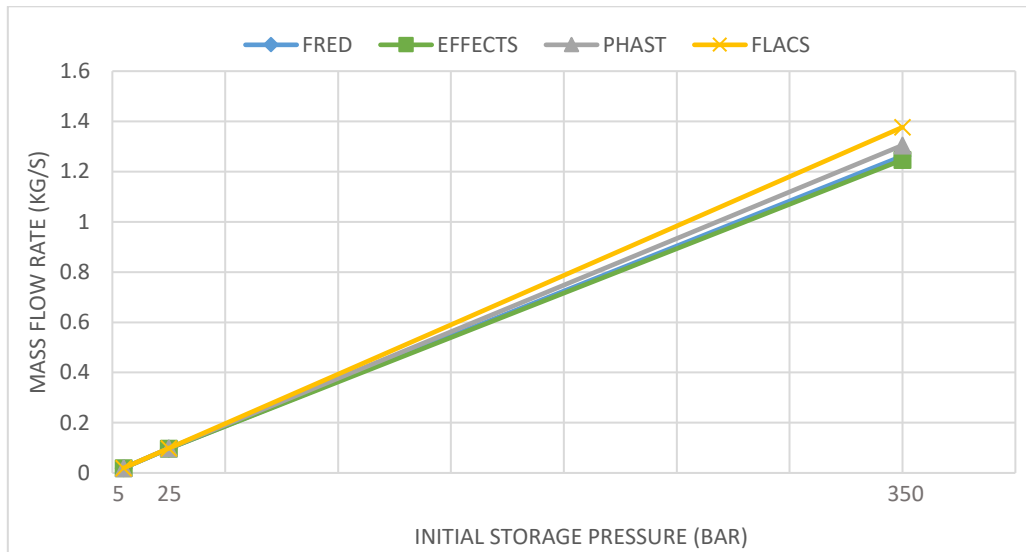


Figure 6.2: Mass flow rates results for hydrogen released at pressure of 5, 25 and 350 bar and temperature of 20 °C through an orifice of 10 mm in diameter.

Effect of orifice cross-sectional area

For a given initial storage pressure and temperature, an increase in the orifice diameter is expected to increase the mass flow rate. This was observed in the results predicted by FLACS, FRED, EFEFCTS and PHAST. This is can be shown in Figure 6.3, where the mass flow rates are given for hydrogen release from a storage tank pressurized at 350 bar through an orifice of different sizes: 1 mm, 3 mm, 5 mm and 10 mm.

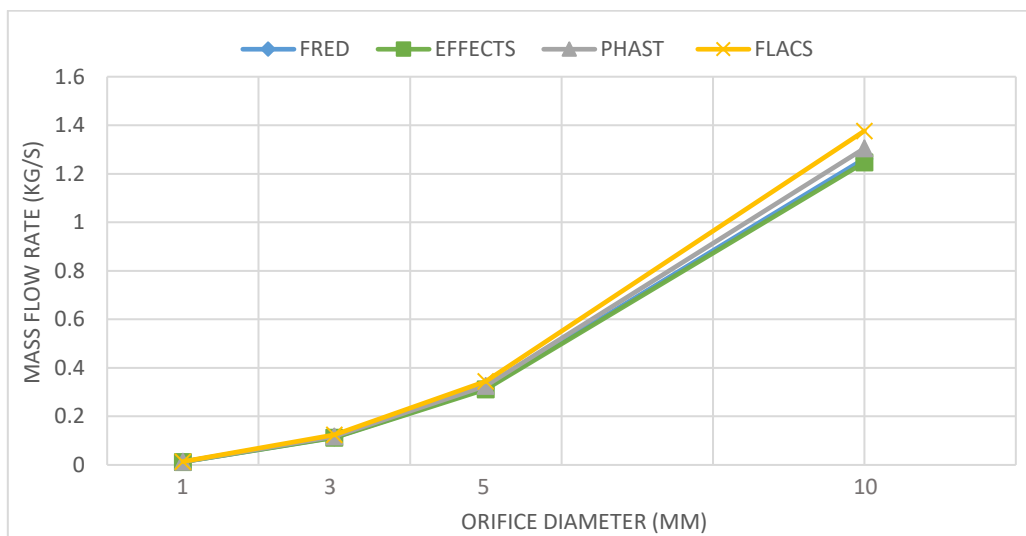


Figure 6.3: Mass flow rates results for hydrogen released at 350 bar and 20°C through various orifice sizes (1, 3, 5, 10 mm).

6.5.2 Dispersion modelling

EFFECTS showed large discrepancies in the results compared to FLACS, PHAST and FRED for all considered release scenarios. For detailed results, please refer to “Appendix B”. Within EFFECTS, a differentiation is made between "neutral gas" and "heavy gas" dispersion models. The neutral gas dispersion model is based on the Gaussian plume model which does not consider the difference in density between the air and the gas. According to EFFECTS’ user and reference manual, “the model must only be used for gases with a density approximately the same as air, or if the gas concentration at the point of release is low” [67, p. 141]. The results of this study were obtained using the dense gas dispersion model which is based on the SLAB-code. The model is mainly for heavy gases, but it can predict the rising flammable cloud for lighter-than-air gases. However, the model was never thoroughly validated for application on light gasses [67].

It was observed that the plume width was too narrow in all scenarios, one explanation could be related on how air is entrained from the sides of the jet; however, more investigation is required. Figure 6.4 shows examples of the flammable gas concentration contours predicted by EFFECTS. For some release scenarios, EFFECTS failed to track the rise of the plume and no results were found. Furthermore, EFFECTS did not provide any results for flammable mass between UFL and LFL as the model calculates the flammable mass from the ground level up to limited height. Thus, the discussion will focus only on the comparison of FLACS, FRED and PHAST.

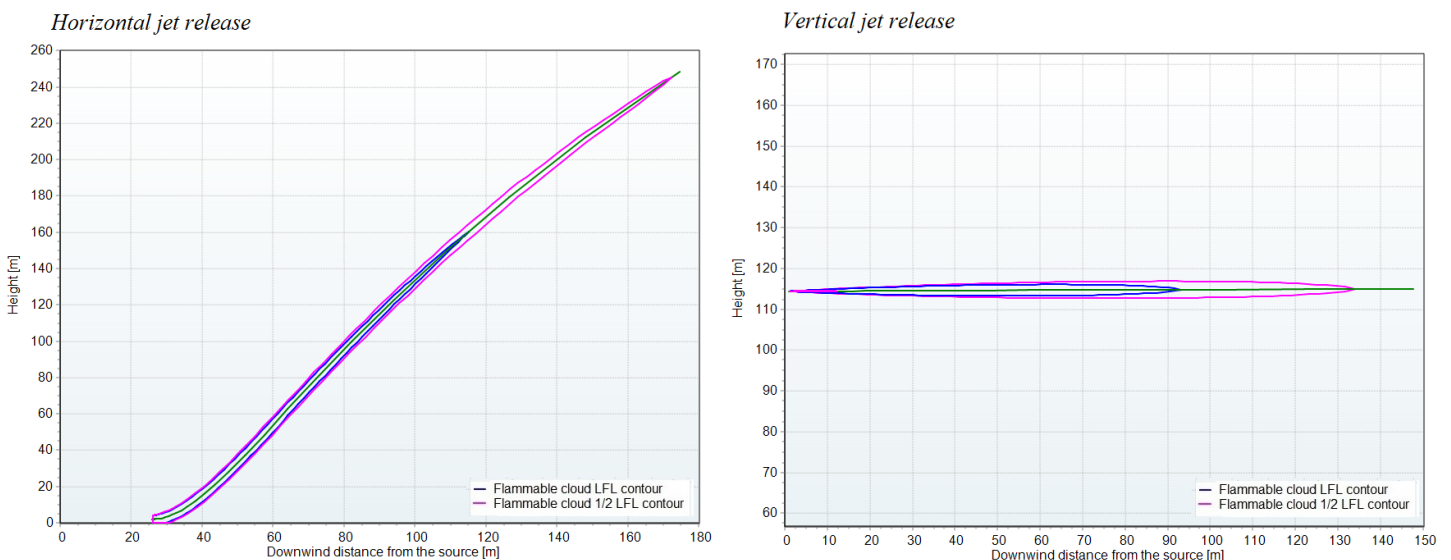


Figure 6.4: EFFECTS concentration contours for horizontal and vertical jet releases.

Dispersion simulations were performed for 81 hydrogen gas release scenarios in each of FRED, EFFECTS, PHAST and EFFECTS: 45 horizontal jet release scenarios along the wind direction and 36 vertical jet release scenarios in crosswind. FLACS predicted longer downwind distances to LFL and ½ LFL compared to FRED and PHAST for most of the considered horizontal jet release scenarios, except for 8 release scenarios in FRED where the tool predicted longer distances to than FLACS; however, the results of these release scenarios were of the same order of magnitude with deviation up to 13%. Table 6.12 shows the average percentage deviation in the results of the distances to LFL and ½ LFL for horizontal jet releases, comparing FLACS with FRED and PHAST. For detailed results, please refer to “Appendix B”.

Table 6.12: Average percentage deviation in the distances to LFL and ½ LFL, comparing FLACS to both FRED and PHAST for horizontal jet releases (45 release scenarios).

	Average percentage deviation between FLACS and FRED	Average percentage deviation between FLACS and PHAST
Distance to LFL (4% vol.)	18%	25%
Distance to 1/2 LFL (2% vol.)	20%	27%

FLACS also predicted longer downwind distances to LFL and ½ LFL compared to FRED and PHAST for most of the considered vertical jet release scenarios, except for 6 release scenarios in FRED and 1 release scenario in PHAST where the tools predicted longer distances than FLACS; however, the results of these release scenarios were of the same order of magnitude with deviation up to 22%. Table 6.13 shows the average percentage deviation in the results of the distances to LFL and ½ LFL for vertical jet releases, comparing FLACS with FRED and PHAST. For detailed results, please refer to “Appendix B”.

Table 6.13: Average percentage deviation in the distances to LFL and ½ LFL, comparing FLACS to both FRED and PHAST for vertical jet releases (36 release scenarios).

	Average percentage deviation between FLACS and FRED	Average percentage deviation between FLACS and PHAST
Distance to LFL (4% vol.)	24%	51%
Distance to 1/2 LFL (2% vol.)	38%	54%

FLACS predicted larger values for flammable mass between UFL and LFL compared to FRED for most of the considered release scenarios, except for 13 release scenarios where FRED predicted larger values; however, the results of these release scenarios were of the same order of magnitude with deviation up to 30%. FLACS predicted larger values for flammable mass between UFL and LFL compared to PHAST for all considered release scenarios. PHAST predicted “zero” flammable mass for 25 out of 81 scenarios. Table 6.14 shows the average percentage deviation in the results of the amount flammable mass, comparing FLACS with FRED and PHAST. For detailed results, please refer to “Appendix B”.

Table 6.14: Average percentage deviation in the flammable mass, comparing FLACS to both FRED and PHAST (81 release scenarios).

	Average percentage deviation between FLACS and FRED	Average percentage deviation between FLACS and PHAST
Amount of flammable mass between UFL and LFL (75 – 4% vol.)	32%	90%

Apart from the physical properties of the released gas and the release conditions (pressure, temperature), the dispersion is dependent on both meteorological conditions and the topographical conditions. In this study, initial storage pressure, release direction, wind speed, atmospheric stability class and surface roughness were varied to analyse their effect on the results predicted by the different tools.

Effect of initial storage pressure

The common argument is that a release of hydrogen gas in an unconfined area will not form a flammable cloud of significant volume due to its high buoyancy [74]. It is expected to rise and disperse relatively quickly upon release; however, this is not always the case. The buoyancy of a hydrogen gas release is only valid outside the part of dispersion which is controlled by the jet momentum [74]. Hydrogen released from a high-pressure source will form a jet which will be dominated by its momentum in the initial phase of dispersion due to the high difference between the jet velocity and the local wind speed. At some distance from the release source, the gas velocity is reduced (due to the air entrainment) to a level at which the dispersion will be dominated by buoyancy force and the gas cloud will start rising; this can be shown by the upward bending of the cloud.

To illustrate, consider the following hydrogen gas release scenarios:

- Initial pressure: 150 and 350 bar
- Initial temperature: 20 °C
- Orifice diameter: 10 mm
- Release height: 2 m
- Release direction: horizontal jet
- Wind speed: 2 m/s
- Wind direction: along release direction
- Stability class: D
- Roughness length: 0.03 m

Figure 6.5 shows the flammable gas concentration contours predicted by FLACS. As expected, a higher initial pressure produces higher momentum and thus, it takes longer for the buoyancy to dominate the flow. This results in longer downwind distances to LFL and ½ LFL. For hydrogen gas released at 150 bar, the distance to ½ LFL is 61 m from the release source and the cloud does not begin to “rise” until 38 m. When the initial pressure increased to 350 bar, the distance to ½ LFL increased to 88 m and the cloud does not begin to “rise” until 58 m. The distance to LFL increased with the increase in the initial pressure from 150 bar to 350 bar; however, the upward bending of the cloud was not observed in these release scenarios. This is mainly because of the ground effect, which will be discussed later in the

coming sections. The upward bending of the cloud was observed in FRED and PHAST. They also agreed to show the same trend as FLACS; the distances to LFL and $\frac{1}{2}$ LFL increased with the increase in the initial pressure.

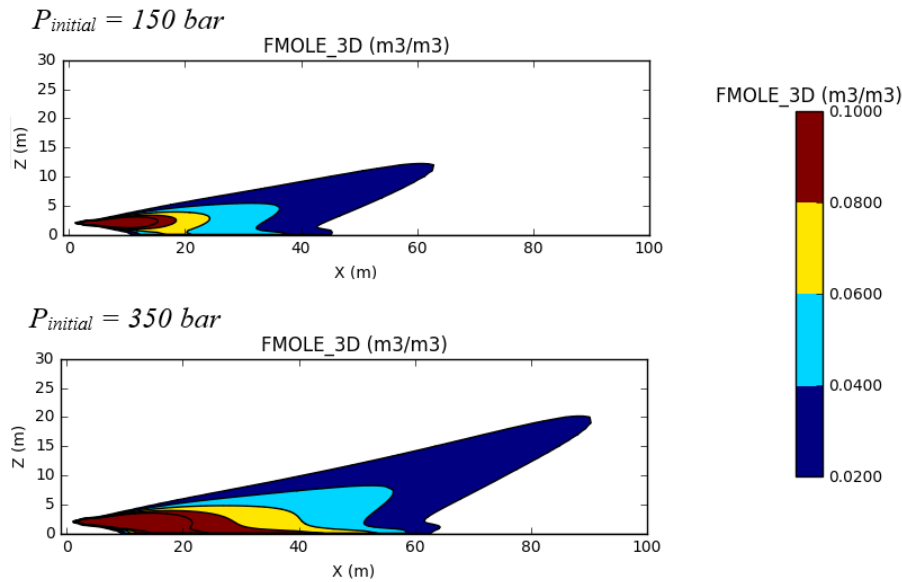


Figure 6.5: FLACS concentration contours for hydrogen release at initial pressure of 150 and 350 bar.

Effect of release height

Another point of interest is the height of the release source. For some release scenarios, hydrogen jets were deflected towards the ground and attached to it causing the LFL and $\frac{1}{2}$ LFL extent to be stretched over longer distances. Bénard et al. [75] explained that this could be due to a phenomenon known as the Coandă effect, which is “the tendency of a fluid jet to flow closer to an adjacent surface due to a lower pressure region that develops between the jet flow and the surface” [10, p. 16414]. When the jet is released closer to the ground, the region between the jet and the ground cannot provide enough air for the entrainment so the pressure in this region is lower than the outer side of the jet leading to a suction pressure which causes the jet to cling to the ground [75].

To illustrate, consider the following hydrogen gas release scenarios:

- Initial storage pressure: 350 bar
- Initial temperature: 20 °C
- Orifice diameter: 10 mm
- Release height: 2 and 5 m
- Release direction: horizontal jet
- Wind speed: 2 m/s
- Wind direction: along release direction
- Stability class: D
- Roughness length: 0.03 m

Figure 6.6 shows the flammable gas concentration contours predicted by FLACS. When the release is positioned at 2 m, the jet was deflected towards the ground and stretched over a

longer distances, whereas when the release is positioned at 5 m, the cloud dispersed faster in air and moved away from the ground. The distance to $\frac{1}{2}$ LFL decreased by 14% and the distance to LFL decreased by 24% at release height of 5 m compared to that at 2 m. This effect was observed in the results predicted by PHAST, as shown in Figure 6.7. The concentration contours plots predicted by FRED showed the deflect of the jet to the ground; however, the distances to LFL and $\frac{1}{2}$ LFL increased when the release height increased from 2 m to 5 m to reduce the ground effect, as shown in Figure 6.8. Figure 6.9 shows the distances to LFL and $\frac{1}{2}$ LFL predicted by FLACS, FRED and PHAST for releases positioned at 2 m and 5 m.

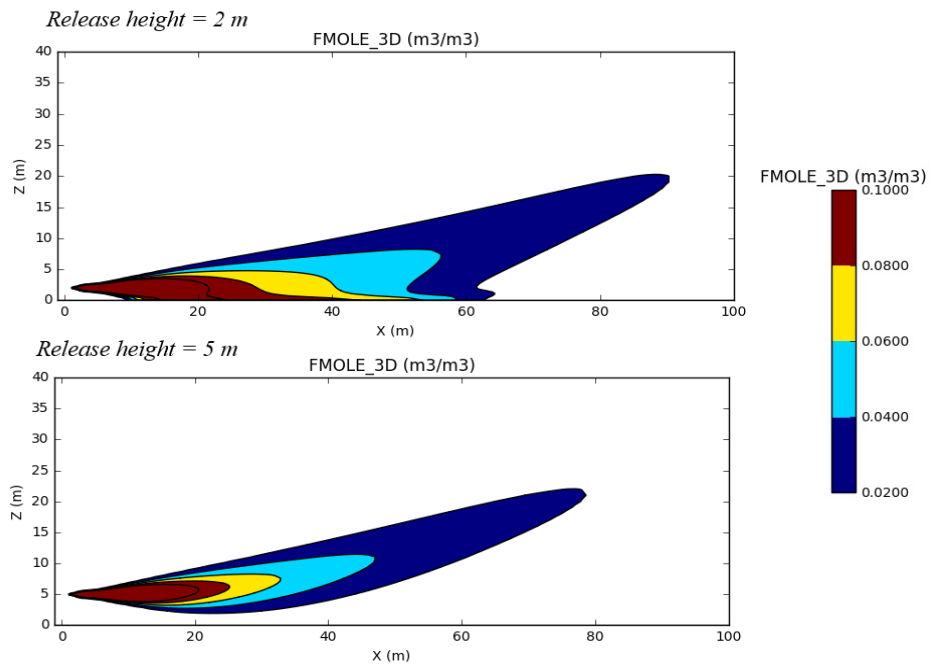


Figure 6.6: Effect of release height – FLACS concentration contours at a release height of 2 m and 5 m.

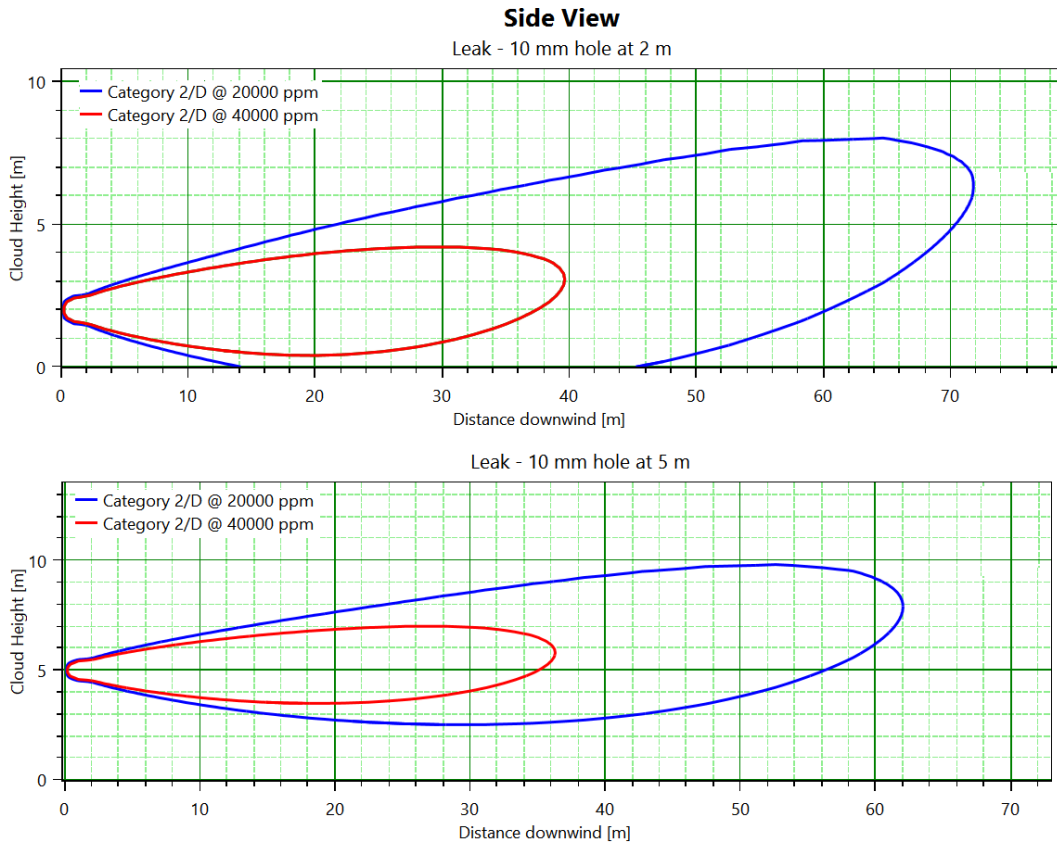


Figure 6.7: Effect of release height – PHAST concentration contours at a release height of 2 m and 5 m.

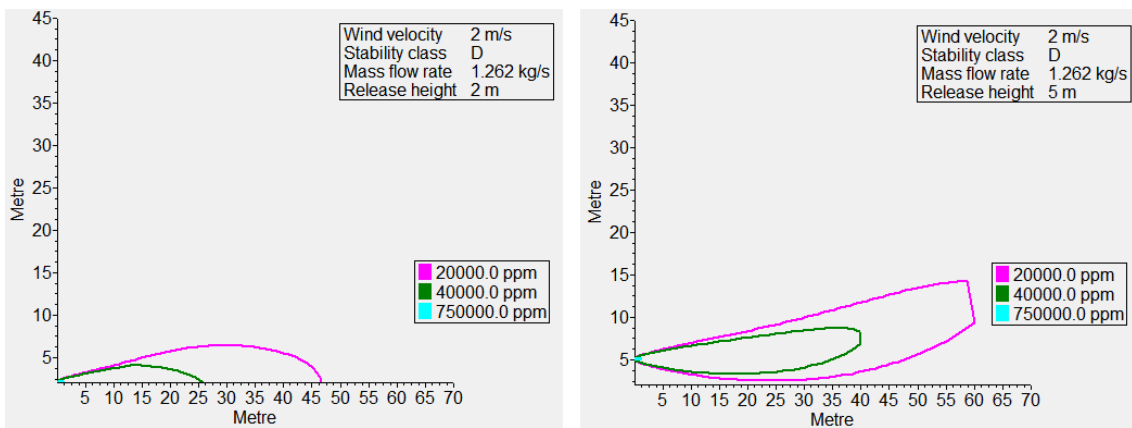


Figure 6.8: Effect of release height – FRED concentration contours at a release height of 2 m and 5 m.

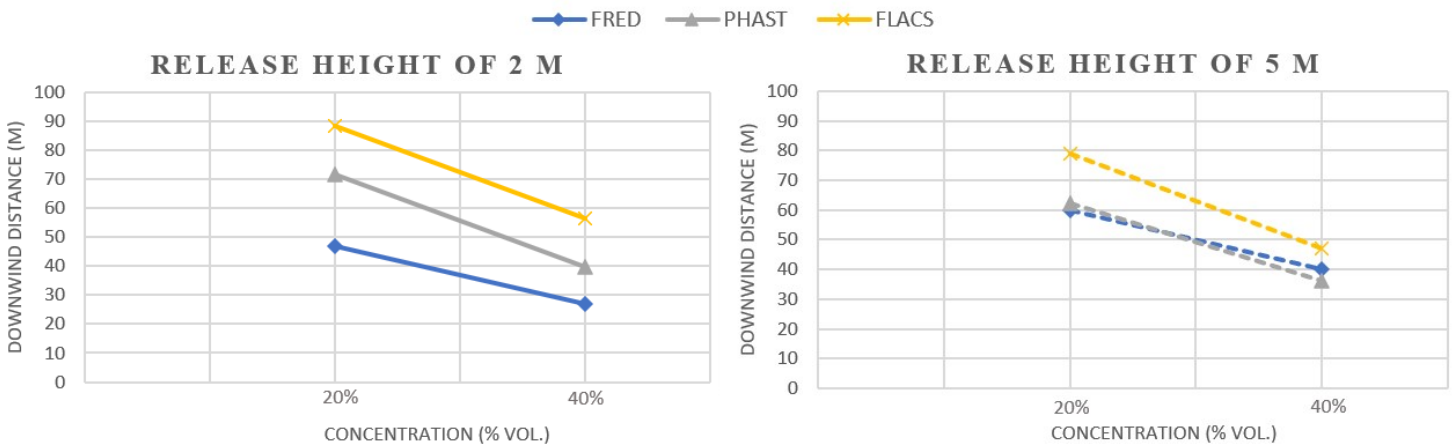


Figure 6.9: Downwind distances to LFL and 1/2 LFL at release height of 2 m and 5 m.

Effect of wind direction and speed

Wind drag at the ground generates turbulence which reduces the wind speed near the ground. This drag has a straightforward frictional component but also an aerodynamic component caused by the complex flow around obstacles such as trees, rocks, buildings, etc. [60]. Higher wind speeds generally increase the level of turbulence in the atmosphere and thus, enhance the dispersion of the gas cloud. Because wind speed increases with height it is specified at a reference height, 10 m is usually taken as a meteorological standard [60].

For a horizontal jet released along wind direction, FLACS, FRED and PHAST agreed to show the same trend for most of the release scenarios; the distances to LFL and 1/2 LFL and the amount of flammable mass decreased with the increase in wind speed. FLACS showed different results for 4 release scenarios where the distance to LFL and 1/2 LFL increased with the increase in wind speed; however, the amount of flammable mass decreased. The discrepancies in the results were mainly because of the effect of the ground. Out of these 4 release scenarios, FRED agreed to show the same trend in the results for 2 release scenarios as FLACS, while PHAST agreed to show the same trend in the results for 1 release scenario.

To illustrate, consider the following hydrogen release scenarios, where both release height and wind speed are varied:

- Initial storage pressure: 350 bar
- Initial temperature: 20 °C
- Orifice diameter: 10 mm
- Release height: 2 and 5 m
- Release direction: horizontal jet
- Wind speed: 2, 5 and 8 m/s
- Wind direction: along release direction
- Stability class: D
- Roughness length: 0.03 m

Figure 6.10 shows the flammable gas concentration contours predicted by FLACS. At a release height of 2 m, the jet was deflected towards the ground and attached to it. The increase in wind speed flattened the flammable cloud causing it to stretch even over a longer distance. Whereas, when the release height is increased to 5 m, this effect was reduced. For

wind speed of 8 m/s, the distance to 1/2 LFL decreased by 42% and the distance to LFL decreased by 50% at release height of 5 m compared to that at 2 m.

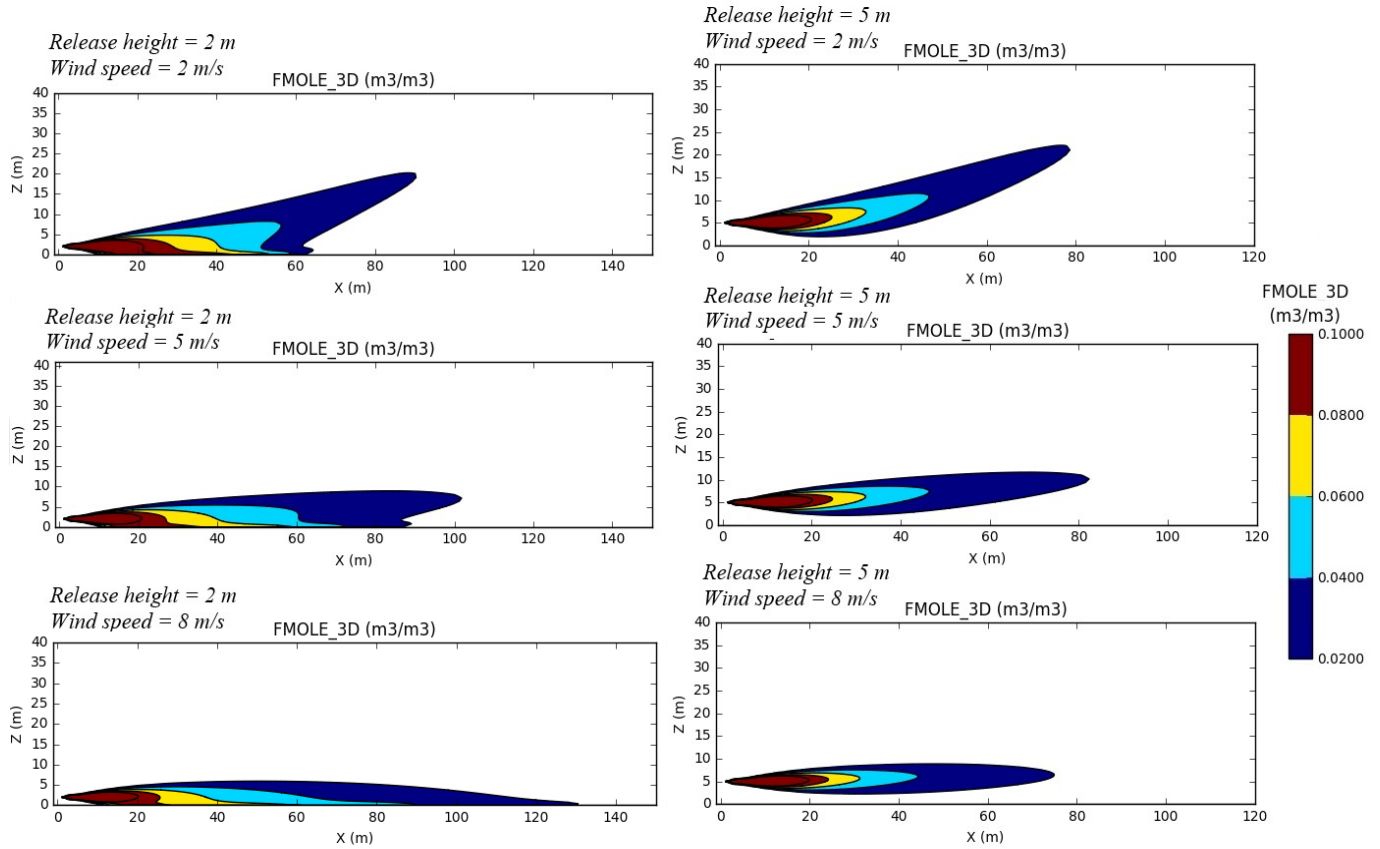


Figure 6.10: Effect of wind speed – FLACS concentration contours at release heights of 2 m and 5 m.

Figures 6.11 and 6.12 show, respectively, the distance to LFL and distance to 1/2 LFL predicted by FLACS, FRED and PHAST for the various wind speeds at both release heights of 2 m and 5 m. At a release height of 5 m, the distances to LFL and 1/2 LFL predicted by FRED and PHAST decreased with the increase in wind speed as the effect of the ground is reduced.

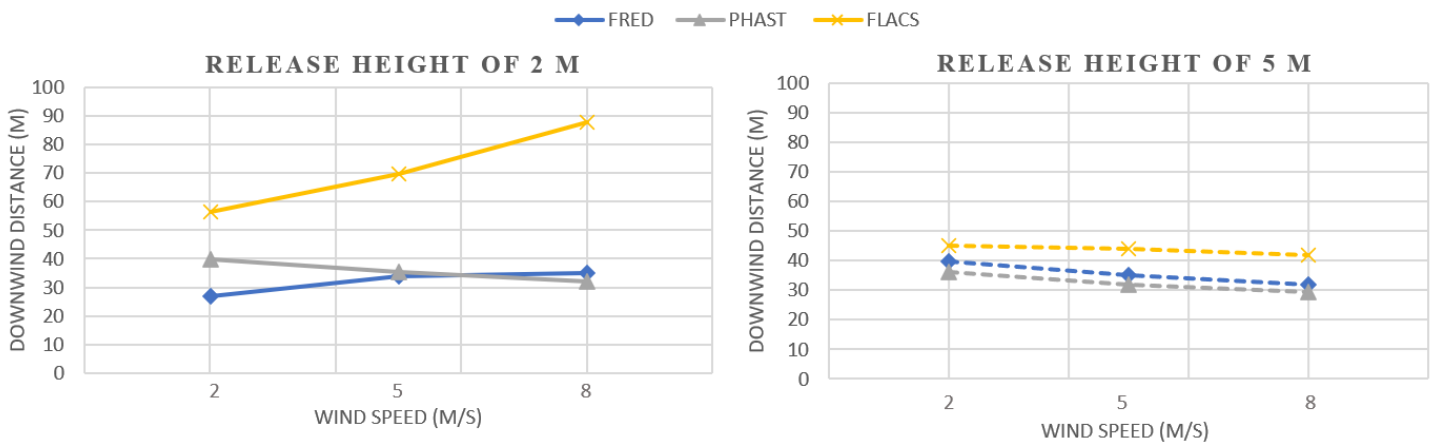


Figure 6.11: Effect of wind speed on distance to LFL for horizontal jet release at height of 2 m and 5 m.

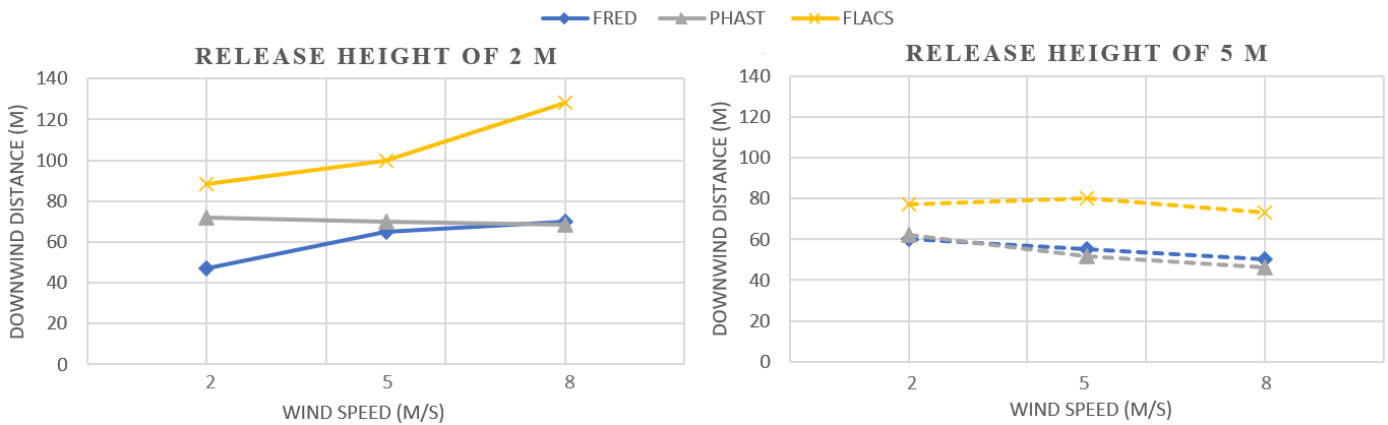


Figure 6.12: Effect of wind speed on distance to 1/2 LFL for horizontal jet release at height of 2 m and 5 m.

A vertical jet released in a crosswind tends to bend towards the downwind direction. According to DeVall et al. [56], there are two contributions from the wind in this bent-over region. The first one arises from entrainment of the air from the wind into the plume, so that total jet momentum gradually deflects towards the downwind direction. The second contribution is related to the pressure force of the wind on the jet which creates a pair of counter-rotating vortices within the plume's body, as shown in Figure 6.13.

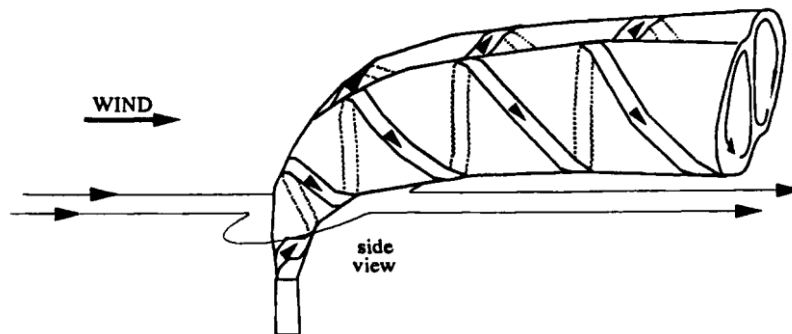


Figure 6.13: Formation of a vortex pair in a jet released in a crosswind [56].

FLACS, FRED and PHAST agreed to show the same trend; the distances to LFL and 1/2 LFL increased and the amount of flammable mass decreased with the increase in wind speed. At low wind speed, the jet disperses vertically and with the increase in wind speed the jet deflects towards the downwind direction. Thus, as the wind speed increases, the flammable gas cloud decreases along the vertical direction and increases along the horizontal direction.

To illustrate, consider the following hydrogen gas release scenarios:

- Initial storage pressure: 350 bar
- Initial temperature: 20 °C
- Orifice diameter: 5 mm
- Release height: 2 m
- Release direction: vertical jet
- Wind speed: 2, 5 and 8 m/s
- Wind direction: normal to release direction
- Stability class: D
- Roughness length: 0.03 m

Figure 6.14 shows the flammable gas concentration contours predicted by FLACS. With the increase in wind speed, the flammable cloud deflects to the downwind direction and reaches longer distances. Figures 6.15 and 6.16 show, respectively, the distance to LFL and distance to ½ LFL predicted by FLACS, FRED and PHAST for the various wind speeds.

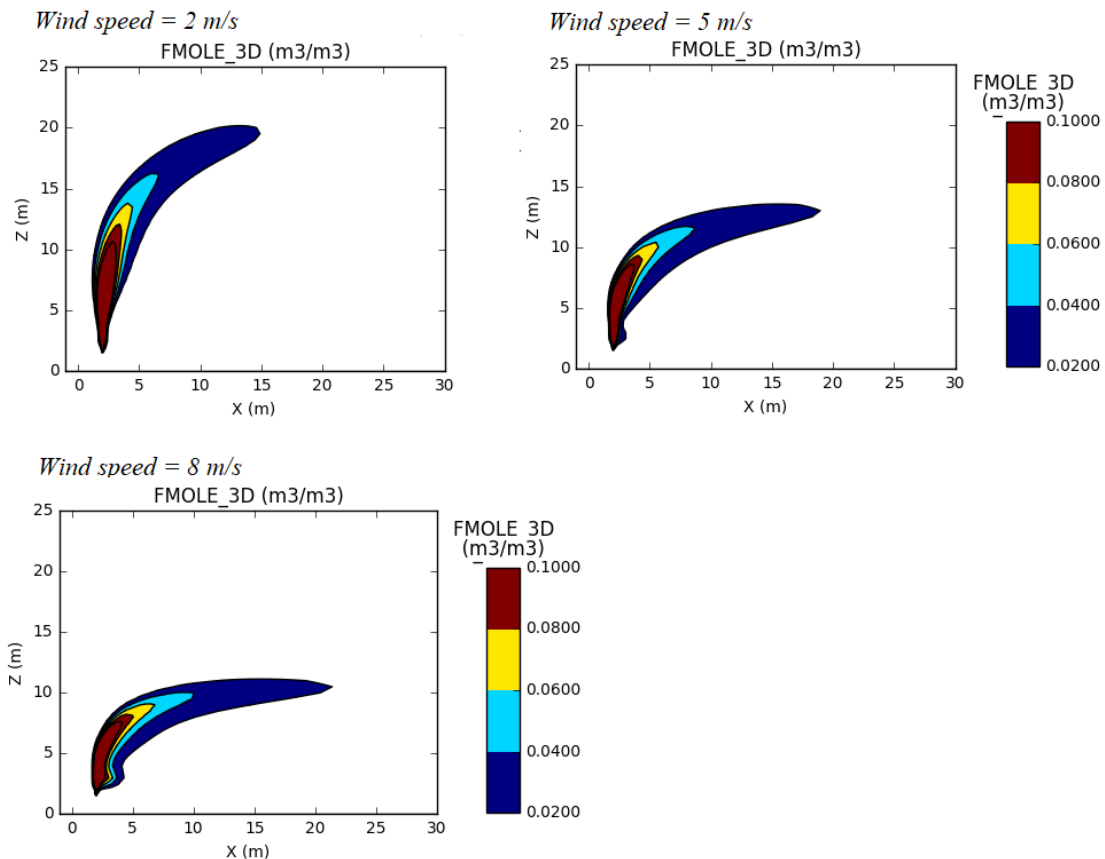


Figure 6.14: Effect of wind speed – FLACS concentration contours for vertical jet releases.

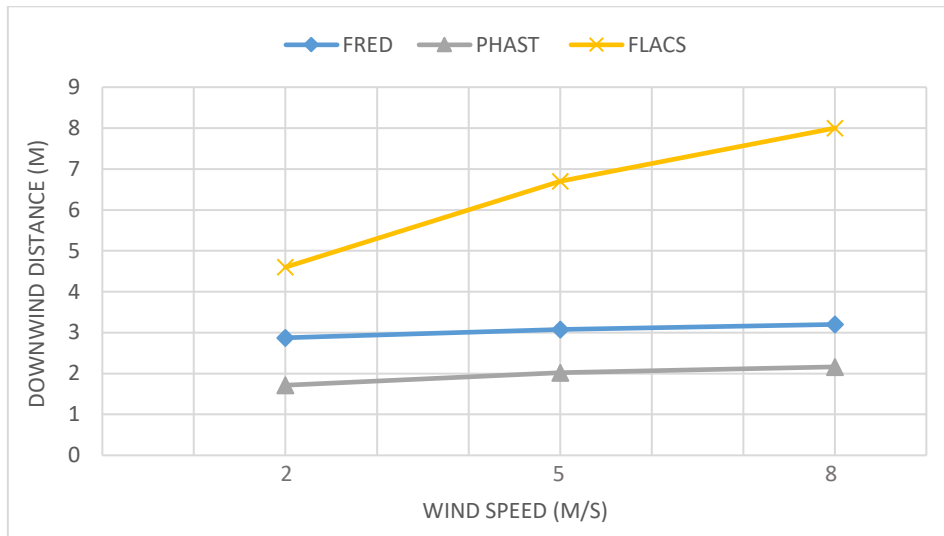


Figure 6.15: Effect of wind speed on distance to LFL for various wind speeds (vertical jet release).

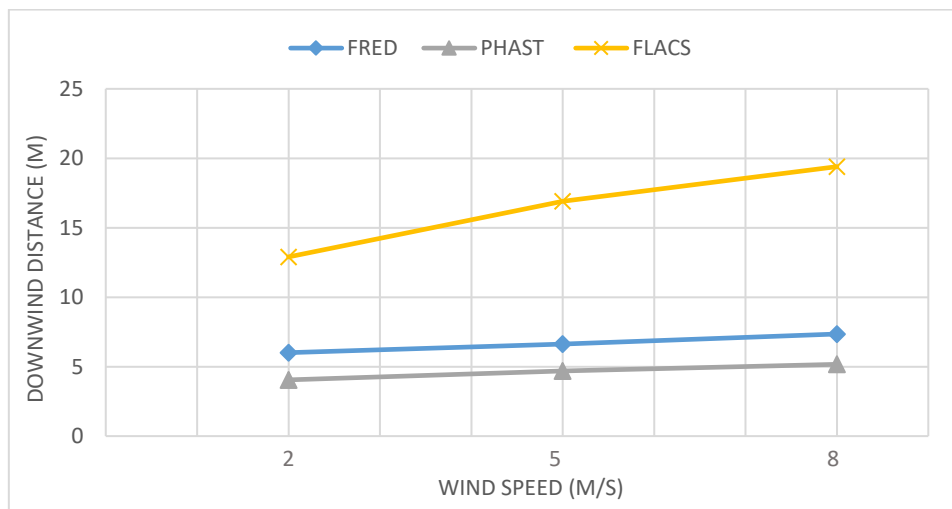


Figure 6.16: Effect of wind speed on distance to 1/2 LFL for various wind speeds (vertical jet release).

Effect of atmospheric stability class

Atmospheric stability describes the tendency for vertical mixing in the atmosphere and hence for turbulence generation by natural forces [4]. Pasquill scheme was used for atmospheric stability classification, assigning letters from A through F for increasingly stable atmospheres. Plume dispersion is at its maximum for unstable atmospheres of stability classes A through C, which typically occur during sunny daytime and low wind speeds. As the ground is heated, vertical updrafts are developed, and the turbulence intensity is increased [4]. Plume dispersion is at its minimum for stable atmospheres of classes E and F, which typically occur during clear nights with light winds. As the ground is cooled by radiation, vertical updrafts are suppressed, and turbulence intensity is reduced [4]. Stability class D

represents neutral stability which occurs in overcast and windy weather conditions (when the heat transfer between the ground and the atmosphere is very small) [56]. Turbulence enhances the dispersion of gas cloud in the atmosphere; thus, it is expected that the downwind distances to LFL and ½ LFL to increase with the increase in atmospheric stability. The use of stability classes A through C is not recommended in FLACS user manual, thus only stability classes D and F were used in this study.

To illustrate, consider the following hydrogen gas release scenarios:

- Initial storage pressure: 5 bar
- Initial temperature: 20 °C
- Orifice diameter: 10 mm
- Release height: 2 m
- Release direction: horizontal jet
- Wind speed: 2 m/s
- Wind direction: along wind direction
- Stability class: D and F
- Roughness length: 0.03 m

Figures 6.17 and 6.18 show, respectively, the distance to LFL and distance to ½ LFL predicted by FLACS, FRED and PHAST for the two stability classes. FLACS and FRED agreed to show the same trend; the distances to LFL and ½ LFL increased with the increase in atmospheric stability, whereas PHAST predicted the opposite. Although the difference between the results for stability class D and stability class F was small, around +/- 9% for these release scenarios. The amount of flammable mass predicted by FLACS, FRED and PHAST increased with the increase in stability class.

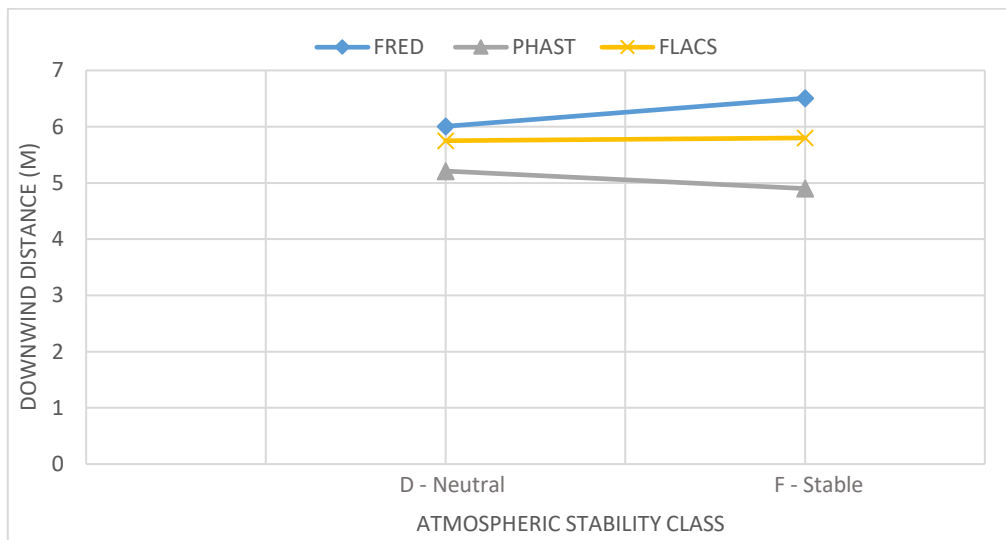


Figure 6.17: Effect of stability class on downwind distance to LFL.

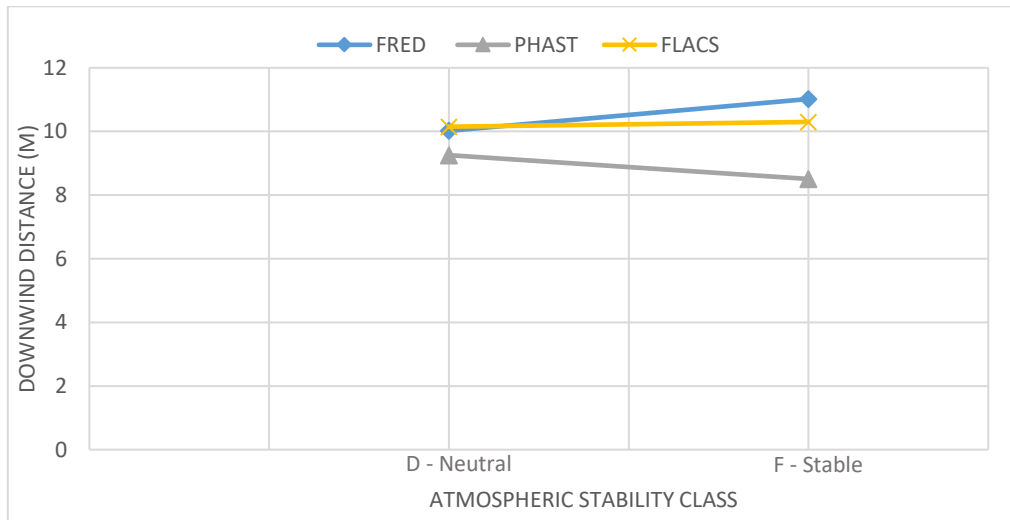


Figure 6.18: Effect of stability class on downwind distance to 1/2 LFL.

Effect of surface roughness length

The surface roughness length is used to characterize the ground roughness (existence of trees, buildings, etc.) and describe its influence on the vertical profile of wind speed and the mechanical turbulence [59]. Higher values of roughness length produce higher turbulence and consequently faster mixing of the gas cloud [4].

To illustrate, consider the following hydrogen gas release scenarios:

- Initial storage pressure: 25 bar
- Initial temperature: 20 °C
- Orifice diameter: 10 mm
- Release height: 2 m
- Release direction: horizontal jet
- Wind speed: 2 m/s
- Wind direction: along release direction
- Stability class: D
- Roughness length: 0.005, 0.03 and 0.1 m

Surface roughness is used differently in integral tools and CFD tools. FRED and PHAST use the surface roughness to represent obstacles and quantify their influence on the gas cloud dispersion. Whereas, FLACS uses the surface roughness to define the wind velocity profile on the wind boundary condition and it is not applied on the ground or surfaces [62].

Figures 6.19 and 6.20 show, respectively, the distance to LFL and distance to 1/2 LFL predicted by FLACS, FRED and PHAST for the various surface roughness lengths. FRED and PHAST agreed to show the same trend; the downwind distances to LFL and 1/2 LFL and the amount of flammable mass decreased with the increase in roughness length. Although the increase in the results was small, around 10% for this release scenario. The increase in roughness length has almost negligible effect on the distances to LFL and 1/2 LFL predicted by FLACS, as shown in Figures 6.19 and 6.20. In addition, the flammable mass calculated by

FLACS increased with the increase in roughness length, showing different results compared to FRED and PHAST.

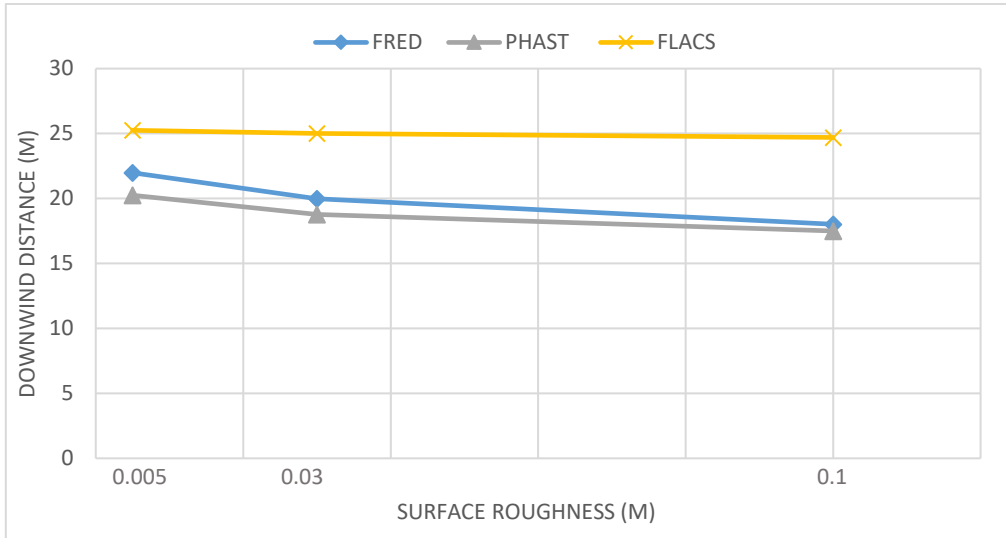


Figure 6.19: Effect of roughness length on downwind distance to LFL.

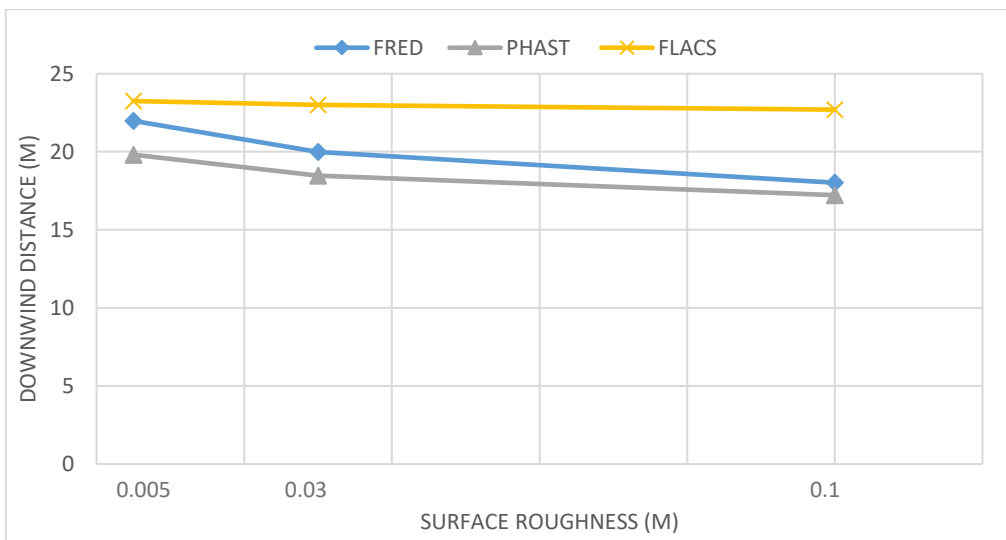


Figure 6.20: Effect of roughness length on downwind distance to 1/2 LFL.

Effect of Obstacles

Turbulence induced by obstacles enhances the dispersion of the gas cloud in the atmosphere. FLACS was used to illustrate the impact of geometry on the dispersion of the flammable gas cloud. Obstructed release scenario, represented by a refuelling gas station, was compared with its corresponding release scenario in an open flat terrain. As shown in Figure 6.21, the distances to LFL and 1/2 LFL for the obstructed release scenario are about half that for the

unobstructed release scenario. Obstruction does help decreasing the jet momentum and allow the buoyancy to have more effect; however, a larger flammable cloud was formed. For detailed results, please refer to “Appendix D”.

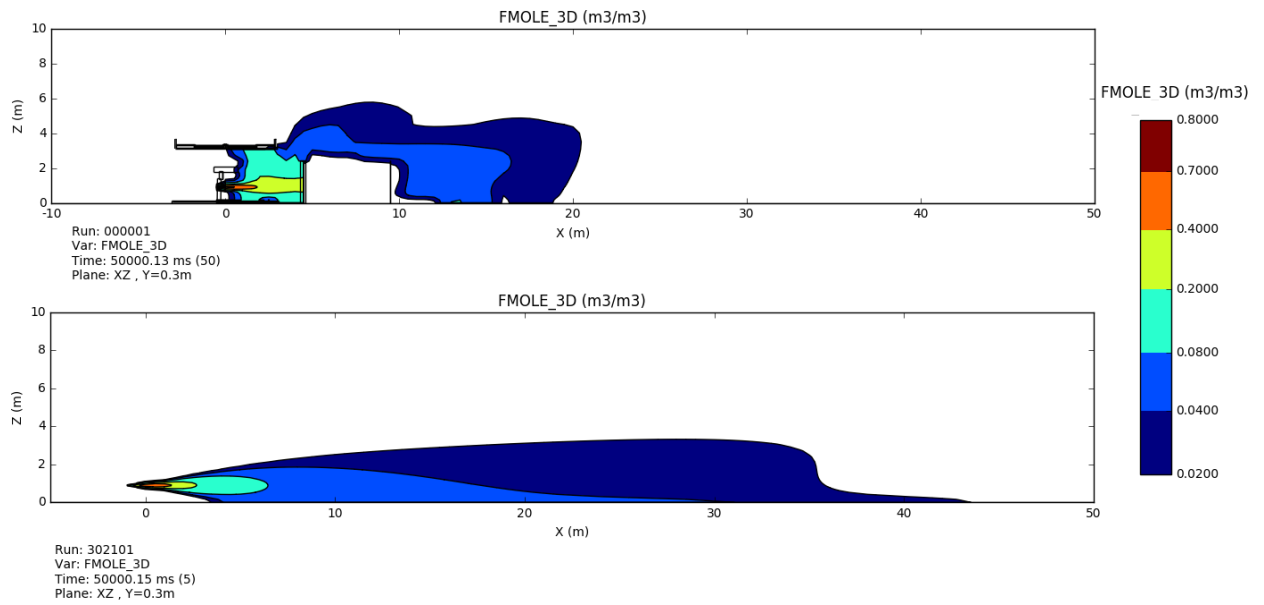


Figure 6.21: Effect of obstacles on the dispersion of flammable gas cloud.

7 Conclusion

This study was performed to compare the results predicted by FRED, EFFECTS, PHAST and FLACS which are used in hydrogen safety studies. Release and dispersion simulations were carried out in each tool for 81 hydrogen gas release scenarios. Variation of input parameters such as initial storage pressure, orifice diameter, release direction, release height, wind speed, atmospheric stability class and surface roughness length were studied. Obstacles effect on the dispersion of the hydrogen gas cloud was studied in FLACS.

Main findings are list below:

- FRED, EFFECTS and PHAST predicted almost the same mass flow rates as FLACS for hydrogen gas releases at 5 bar and 25 bar. However, for hydrogen gas releases at 350 bar, FLACS predicted higher values than FRED, EFFECTS and PHAST, with deviation up to 9%.
- Another version of the JET utility program was developed in FLACS to account for the non-ideal behaviour of hydrogen gas release at high pressures. The mass flow rates predicted by the model using the Abel-Noble EOS were 0.2% higher than that predicted by the model using ideal gas EOS.
- EFFECTS showed large discrepancies in the results of distances to LFL and ½ LFL compared to FLACS, FRED and PHAST. From the results of this study, the use of EFFECTS is not recommended for hydrogen safety studies.
- FLACS predicted longer downwind distances to LFL and ½ LFL compared to FRED and PHAST for most of the considered horizontal and vertical jet release scenarios, except for 14 release scenarios in FRED and 1 release scenario in PHAST where the tools predicted longer distances than FLACS; however, the results of these scenarios were of the same order of magnitude. FLACS predicted larger values for flammable mass between UFL and LFL compared to FRED and PHAST, except for 13 scenarios where FRED predicted larger values; however, the results of these scenarios were of the same order of magnitude. It is not possible to recommend one tool over the other based only on the results of this study as the results predicted by the tools need to be compared against experimental data.

Effect of varying parameters:

- Hydrogen buoyancy is only relevant outside the part of dispersion which is controlled by the jet momentum. Increasing the initial release pressure produces jets with higher momentum and thus, longer time is taken for buoyancy to dominate the flow.
- Hydrogen buoyancy does not prevent the formation of a large flammable gas cloud for high pressure hydrogen release near the ground. However, as the distance between the ground and the leak source increases, the gas cloud disperses faster and moves away from the ground.

- Increasing wind speed generally increases the level of turbulence in the atmosphere and thus, enhance the dispersion of the gas cloud. However, for hydrogen gas released near the ground, the increase in wind speed flattens the flammable cloud causing it to stretch even over a longer distance. This effect disappears as the distance between the ground and the leak source increases.
- Hydrogen jet released in crosswind tends to bend towards the downwind direction. As the wind speed increases, the flammable gas cloud decreases along the vertical direction and increases along the horizontal direction, and thus it reaches longer distance.
- Turbulence intensity is reduced with the increase in atmospheric stability. Increasing atmospheric stability from class D to F reduces the turbulence in the atmosphere causing an increase in the distances to LFL and $\frac{1}{2}$ LFL. PHAST showed different trend in the results compared to FLACS and FRED, although the increase in atmospheric stability had minor effects on the distances to LFL and $\frac{1}{2}$ LFL in the three tools.
- Surface roughness is used differently in integral tools and CFD tools. FRED and PHAST use the surface roughness to represent obstacles and quantify their influence on the gas cloud dispersion. Whereas, FLACS uses the surface roughness to define the wind velocity profile on the wind boundary condition and it is not applied on the ground or surfaces [62]. Increasing roughness length increases the turbulence in the atmosphere causing a decrease in the distances to LFL and $\frac{1}{2}$ LFL. FRED and PHAST showed the same trend in the results, whereas the increase in roughness length had negligible effect on the results predicted by FLACS.
- The presence of obstacles in the path of the gas cloud has significant influence on its dispersion due to the recirculation zones and wakes they can introduce. Comparing an obstructed release scenario with its unobstructed counterpart showed that obstacles help decreasing the jet momentum and allow the buoyancy to have more effect; however, a larger flammable cloud was still formed.

8 Further Work

- Study the dispersion models used in FLACS, FRED, PHAST and EFFECTS to understand the discrepancies in the results.
- The results predicted by FLACS, FRED and PHAST should be compared against experimental data. As at this point, it is not possible to recommend one tool over the other.
- Study the effect of forced ventilation over accidental hydrogen gas releases occurring in enclosed volumes. Hypothetical hydrogen gas release scenarios to be simulated in FLACS in partially to fully enclosed rooms under forced ventilation. Sensitivity studies can be performed by using variations of mass flow rate, room size and ventilation rate (air change per hour) in order to categorize release scenarios as relevant for area classification or major accidents.

9 References

- [1] O. R. Hansen and P. Middha, “CFD-Based Risk Assessment for Hydrogen Applications,” *Process Saf. Prog.*, vol. 27, no. 1, pp. 29–34, 2007.
- [2] E. N. Ekerold, “Interpretation of geometrical effects in consequence modelling. Comparison study between the commercial consequence assessment tools FLACS and PHAST for flammable gas dispersion (MSc Thesis),” University of Bergen, 2014.
- [3] T. Skjold *et al.*, “3D risk management for hydrogen installations,” *Int. J. Hydrog. Energy*, vol. 42, pp. 7721–7730, 2017.
- [4] J. L. Woodward, *Estimating the flammable mass of a vapor cloud*. Center for Chemical Process Safety (CCPS), 1998.
- [5] CPR 14E, *The Yellow Book - Methods for the calculations of Physical Effects, due to release of hazardous materials (liquids and gases)*, Third Edition. Committee for the Prevention of Disasters (CPR), 2005.
- [6] Sandpower AS and SINTEF, *Handbook for fire calculations and fire risk assessment in the process industry*. 2003.
- [7] “CCPS Process Safety Glossary,” *Center of Chemical Process Safety (CCPS)*. Retrieved from: <https://www.aisc.org/ccps/resources/glossary> (accessed May 22, 2020).
- [8] D. Bjerketvedt, J. R. Bakke, and K. van Wingerden, *Gas Explosion Handbook*. Gexcon AS, 1992.
- [9] ISO, “ISO/TR15916:2015 - Basic considerations for the safety of hydrogen systems, Second Edition,” 2015.
- [10] E. M. Edelia, R. Winkler, D. Sengupta, M. M. El-Halwagi, and M. S. Mannan, “A computational fluid dynamics evaluation of unconfined hydrogen explosion in high pressure applications,” *Int. J. Hydrog. Energy*, vol. 43, pp. 16411–16420, 2018.
- [11] P. Middha, “Development, use, and validation of the CFD tool FLACS for hydrogen safety studies (PhD Thesis),” University of Bergen, 2010.
- [12] Standard Norway, “NORSOK Z-013 Standard—Risk and emergency preparedness assessment.” Standard Norway, 2010.
- [13] T. Aven, *Risk Analysis*, Second Edition. John Wiley & Sons, Incorporated, 2015.
- [14] COAG Energy Council, *Australia’s National Hydrogen Strategy*. Australian Government - Department of Industry, Science, Energy and Resources, 2019.
- [15] International Energy Agency (IEA), “The Future of Hydrogen - Seizing today’s opportunities,” Japan, 2019.
- [16] History.com Editors, “The Hindenburg disaster,” *HISTORY*, 2020. Retrieved from: <https://www.history.com/this-day-in-history/the-hindenburg-disaster> (accessed May 24, 2020).
- [17] G. R. Astbury, “A review of the properties and hazards of some alternative fuels,” *Process Saf. Environ. Prot.*, vol. 86, pp. 397–414, 2008.

- [18] CPR 18E, *The Purple Book - Guideline for quantitative risk assessment*. Committee for the Prevention of Disasters (CPR), 2005.
- [19] T. Aven, *Quantitative Risk Assessment: The Scientific Platform*. Cambridge University Press, 2011.
- [20] ISO, “ISO 31000 Risk Management—Principles and Guidelines.” International Organization for Standardization, 2009.
- [21] ISO, “ISO/FDIS 31000 Risk Management - Principles and Guidelines.” International Organization for Standardization, 2017.
- [22] A. Hallgarth, A. Zayer, A. Gatward, and J. Davies, “Large Scale Outdoor Flammable & Toxic Gas Dispersion Modelling in Industrial Environments,” COMSOL, Milan, Excerpt from the Proceedings of the COMSOL Conference, 2009. [Online]. Retrieved from: <https://www.comsol.no/paper/download/46197/Hallgarth.pdf>.
- [23] D. Baraldi *et al.*, “JRC Reference Reports - Prioritisation of Research and Development for modelling the safe production, storage, delivery and use of hydrogen,” Joint Research Centre of the European Commission, 2011.
- [24] K. Wingerden, D. Siccama, A. Lindtner, and F. Gavelli, “Modelling of gas dispersion in congested areas - A comparison of a CFD-model and integral models, GEXCON In-house - not officially published,” GEXCON AS.
- [25] A. Fiorucci *et al.*, “Risk assessment of dangerous products release and dispersion: a comparison between CFD and integral models,” 2008.
- [26] T. Egeberg, T. Davidsen, M. M. Venkatraman, and S. Nassiri, “Comparative study on gas dispersion,” Civil Protection and Emergency Planning (DSB) and Scandpower AS.
- [27] HySafe, “Biennial Report on Hydrogen Safety,” 2007. Retrieved from: <http://www.hysafe.org/index.php?ID=40&author=59> (accessed Jul. 02, 2020).
- [28] V. Molkov, *Fundamentals of Hydrogen Safety Engineering*, 1st Edition. 2012.
- [29] J. M. Kuchta, “Investigation of fire and explosion accidents in the chemical, mining and fuel-related industries - A manual,” United States Department of The Interior, Bureau of Mines, 1985.
- [30] IRENA, “Hydrogen: A Renewable Energy Perspective,” The International Renewable Energy Agency, Abu Dhabi, 2019. [Online]. Retrieved from: <https://www.irena.org/publications/2019/Sep/Hydrogen-A-renewable-energy-perspective>.
- [31] Committee on Climate Change, “Hydrogen in a low-carbon economy,” 2018. Accessed: May 19, 2020. [Online]. Retrieved from: <https://www.theccc.org.uk/wp-content/uploads/2018/11/Hydrogen-in-a-low-carbon-economy.pdf>.
- [32] U.S. Department of Energy’s Office of Energy Efficiency and Renewable Energy (EERE), “Hydrogen Production: Natural Gas Reforming.” Retrieved from: <https://www.energy.gov/eere/fuelcells/hydrogen-production-natural-gas-reforming> (accessed Apr. 04, 2020).
- [33] U.S. Department of Energy’s Office of Energy Efficiency and Renewable Energy (EERE), “Hydrogen Production: Coal Gasification.” Retrieved from:

- <https://www.energy.gov/eere/fuelcells/hydrogen-production-coal-gasification> (accessed May 19, 2020).
- [34] Shell, “Shell hydrogen study: Energy of the future? Sustainable mobility through fuel cells and hydrogen,” 2017. Accessed: Feb. 04, 2020. [Online]. Retrieved from: https://www.shell.com/energy-and-innovation/new-energies/hydrogen/_jcr_content/par/keybenefits_150847174/link.stream/1496312627865/6a3564d61b9aff43e087972db5212be68d1fb2e8/shell-h2-study-new.pdf.
- [35] DNV GL, “Produksjon og bruk av Hydrogen i Norge - Klima- og miljødepartementet og Olje- og energidepartementet,” 2019. [Online]. Retrieved from: <https://www.regjeringen.no/contentassets/0762c0682ad04e6abd66a9555e7468df/hydrogen-i-norge---synteserapport.pdf>.
- [36] FCHEA, “Fuel Cell Basics,” *Fuel Cell & Hydrogen Energy Association (FCHEA)*. Retrieved from: <http://www.fchea.org/fuelcells> (accessed Apr. 25, 2020).
- [37] FCHEA, “Fuel Cells and Hydrogen - Stationary Power,” *The Fuel Cell and Hydrogen Energy Association (FCHEA)*. Retrieved from: <http://www.fchea.org/stationary> (accessed May 19, 2020).
- [38] FuelCellsWorks, “SP Group sets up first zero-emission building powered by green hydrogen in Southeast Asia.” Retrieved from: <https://fuelcellsworks.com/news/sp-group-sets-up-first-zero-emission-building-powered-by-green-hydrogen-in-southeast-asia/> (accessed May 19, 2020).
- [39] I. Staffell *et al.*, “The role of hydrogen and fuel cells in the global energy system,” *Energy Environ. Sci.*, vol. 12, pp. 463–491, 2019.
- [40] U.S. Department of Energy’s Office of Energy Efficiency and Renewable Energy (EERE), “Hydrogen Storage.” Retrieved from: <https://www.energy.gov/eere/fuelcells/hydrogen-storage> (accessed Apr. 03, 2020).
- [41] Toyota, “Mirai - Fuel Cell Vehicle, Brochure 2020.” Accessed: May 19, 2020. [Online]. Retrieved from: https://www.toyota.co.uk/download/cms/gben/Mirai-brochure-2020_tcm-3060-1884525.pdf.
- [42] AFC TCP, “Hydrogen as fuel,” *Advanced Fuel Cells Technology Collaboration Programme (AFC TCP)*. Retrieved from: <https://www.ieafuelcell.com/index.php?id=33> (accessed May 19, 2020).
- [43] J.-E. Vinnem, *Offshore Risk Assessment Volume 2 - Principles, Modelling and Applications of QRA Studies*, Third Edition. Springer Series in Reliability Engineering, 2014.
- [44] R. B. Gupta, *Hydrogen Fuel - Production, Transport and Storage*. CRC Press, Taylor & Francis Group, 2009.
- [45] N. Salaün, “TiZir Tyssedal - Safety Philosophy Documentation. Ilmenite-hydrogen upgrade of pre-reduction process (Gexcon in-house document),” 2016.
- [46] G. R. Astbury and S. J. Hawksworth, “Spontaneous ignition of hydrogen leaks: A review of postulated mechanisms,” *Int. J. Hydrog. Energy*, vol. 32, pp. 2178–2185, 2007.

- [47] F. L. Dryer, M. Chaos, Z. Zhao, J. N. Stein, J. Y. Alpert, and C. J. Homer, "Spontaneous Ignition of Pressurized Releases of Hydrogen and Natural Gas into Air," *Combust. Sci. Technol.*, vol. 179, pp. 663–694, 2007.
- [48] V. V. Golub *et al.*, "Hydrogen Auto-Ignition During Accidental or Technical Opening of High Pressure Tank," *J. Loss Prev. Process Ind.*, vol. 20, pp. 439–446, 2007.
- [49] V. V. Golub *et al.*, "Mechanisms of high-pressure hydrogen gas self-ignition in tubes," *J. Loss Prev. Process Ind.*, vol. 21, pp. 185–198, 2008.
- [50] V. V. Golub *et al.*, "Experimental and numerical investigation of hydrogen gas auto-ignition," *Int. J. Hydrog. Energy*, vol. 34, pp. 5946–5953, 2009.
- [51] V. V. Golub *et al.*, "Shock-induced ignition of hydrogen gas during accidental or technical opening of high-pressure tanks," *J. Loss Prev. Process Ind.*, vol. 20, pp. 439–466, 2007.
- [52] T. Mogi, D. Kim, H. Shiina, and S. Horiguchi, "Self-ignition and explosion during discharge of high-pressure hydrogen," *J. Loss Prev. Process Ind.*, vol. 21, pp. 199–204, 2008.
- [53] B. P. Xu, L. El Hima, J. X. Wen, S. Dembele, V. H. Y. Tam, and T. Donchev, "Numerical study on the spontaneous ignition of pressurized hydrogen release through a tube into air," *J. Loss Prev. Process Ind.*, vol. 21, pp. 205–213, 2008.
- [54] E. Yamada, S. Watanabe, A. K. Hayashi, and N. Tsuboi, "Numerical analysis on auto-ignition of a high pressure hydrogen jet spouting from a tube," *Proceedings Combust. Inst.*, vol. 32, pp. 2363–2369, 2009.
- [55] P. K. Pahwa and G. K. Pahwa, *Hydrogen Economy*. The Energy and Resources Institute (TERI), 2014.
- [56] G. E. DeVaull, J. A. King, R. J. Lantzy, and D. J. Fontaine, *Understanding Atmospheric Dispersion of Accidental Releases - A CCPS Concept Book*. Center for Chemical Process Safety, 1995.
- [57] S. R. Hanna, P. J. Drivas, and J. J. Chang, *Guidelines for Use of Vapor Cloud Dispersion Models*, Second Edition. Center for Chemical Process Safety (CCPS), 1996.
- [58] J. M. Kuchta, "Investigation of fire and explosion accidents in the chemical, mining and fuel-related industries - A manual," United States Department of The Interior, Bureau of Mines, 1985.
- [59] J. Casal, *Evaluation of the Effects and Consequences of Major Accidents in Industrial Plants*. Elsevier Science & Technology, 2017.
- [60] "Shell FRED 7.1 - Technical Guide." Shell Global Solutions, 2019.
- [61] S. Mannan, *Lees' Loss Prevention in the Process Industries: Hazard Identification, Assessment and Control*. Elsevier Science & Technology, 2012.
- [62] Gexcon AS, "FLACS v10.9 User's Manual." 2019.
- [63] S. Dharmavaram, S. R. Hanna, and O. R. Hansen, "Consequence Analysis - Using a CFD Model for Industrial Sites," *Wiley Intersci.*, 2005.

- [64] Gexcon AS, “FRED Software,” 2018. Retrieved from: <https://www.gexcon.com/products-services/FRED-Software/26/en> (accessed Mar. 05, 2020).
- [65] Gexcon AS, “EFFECTS,” 2020. Retrieved from: <https://www.gexcon.com/products-services/EFFECTS/31/en> (accessed Mar. 07, 2020).
- [66] CPR 16E, *The Green Book - Methods for the determination of possible damage, to people and objects resulting from release of hazardous materials*, First Edition. Committee for the Prevention of Disasters (CPR), 1992.
- [67] “EFFECTS Version 11 - User and reference manual.” Gexcon AS, 2020.
- [68] DNV GL, “Process hazard analysis software - Phast.” Retrieved from: <https://www.dnvgl.com/services/process-hazard-analysis-software-phast-1675> (accessed Mar. 15, 2020).
- [69] DNV GL - Software, “PHAST Technical Reference.” DNV GL, 2017.
- [70] B. E. Launder and D. B. Spalding, “The numerical computation of turbulent flows,” vol. 3, no. 2, pp. 269–289, 1974.
- [71] A. D. Birch, D. R. Brown, M. G. Dodson, and F. Swaffield, “The Structure and Concentration Decay of High Pressure Jets of Natural Gas,” vol. 36, pp. 249–261, 1984.
- [72] K. C. Cornelius and K. Srinivas, “Isentropic Compressible Flow for Non Ideal Gas Models for a Venturi,” vol. 126, no. 2, pp. 238–244, 2004.
- [73] L. Post, “HGSYSTEM 3.0: Technical Reference Manual and User’s Guide.” 1995.
- [74] J. K. Thomas, C. Eastwood, and M. Goodrich, “Are Unconfined Hydrogen Vapor Cloud Explosions Credible?,” *Process Saf. Prog.*, vol. 34, no. 1, pp. 36–43, 2015.
- [75] P. Bénard, A. Hourri, B. Angers, and A. Tchouvelev, “Adjacent surface effect on the flammable cloud of hydrogen and methane jets: Numerical investigation and engineering correlations,” *Int. J. Hydrog. Energy*, vol. 41, pp. 18654–18662, 2016.

Appendices

Appendix A Comparison Tool

A.1 Deliverables

Table A.1: Comparative study deliverables.

File name (.xlsx)	Content
Comparison Tool	This file is in the form of a comparison tool for the results of the 72 hydrogen gas release scenarios which were simulated in each of FRED, EFFECTS, PHAST and FLACS. The user can choose from predefined inputs, including initial storage pressure, orifice diameter, release direction and wind speed. The outputs are mass flow rate, downwind distances to lower flammability limit (LFL) and half of the lower flammability limit (1/2 LFL), and amount of flammable mass between upper and lower flammability limits.

A.2 Attachments

The tool is available on: [Comparison Tool.xlsx](#)

Figures A.1 and A.2 show screenshots of the two worksheets of the comparison tool. The user can only change the input cells highlighted in yellow with a predefined drop list. The results are given in both a table and a graph.

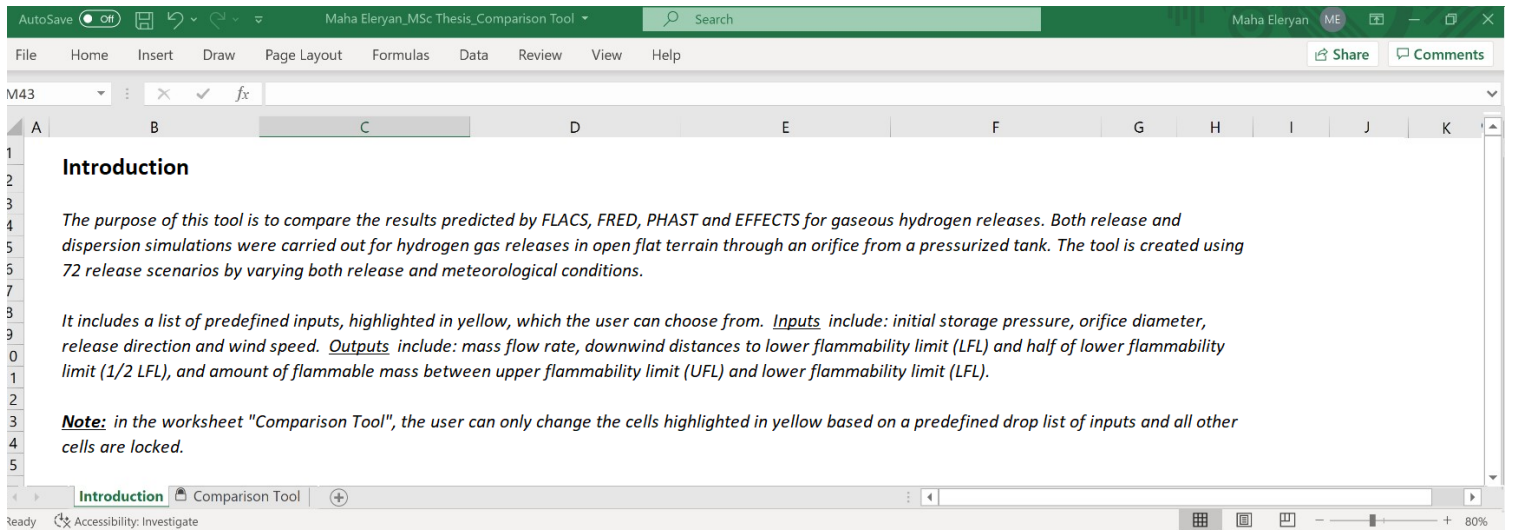


Figure A.1: Comparison tool – “Introduction” worksheet.

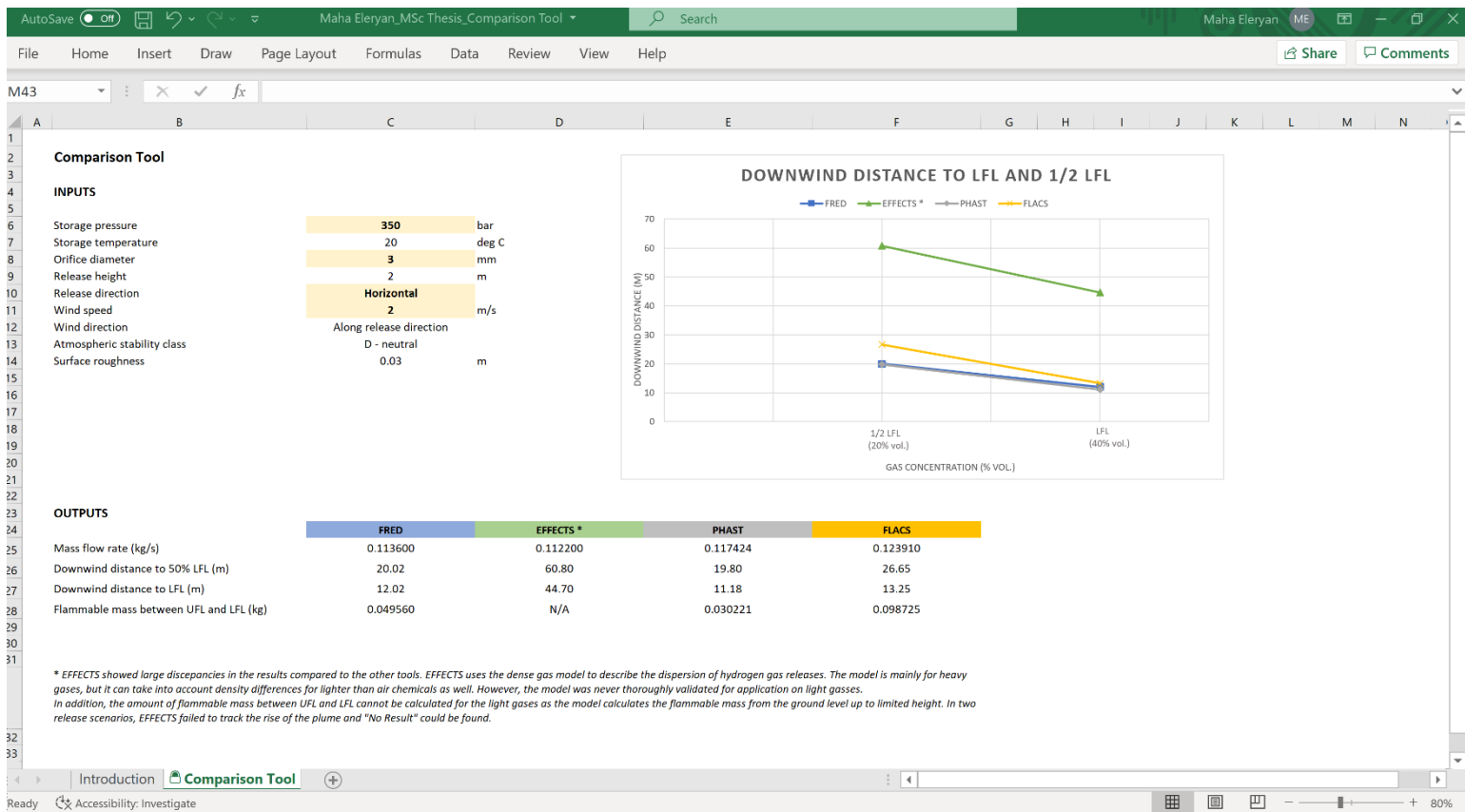


Figure A.2: Comparison tool – “Comparison Tool” worksheet.

Downwind distance to lower flammability limits (LFL) – 4% vol.

Scenario: a|b|c|d

- a: storage pressure (bar)
- b: orifice diameter (mm)
- c: release direction
- d: wind speed (m/s)

Table B.2: Case 1 – downwind distance to LFL results

Scenario	FRED	EFFECTS	PHAST	FLACS
5bar 3mm Horizontal 2m/s	2.00	4.00	1.67	2.60
5bar 3mm Horizontal 5m/s	1.90	3.60	1.60	2.55
5bar 3mm Horizontal 8m/s	1.80	3.50	1.49	2.40
5bar 5mm Horizontal 2m/s	3.00	8.40	2.71	3.40
5bar 5mm Horizontal 5m/s	3.00	5.40	2.48	3.30
5bar 5mm Horizontal 8m/s	2.50	4.70	2.36	3.20
5bar 10mm Horizontal 2m/s	6.01	19.20	5.21	5.75
5bar 10mm Horizontal 5m/s	5.50	10.80	4.64	5.53
5bar 10mm Horizontal 8m/s	5.00	8.50	4.32	5.32
5bar 50mm Horizontal 2m/s	22.98	72.11	23.56	36.40
5bar 50mm Horizontal 5m/s	22.02	51.33	19.65	29.80
5bar 50mm Horizontal 8m/s	20.01	41.42	17.35	25.30
Scenario	FRED	EFFECTS	PHAST	FLACS
5bar 3mm Vertical 2m/s	0.28	2.40	0.15	0.25
5bar 3mm Vertical 5m/s	0.31	1.70	0.18	0.26
5bar 3mm Vertical 8m/s	0.28	1.60	0.19	0.23
5bar 5mm Vertical 2m/s	0.47	6.60	0.23	0.39
5bar 5mm Vertical 5m/s	0.49	4.00	0.38	0.51
5bar 5mm Vertical 8m/s	0.51	3.20	0.43	0.48
5bar 10mm Vertical 2m/s	0.87	17.00	0.48	0.85
5bar 10mm Vertical 5m/s	0.91	9.10	0.57	1.19
5bar 10mm Vertical 8m/s	1.02	6.70	0.62	1.18
5bar 50mm Vertical 2m/s	4.37	117.30	2.50	4.40
5bar 50mm Vertical 5m/s	4.69	50.30	2.91	8.00
5bar 50mm Vertical 8m/s	4.99	38.30	3.15	10.00

Downwind distance to half of lower flammability limits (1/2 LFL) – 2% vol.

Scenario: a|b|c|d

- a: storage pressure (bar)
- b: orifice diameter (mm)
- c: release direction
- d: wind speed (m/s)

Table B.3: Case 1 – downwind distance to ½ LFL results

Scenario	FRED	EFFECTS	PHAST	FLACS
5bar 3mm Horizontal 2m/s	3.50	4.50	3.12	3.80
5bar 3mm Horizontal 5m/s	3.00	3.70	2.75	3.60
5bar 3mm Horizontal 8m/s	3.00	3.60	2.55	3.30
5bar 5mm Horizontal 2m/s	5.51	11.10	4.97	5.60
5bar 5mm Horizontal 5m/s	5.00	6.50	4.29	5.15
5bar 5mm Horizontal 8m/s	4.50	5.30	3.93	4.70
5bar 10mm Horizontal 2m/s	10.02	26.60	9.25	10.15
5bar 10mm Horizontal 5m/s	9.00	14.80	7.78	9.41
5bar 10mm Horizontal 8m/s	8.00	10.90	7.02	8.48
5bar 50mm Horizontal 2m/s	37.94	97.42	40.88	56.70
5bar 50mm Horizontal 5m/s	44.98	70.00	34.90	68.50
5bar 50mm Horizontal 8m/s	43.00	56.69	33.86	88.00
Scenario	FRED	EFFECTS	PHAST	FLACS
5bar 3mm Vertical 2m/s	0.59	3.10	0.45	0.69
5bar 3mm Vertical 5m/s	0.68	2.20	0.59	0.67
5bar 3mm Vertical 8m/s	0.73	1.90	0.67	0.58
5bar 5mm Vertical 2m/s	0.98	9.60	0.58	1.33
5bar 5mm Vertical 5m/s	1.11	5.60	1.01	1.35
5bar 5mm Vertical 8m/s	1.17	4.40	1.04	1.10
5bar 10mm Vertical 2m/s	1.83	24.70	1.14	2.23
5bar 10mm Vertical 5m/s	2.18	13.50	1.37	3.30
5bar 10mm Vertical 8m/s	2.18	10.70	1.51	3.10
5bar 50mm Vertical 2m/s	8.88	155.90	5.74	10.70
5bar 50mm Vertical 5m/s	10.27	69.20	6.79	21.50
5bar 50mm Vertical 8m/s	11.26	55.00	7.50	24.25

Amount of flammable mass between upper and lower flammability limits (75 - 4% vol.)

Scenario: a|b|c|d

a: storage pressure (bar)

b: orifice diameter (mm)

c: release direction

d: wind speed (m/s)

Table B.4: Case 1 – flammable mass between UFL and LFL results

Scenario	FRED	EFFECTS	PHAST	FLACS
5bar 3mm Horizontal 2m/s	0.000161	N/A	0.000000	0.000143
5bar 3mm Horizontal 5m/s	0.000131	N/A	0.000000	0.000119
5bar 3mm Horizontal 8m/s	0.000110	N/A	0.000000	0.000096
5bar 5mm Horizontal 2m/s	0.000786	N/A	0.000000	0.000606
5bar 5mm Horizontal 5m/s	0.000590	N/A	0.000000	0.000475
5bar 5mm Horizontal 8m/s	0.000456	N/A	0.000000	0.000384
5bar 10mm Horizontal 2m/s	0.005898	N/A	0.000000	0.005409
5bar 10mm Horizontal 5m/s	0.004352	N/A	0.000000	0.004104
5bar 10mm Horizontal 8m/s	0.003544	N/A	0.000000	0.003150
5bar 50mm Horizontal 2m/s	0.636100	N/A	0.338384	0.915980
5bar 50mm Horizontal 5m/s	0.454300	N/A	0.233788	0.638400
5bar 50mm Horizontal 8m/s	0.343500	N/A	0.180778	0.457590
Scenario	FRED	EFFECTS	PHAST	FLACS
5bar 3mm Vertical 2m/s	0.000105	N/A	0.000000	0.000146
5bar 3mm Vertical 5m/s	0.000059	N/A	0.000000	0.000071
5bar 3mm Vertical 8m/s	0.000043	N/A	0.000000	0.000037
5bar 5mm Vertical 2m/s	0.000523	N/A	0.000000	0.000641
5bar 5mm Vertical 5m/s	0.000275	N/A	0.000000	0.000334
5bar 5mm Vertical 8m/s	0.000194	N/A	0.000000	0.000203
5bar 10mm Vertical 2m/s	0.003805	N/A	0.000000	0.004545
5bar 10mm Vertical 5m/s	0.001994	N/A	0.000000	0.002704
5bar 10mm Vertical 8m/s	0.001488	N/A	0.000000	0.001856
5bar 50mm Vertical 2m/s	0.438700	N/A	0.000000	0.557830
5bar 50mm Vertical 5m/s	0.224600	N/A	0.000000	0.426910
5bar 50mm Vertical 8m/s	0.156600	N/A	0.000000	0.336190

Downwind distance to lower flammability limit (LFL) – 4% vol.

Scenario: a|b|c|d

- a: storage pressure (bar)
- b: orifice diameter (mm)
- c: release direction
- d: wind speed (m/s)

Table B.6: Case 2 – downwind distance to LFL results

 * *EFFECTS failed to track the rise of the plume and "No Result" could be found.*

Scenario	FRED	EFFECTS	PHAST	FLACS
25bar 3mm Horizontal 2m/s	4.00	10.20	3.38	4.30
25bar 3mm Horizontal 5m/s	3.50	7.00	3.11	5.60
25bar 3mm Horizontal 8m/s	3.50	6.30	2.92	5.40
25bar 5mm Horizontal 2m/s	6.50	20.70	5.50	6.20
25bar 5mm Horizontal 5m/s	5.50	12.10	4.96	5.90
25bar 5mm Horizontal 8m/s	5.00	9.80	4.60	5.60
25bar 10mm Horizontal 2m/s	12.01	46.10	10.59	11.55
25bar 10mm Horizontal 5m/s	10.01	26.10	9.25	11.10
25bar 10mm Horizontal 8m/s	9.50	19.50	8.45	10.70
25bar 50mm Horizontal 2m/s	33.98	114.40	49.31	70.30
25bar 50mm Horizontal 5m/s	48.91	99.20	50.50	74.80
25bar 50mm Horizontal 8m/s	50.03	85.80	50.06	76.00
Scenario	FRED	EFFECTS	PHAST	FLACS
25bar 3mm Vertical 2m/s	0.51	7.30	0.24	0.54
25bar 3mm Vertical 5m/s	0.59	4.30	0.50	0.71
25bar 3mm Vertical 8m/s	0.61	3.40	0.61	0.66
25bar 5mm Vertical 2m/s	0.89	17.10	0.47	0.90
25bar 5mm Vertical 5m/s	0.82	9.10	0.58	1.40
25bar 5mm Vertical 8m/s	1.02	6.70	0.63	1.48
25bar 10mm Vertical 2m/s	1.77	43.90	1.00	1.90
25bar 10mm Vertical 5m/s	1.87	21.60	1.18	3.20
25bar 10mm Vertical 8m/s	1.81	15.70	1.26	3.90
25bar 50mm Vertical 2m/s	8.55	No Result*	5.09	10.20
25bar 50mm Vertical 5m/s	9.19	124.00	5.90	16.50
25bar 50mm Vertical 8m/s	9.84	91.70	6.35	21.00

Downwind distance to half of lower flammability limit (1/2 LFL) – 2% vol.

Scenario: a|b|c|d

- a: storage pressure (bar)
- b: orifice diameter (mm)
- c: release direction
- d: wind speed (m/s)

Table B.7: Case 2 – downwind distance to ½ LFL results

* *EFFECTS failed to track the rise of the plume and "No Result" could be found.*

Scenario	FRED	EFFECTS	PHAST	FLACS
25bar 3mm Horizontal 2m/s	7.01	13.30	6.23	7.20
25bar 3mm Horizontal 5m/s	6.00	8.20	5.39	8.10
25bar 3mm Horizontal 8m/s	5.50	6.90	4.89	7.50
25bar 5mm Horizontal 2m/s	11.01	28.30	9.91	11.15
25bar 5mm Horizontal 5m/s	9.50	16.00	8.36	10.25
25bar 5mm Horizontal 8m/s	8.50	12.10	7.55	9.30
25bar 10mm Horizontal 2m/s	19.99	65.20	18.47	23.00
25bar 10mm Horizontal 5m/s	16.02	36.30	15.06	20.45
25bar 10mm Horizontal 8m/s	15.00	26.70	13.38	18.80
25bar 50mm Horizontal 2m/s	59.42	163.70	56.66	106.50
25bar 50mm Horizontal 5m/s	89.98	136.00	60.41	123.30
25bar 50mm Horizontal 8m/s	100.00	119.20	65.28	129.00
Scenario	FRED	EFFECTS	PHAST	FLACS
25bar 3mm Vertical 2m/s	1.10	10.50	0.67	1.45
25bar 3mm Vertical 5m/s	1.10	6.20	1.02	1.95
25bar 3mm Vertical 8m/s	1.37	4.80	1.14	1.80
25bar 5mm Vertical 2m/s	1.85	25.10	1.17	2.45
25bar 5mm Vertical 5m/s	1.98	13.50	1.38	4.30
25bar 5mm Vertical 8m/s	2.01	10.30	1.52	3.80
25bar 10mm Vertical 2m/s	3.71	64.50	2.37	5.38
25bar 10mm Vertical 5m/s	4.05	32.50	2.77	8.20
25bar 10mm Vertical 8m/s	4.52	23.90	3.02	9.50
25bar 50mm Vertical 2m/s	17.33	No Result*	11.42	24.40
25bar 50mm Vertical 5m/s	20.00	172.40	14.05	43.50
25bar 50mm Vertical 8m/s	22.38	128.50	15.49	53.50

Amount of flammable mass between upper and lower flammability limit (75 - 4% vol.)

Scenario: a|b|c|d

- a: storage pressure (bar)
- b: orifice diameter (mm)
- c: release direction
- d: wind speed (m/s)

Table B.8: Case 2 – flammable mass between UFL and LFL results

Scenario	FRED	EFFECTS	PHAST	FLACS
25bar 3mm Horizontal 2m/s	0.001342	N/A	0.000000	0.001631
25bar 3mm Horizontal 5m/s	0.001104	N/A	0.000000	0.001374
25bar 3mm Horizontal 8m/s	0.000910	N/A	0.000000	0.001132
25bar 5mm Horizontal 2m/s	0.006372	N/A	0.000000	0.007350
25bar 5mm Horizontal 5m/s	0.004866	N/A	0.000000	0.005539
25bar 5mm Horizontal 8m/s	0.003853	N/A	0.000000	0.004378
25bar 10mm Horizontal 2m/s	0.048940	N/A	0.025805	0.064412
25bar 10mm Horizontal 5m/s	0.036140	N/A	0.019619	0.047364
25bar 10mm Horizontal 8m/s	0.029210	N/A	0.015783	0.036529
25bar 50mm Horizontal 2m/s	3.093000	N/A	3.672280	13.578000
25bar 50mm Horizontal 5m/s	3.656000	N/A	3.133120	10.755000
25bar 50mm Horizontal 8m/s	3.402000	N/A	2.531250	8.639600
Scenario	FRED	EFFECTS	PHAST	FLACS
25bar 3mm Vertical 2m/s	0.000929	N/A	0.000000	0.001374
25bar 3mm Vertical 5m/s	0.000568	N/A	0.000000	0.000852
25bar 3mm Vertical 8m/s	0.000398	N/A	0.000000	0.000536
25bar 5mm Vertical 2m/s	0.004522	N/A	0.000000	0.006389
25bar 5mm Vertical 5m/s	0.002416	N/A	0.000000	0.004075
25bar 5mm Vertical 8m/s	0.001564	N/A	0.000000	0.002835
25bar 10mm Vertical 2m/s	0.035440	N/A	0.000000	0.053327
25bar 10mm Vertical 5m/s	0.019650	N/A	0.000000	0.035276
25bar 10mm Vertical 8m/s	0.013440	N/A	0.000000	0.027130
25bar 50mm Vertical 2m/s	3.802000	N/A	0.284718	6.188300
25bar 50mm Vertical 5m/s	2.018000	N/A	0.348923	4.396400
25bar 50mm Vertical 8m/s	1.405000	N/A	0.350885	3.469800

B.3 Case 3 – hydrogen gas release from storage tank at 350 bar

The following tables give the results of the 24 release scenarios that were simulated FRED, EFFECTS, PHAST and FLACS.

Mass flow rate (kg/s)

Scenario: **a|b**

a: storage pressure (bar)

b: orifice diameter (mm)

Table B.9: Case 3 – mass flow rate results

Scenario	FRED	EFFECTS	PHAST	FLACS
350bar 1mm orifice diameter	0.012620	0.012467	0.013047	0.013767
350bar 3mm orifice diameter	0.113600	0.112200	0.117424	0.123910
350bar 5mm orifice diameter	0.315500	0.311660	0.326179	0.344180
350bar 10mm orifice diameter	1.262000	1.246700	1.304710	1.376700

For hydrogen gas released at 350 bar, the mass flow rate was calculated using another version of the JET utility program in FLACS to account for the non-ideal behaviour of hydrogen release at high pressures. Table A.11 shows the mass flow rate predicted by the jet utility using ideal gas EOS and Abel-Noble EOS.

Table B.10: Case 3 – FLACS mass flow rate results using ideal gas EOS and Abel-Noble EOS

Scenario	Mass flow rate using ideal gas EOS (kg/s)	Mass flow rate using Abel-Noble EOS (kg/s)
350bar 1mm orifice diameter	0.0137390	0.0137670
350bar 3mm orifice diameter	0.1236520	0.1239100
350bar 5mm orifice diameter	0.3434780	0.3441800
350bar 10mm orifice diameter	1.3739100	1.3767000

Downwind distance to lower flammability limit (LFL) – 4% vol.

Scenario: a|b|c|d

- a: storage pressure (bar)
- b: orifice diameter (mm)
- c: release direction
- d: wind speed (m/s)

Table B.11: Case 3 – downwind distance to LFL results

* *EFFECTS failed to track the rise of the plume and "No Result" could be found.*

Scenario	FRED	EFFECTS	PHAST	FLACS
350bar 1mm Horizontal 2m/s	4.50	14.40	3.94	4.82
350bar 1mm Horizontal 5m/s	4.00	10.10	3.61	4.72
350bar 1mm Horizontal 8m/s	3.50	9.50	3.39	4.52
350bar 3mm Horizontal 2m/s	12.02	44.70	11.18	13.25
350bar 3mm Horizontal 5m/s	11.00	27.00	9.81	12.50
350bar 3mm Horizontal 8m/s	10.00	21.80	8.98	12.10
350bar 5mm Horizontal 2m/s	17.99	85.10	18.13	23.75
350bar 5mm Horizontal 5m/s	16.02	49.20	15.52	22.70
350bar 5mm Horizontal 8m/s	15.01	37.20	14.01	20.75
350bar 10mm Horizontal 2m/s	27.09	115.20	39.63	56.50
350bar 10mm Horizontal 5m/s	34.02	96.30	35.52	69.80
350bar 10mm Horizontal 8m/s	35.01	82.70	31.99	87.50
Scenario	FRED	EFFECTS	PHAST	FLACS
350bar 1mm Vertical 2m/s	0.58	10.70	0.25	0.62
350bar 1mm Vertical 5m/s	0.64	5.40	0.33	0.93
350bar 1mm Vertical 8m/s	0.67	4.00	0.70	0.85
350bar 3mm Vertical 2m/s	1.73	36.50	1.02	2.35
350bar 3mm Vertical 5m/s	1.85	18.30	1.21	3.80
350bar 3mm Vertical 8m/s	1.94	13.30	1.29	4.75
350bar 5mm Vertical 2m/s	2.88	86.10	1.71	4.60
350bar 5mm Vertical 5m/s	3.08	38.30	2.02	6.70
350bar 5mm Vertical 8m/s	3.20	27.00	2.16	8.00
350bar 10mm Vertical 2m/s	5.68	No Result*	3.48	8.10
350bar 10mm Vertical 5m/s	6.05	93.20	4.10	13.10
350bar 10mm Vertical 8m/s	6.08	65.90	4.35	17.00

Downwind distance to half of lower flammability limit (1/2 LFL) – 2% vol.

Scenario: a|b|c|d

- a: storage pressure (bar)
- b: orifice diameter (mm)
- c: release direction
- d: wind speed (m/s)

Table B.12: Case 3 – downwind distance to ½ LFL results

* *EFFECTS failed to track the rise of the plume and "No Result" could be found.*

Scenario	FRED	EFFECTS	PHAST	FLACS
350bar 1mm Horizontal 2m/s	8.00	18.80	7.28	8.15
350bar 1mm Horizontal 5m/s	7.00	11.40	6.24	7.80
350bar 1mm Horizontal 8m/s	6.00	10.10	5.70	7.15
350bar 3mm Horizontal 2m/s	20.02	60.80	19.80	26.65
350bar 3mm Horizontal 5m/s	17.01	35.30	16.13	24.40
350bar 3mm Horizontal 8m/s	15.01	27.40	14.28	21.65
350bar 5mm Horizontal 2m/s	29.06	123.80	35.11	47.25
350bar 5mm Horizontal 5m/s	30.99	67.40	29.05	49.00
350bar 5mm Horizontal 8m/s	27.01	50.20	24.48	68.00
350bar 10mm Horizontal 2m/s	46.75	172.40	71.81	88.40
350bar 10mm Horizontal 5m/s	64.99	134.90	69.87	99.80
350bar 10mm Horizontal 8m/s	69.99	115.20	68.34	128.00
Scenario	FRED	EFFECTS	PHAST	FLACS
350bar 1mm Vertical 2m/s	1.20	16.20	0.78	1.78
350bar 1mm Vertical 5m/s	1.32	8.60	0.95	2.70
350bar 1mm Vertical 8m/s	1.25	6.20	1.39	2.42
350bar 3mm Vertical 2m/s	3.63	53.20	2.45	6.30
350bar 3mm Vertical 5m/s	4.06	27.90	2.84	9.75
350bar 3mm Vertical 8m/s	4.27	20.70	3.09	11.20
350bar 5mm Vertical 2m/s	6.01	126.40	4.05	12.90
350bar 5mm Vertical 5m/s	6.62	57.70	4.69	16.90
350bar 5mm Vertical 8m/s	7.35	42.50	5.17	19.40
350bar 10mm Vertical 2m/s	11.76	No Result*	8.11	21.80
350bar 10mm Vertical 5m/s	12.98	134.00	9.57	33.10
350bar 10mm Vertical 8m/s	14.31	100.00	10.54	45.00

Amount of flammable mass between upper and lower flammability limit (75 - 4% vol.)

Scenario: a|b|c|d

a: storage pressure (bar)

b: orifice diameter (mm)

c: release direction

d: wind speed (m/s)

Table B.13: Case 3 – flammable mass between UFL and LFL results

Scenario	FRED	EFFECTS	PHAST	FLACS
350bar 1mm Horizontal 2m/s	0.001870	N/A	0.000000	0.002813
350bar 1mm Horizontal 5m/s	0.001582	N/A	0.000000	0.002209
350bar 1mm Horizontal 8m/s	0.001291	N/A	0.000000	0.001764
350bar 3mm Horizontal 2m/s	0.049560	N/A	0.030221	0.098725
350bar 3mm Horizontal 5m/s	0.038340	N/A	0.023004	0.071761
350bar 3mm Horizontal 8m/s	0.031630	N/A	0.018731	0.053947
350bar 5mm Horizontal 2m/s	0.225800	N/A	0.137097	0.585130
350bar 5mm Horizontal 5m/s	0.169800	N/A	0.100262	0.436900
350bar 5mm Horizontal 8m/s	0.136800	N/A	0.081634	0.268460
350bar 10mm Horizontal 2m/s	1.219000	N/A	1.272500	5.518900
350bar 10mm Horizontal 5m/s	1.246000	N/A	0.937383	4.297600
350bar 10mm Horizontal 8m/s	1.069000	N/A	0.724132	3.397500
Scenario	FRED	EFFECTS	PHAST	FLACS
350bar 1mm Vertical 2m/s	0.001518	N/A	0.000000	0.002512
350bar 1mm Vertical 5m/s	0.000784	N/A	0.000000	0.001555
350bar 1mm Vertical 8m/s	0.000593	N/A	0.000000	0.001052
350bar 3mm Vertical 2m/s	0.038200	N/A	0.000000	0.076766
350bar 3mm Vertical 5m/s	0.021820	N/A	0.000000	0.052125
350bar 3mm Vertical 8m/s	0.015360	N/A	0.000000	0.040728
350bar 5mm Vertical 2m/s	0.167500	N/A	0.000000	0.372360
350bar 5mm Vertical 5m/s	0.093310	N/A	0.000000	0.251950
350bar 5mm Vertical 8m/s	0.064670	N/A	0.000000	0.194080
350bar 10mm Vertical 2m/s	1.277000	N/A	0.000000	2.648300
350bar 10mm Vertical 5m/s	0.697800	N/A	0.000000	1.897600
350bar 10mm Vertical 8m/s	0.482300	N/A	0.121301	1.614400

Appendix C Results of Sensitivity Study

C.1 Case 1 – hydrogen gas release from storage tank at 5 bar

C.1.1 Base Case 1

Hydrogen gas is hypothetically released from a pressurized storage tank through an orifice on its side. The storage pressure is 5 bar at a temperature of 20 °C. The size of the orifice is 10 mm in diameter with the leak positioned at a height of 2 m above the ground in the positive x-axis direction. For boundary conditions, Pasquill atmospheric stability class D and wind speed of 2 m/s are used. Wind direction is at 270°, in the same direction as that of the leak. The ground is assumed to be an open flat terrain with few obstacles, with roughness length of 0.03 m.

The results are given in tables, graphs and concentration contours:

- Table C.1 gives the mass flow rate.
- Table C.2 gives the downwind distances to LFL and ½ LFL.
- Figure C.1 gives the downwind distance to LFL and ½ LFL.
- Figures C.2, C.3, C.4 and C.5 give the concentration contours plots predicted by FRED, EFFECTS, PHAST and FLACS, respectively.

Table C.1: Base case 1 - mass flow rate results.

	FRED	EFFECTS	PHAST	FLACS
Mass flow rate (kg/s)	0.019590	0.019568	0.019654	0.019627

Table C.2: Base case 1 - distances to LFL and ½ LFL results.

Downwind distance (m)	FRED	EFFECTS	PHAST	FLACS
LFL (40% vol.)	6.01	19.20	5.21	5.75
1/2 LFL (20% vol.)	10.02	26.60	9.25	10.15

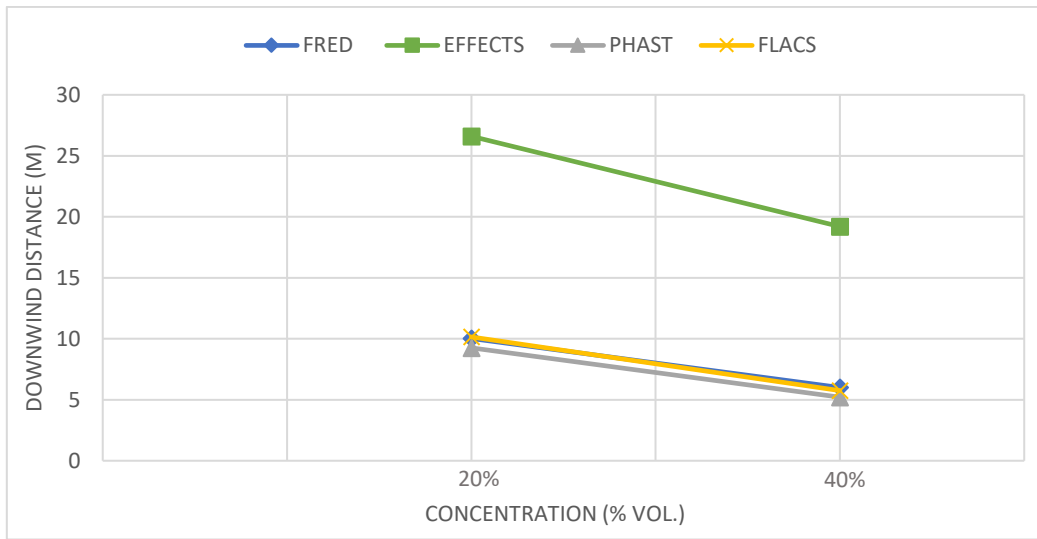


Figure C.1: Base case 1 - distances to LFL and 1/2 LFL for the different tools.

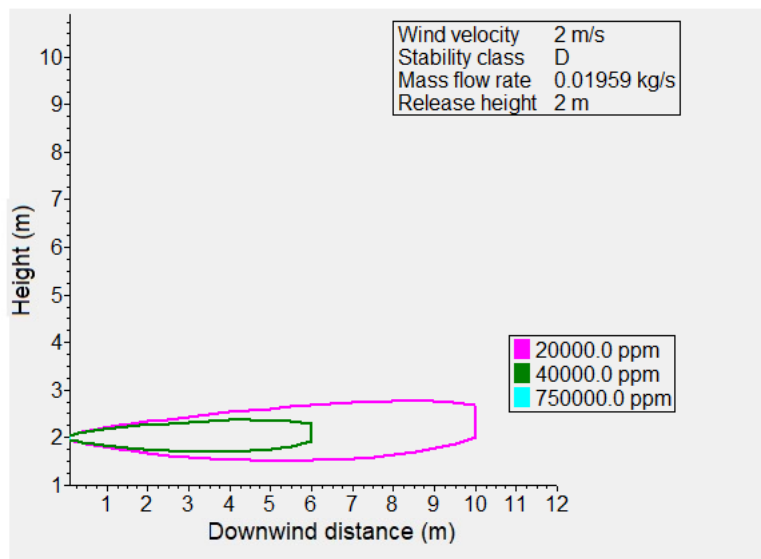


Figure C.2: Base case 1 - concentration contours plot predicted by FRED.

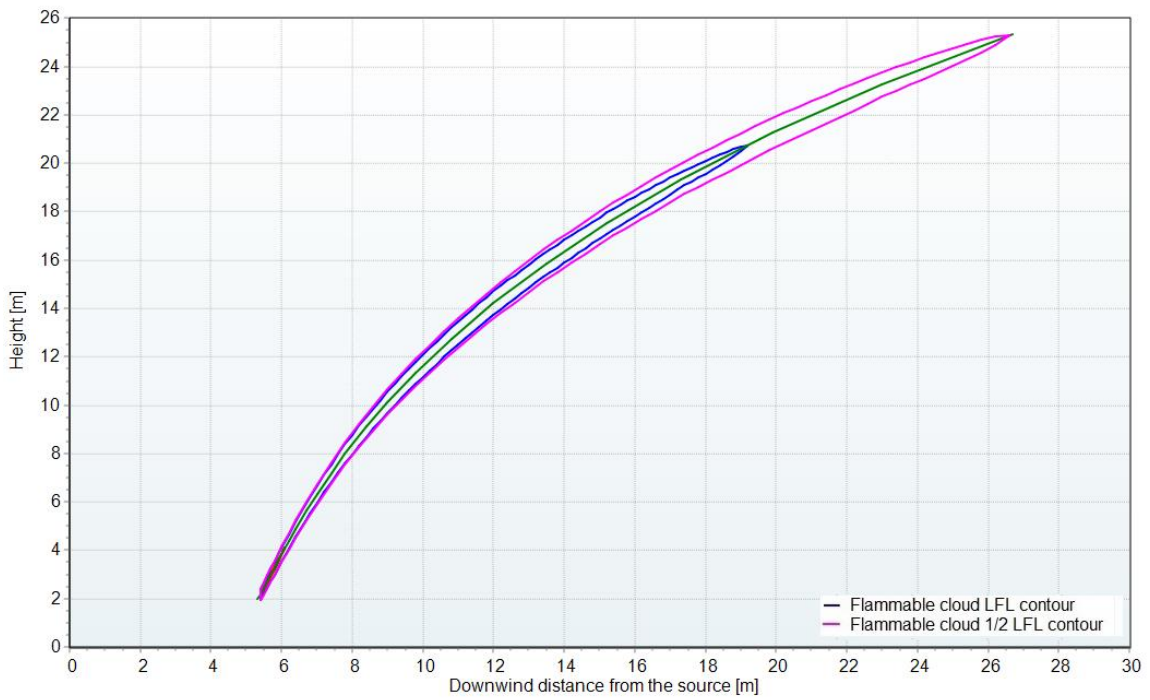


Figure C.3: Base case 1 - concentration contours plot predicted by EFFECTS.

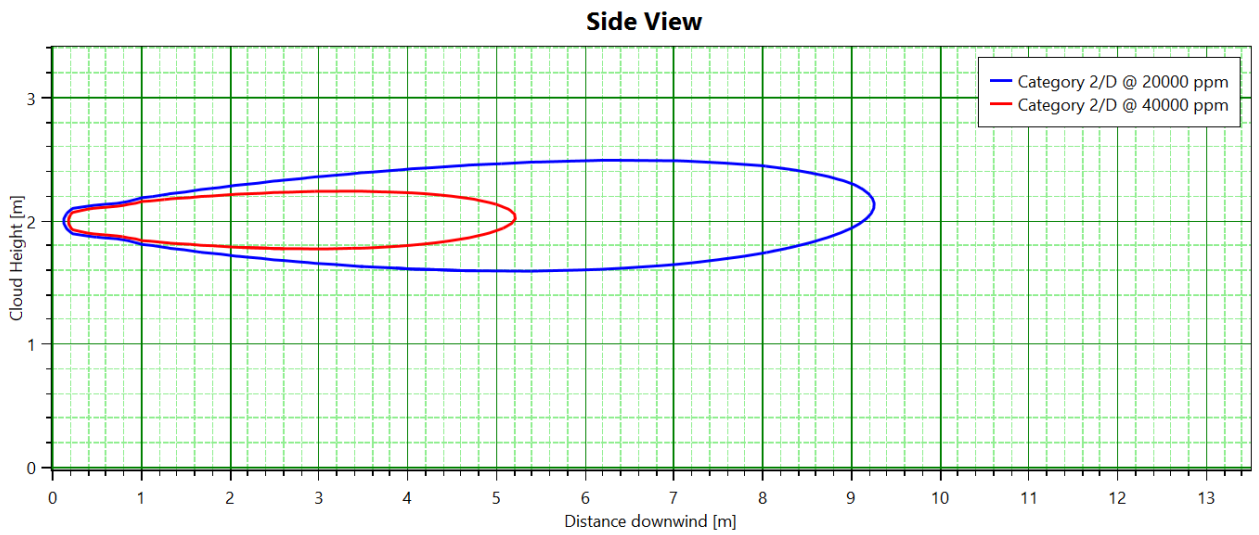


Figure C.4: Base case 1 - concentration contours plot predicted by PHAST.

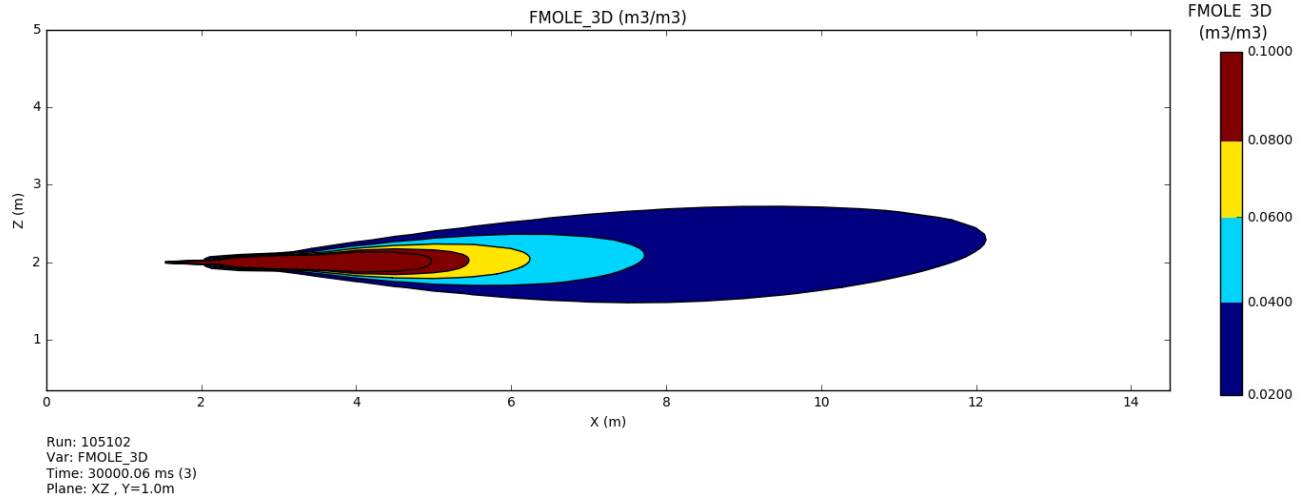


Figure C.5: Base case 1 - concentration contours plot predicted by FLACS.

C.1.2 Effect of orifice size

FRED, EFFECTS, PHAST and FLACS were used to study the effect of orifice size on both the mass flow rate and downwind distances to LFL and ½ LFL. Four leak sizes were used by varying the orifice diameter: 3 mm, 5 mm, 10 mm and 50 mm. The remaining parameters were kept the same as the base case release scenario.

The results are given in tables and graphs:

- Table C.3 gives the mass flow rate for the various orifice sizes.
- Tables C.4, C.5, C.6 and C.7 give the downwind distances to LFL and ½ LFL for orifice sizes of 3 mm, 5 mm, 10 mm and 50 mm, respectively.
- Figure C.6 gives the mass flow rate for the various orifice sizes.
- Figures C.7 and C.8 give, respectively, the downwind distance to LFL and the downwind distance to ½ LFL for the various orifice sizes.

Table C.3: Case 1 - mass flow rate for the various orifice diameters.

Orifice diameter (mm)	Mass flow rate (kg/s)			
	FRED	EFFECTS	PHAST	FLACS
3	0.001763	0.001761	0.001789	0.001766
5	0.004897	0.004892	0.004913	0.004907
10	0.019590	0.019568	0.019654	0.019627
50	0.489700	0.489190	0.491349	0.490683

Table C.4: Case 1 - distances to LFL and ½ LFL for orifice diameter of 3 mm.

Downwind distance (m)	FRED	EFFECTS	PHAST	FLACS
LFL (40% vol.)	2.00	4.00	1.67	2.60
1/2 LFL (20% vol.)	3.50	4.50	3.12	3.80

Table C.5: Case 1 - distances to LFL and 1/2 LFL for orifice diameter of 5 mm.

Downwind distance	FRED	EFFECTS	PHAST	FLACS
LFL (40% vol.)	3.00	8.40	2.71	3.40
1/2 LFL (20% vol.)	5.51	11.10	4.97	5.60

Table C.6: Case 1- distances to LFL and 1/2 LFL for orifice diameter of 10 mm.

Downwind distance	FRED	EFFECTS	PHAST	FLACS
LFL (40% vol.)	6.01	19.20	5.21	5.75
1/2 LFL (20% vol.)	10.02	26.60	9.25	10.15

Table C.7: Case 1 - distances to LFL and 1/2 LFL for orifice diameter of 50 mm.

Downwind distance	FRED	EFFECTS	PHAST	FLACS
LFL (40% vol.)	22.98	72.11	23.56	36.40
1/2 LFL (20% vol.)	37.94	97.42	40.88	56.70

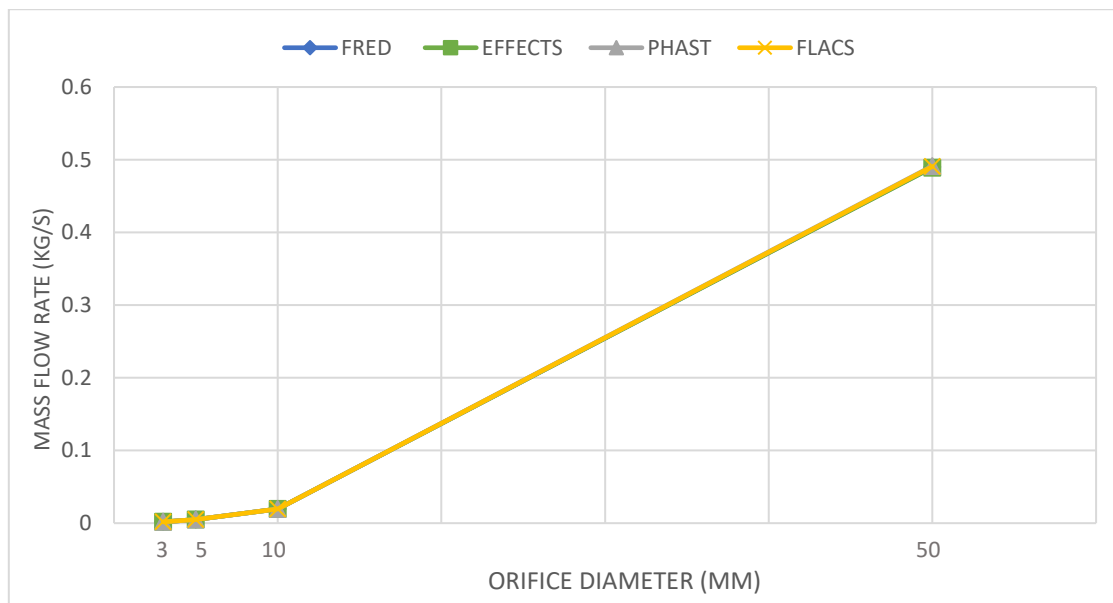


Figure C.6: Case 1 - mass flow rate for the various orifice diameters.

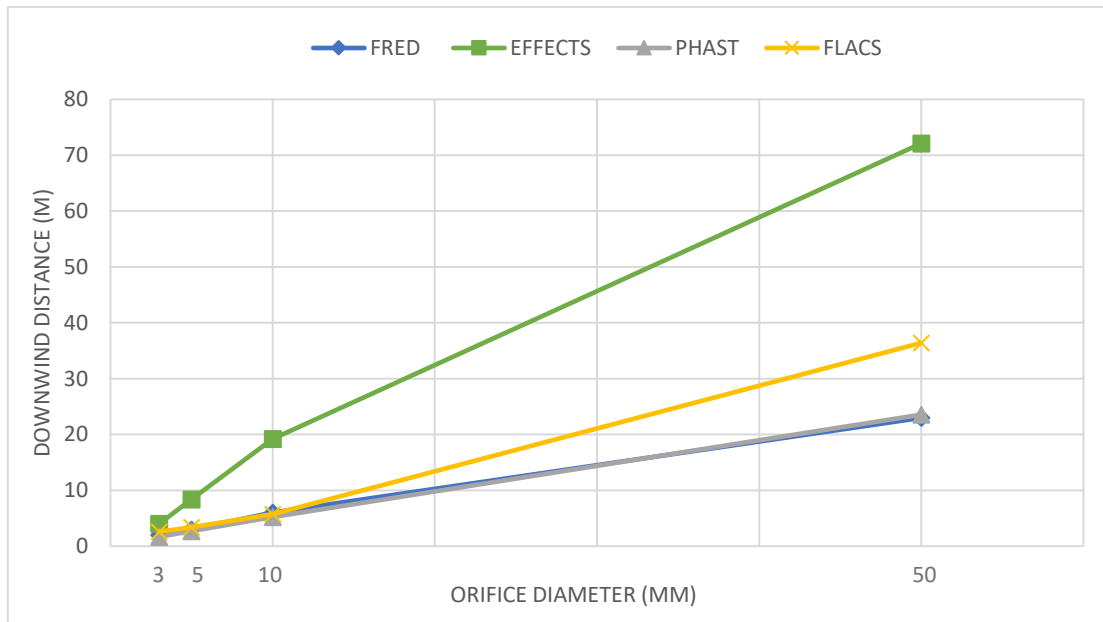


Figure C.7: Case 1 - effect of orifice size on downwind distance to LFL.

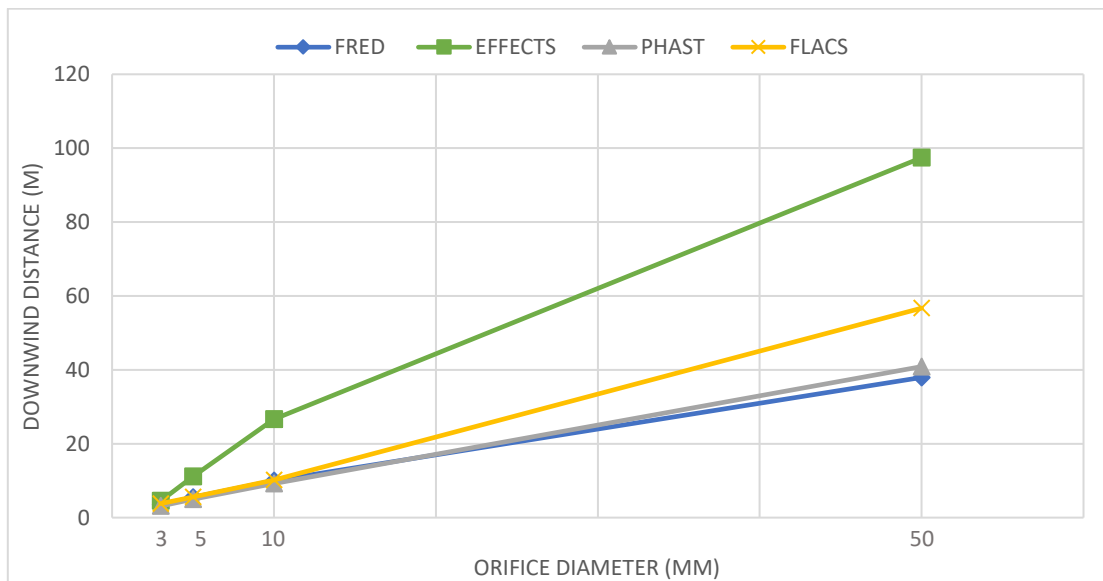


Figure C.8: Case 1 - effect of orifice size on downwind distance to 1/2 LFL.

C.1.3 Effect of release direction

FRED, EFFECTS, PHAST and FLACS were used to study the effect of the release direction of the jet on the downwind distances to LFL and ½ LFL. Both horizontal (+ x-axis direction) and vertical (+z-axis direction) releases were used. The remaining parameters were kept the same as the base case release scenario.

The results are given in tables and graphs:

- Tables C.8 and C.9 give the downwind distances to LFL and ½ LFL for horizontal and vertical jet releases, respectively.
- Figures C.9 and C.10 give, respectively, the downwind distance to LFL and the downwind distance to ½ LFL for both release directions.

Table C.8: Case 1 - distances to LFL and ½ LFL for horizontal jet release.

Downwind distance (m)	FRED	EFFECTS	PHAST	FLACS
LFL (40% vol.)	6.01	19.20	5.21	5.75
1/2 LFL (20% vol.)	10.02	26.60	9.25	10.15

Table C.9: Case 1 - distances to LFL and ½ LFL for vertical jet release.

Downwind distance (m)	FRED	EFFECTS	PHAST	FLACS
LFL (40% vol.)	0.87	17.00	0.48	0.85
1/2 LFL (20% vol.)	1.83	24.70	1.14	2.23

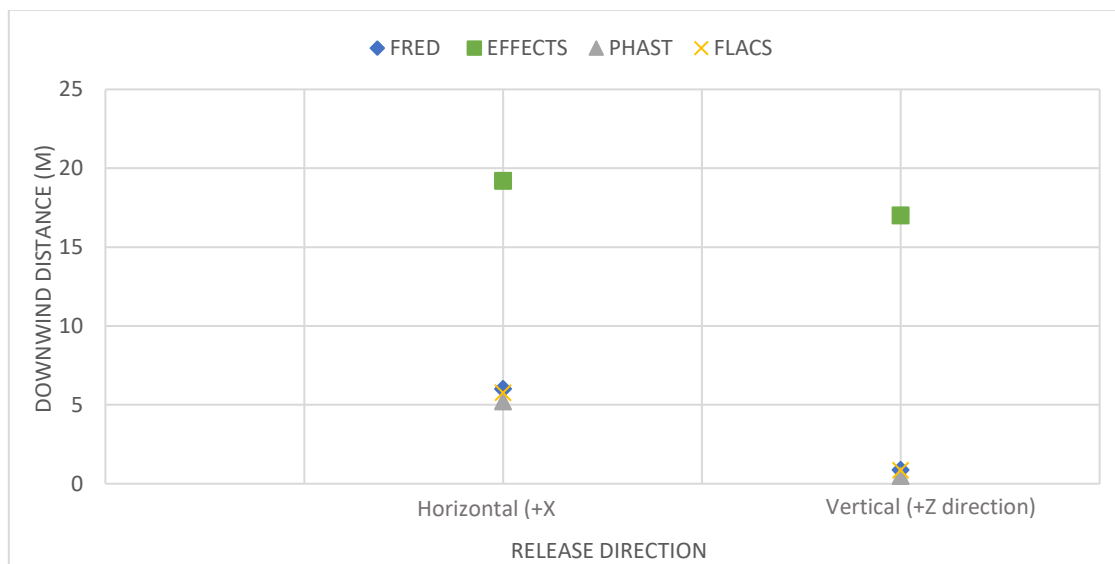


Figure C.9: Case 1 – effect of release direction on downwind distance to LFL.



Figure C.10: Case 1 – effect of release direction on downwind distance to ½ LFL.

C.1.4 Effect of wind speed

FRED, EFFECTS, PHAST and FLACS were used to study the effect of the wind speed on the downwind distances to LFL and ½ LFL. Three wind speeds were used: 2 m/s, 5 m/s and 8 m/s. The remaining parameters were kept the same as the base case release scenario.

The results are given in tables and graphs:

- Tables C.10, C.11 and C.12 give the downwind distances to LFL and ½ LFL for wind speed of 2 m/s, 5 m/s and 8 m/s, respectively.
- Figures C.11 and C.12 give, respectively, the downwind distance to LFL and the downwind distance to ½ LFL for the various wind speeds.

Table C.10: Case1 - distances to LFL and ½ LFL for wind speed of 2 m/s.

Downwind distance (m)	FRED	EFFECTS	PHAST	FLACS
LFL (40% vol.)	6.01	19.20	5.21	5.75
1/2 LFL (20% vol.)	10.02	26.60	9.25	10.15

Table C.11: Case 1 - distances to LFL and ½ LFL for wind speed of 5 m/s.

Downwind distance (m)	FRED	EFFECTS	PHAST	FLACS
LFL (40% vol.)	5.50	10.80	4.64	5.53
1/2 LFL (20% vol.)	9.00	14.80	7.78	9.41

Table C.12: Case 1 - distances to LFL and 1/2 LFL for wind speed of 8 m/s.

Downwind distance (m)	FRED	EFFECTS	PHAST	FLACS
LFL (40% vol.)	5.00	8.50	4.32	5.32
1/2 LFL (20% vol.)	8.00	10.90	7.02	8.48

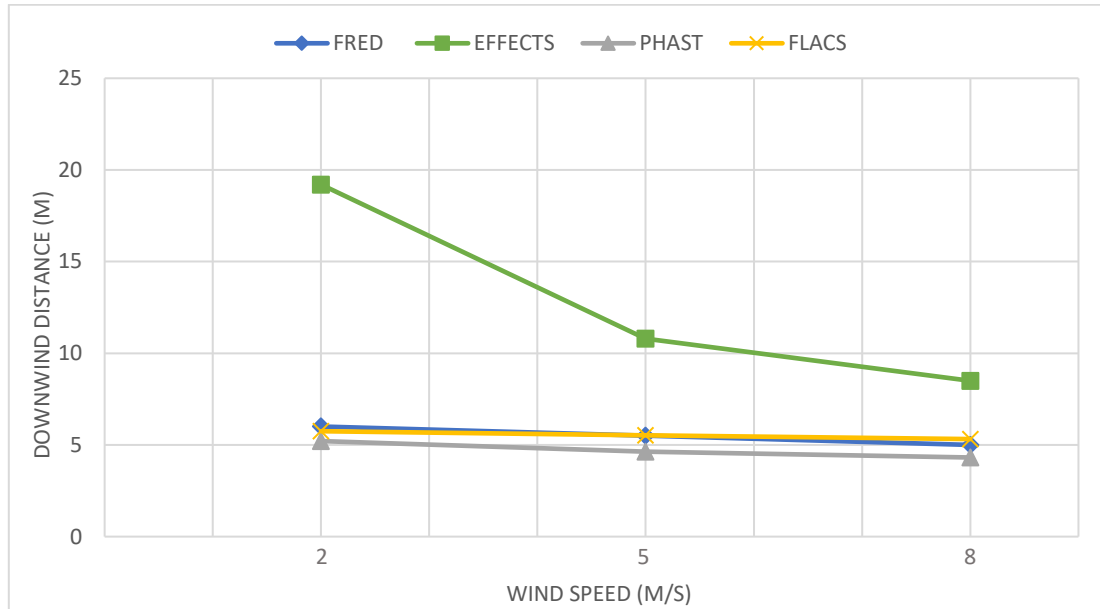


Figure C.11: Case 1 – effect of wind speed on downwind distance to LFL.

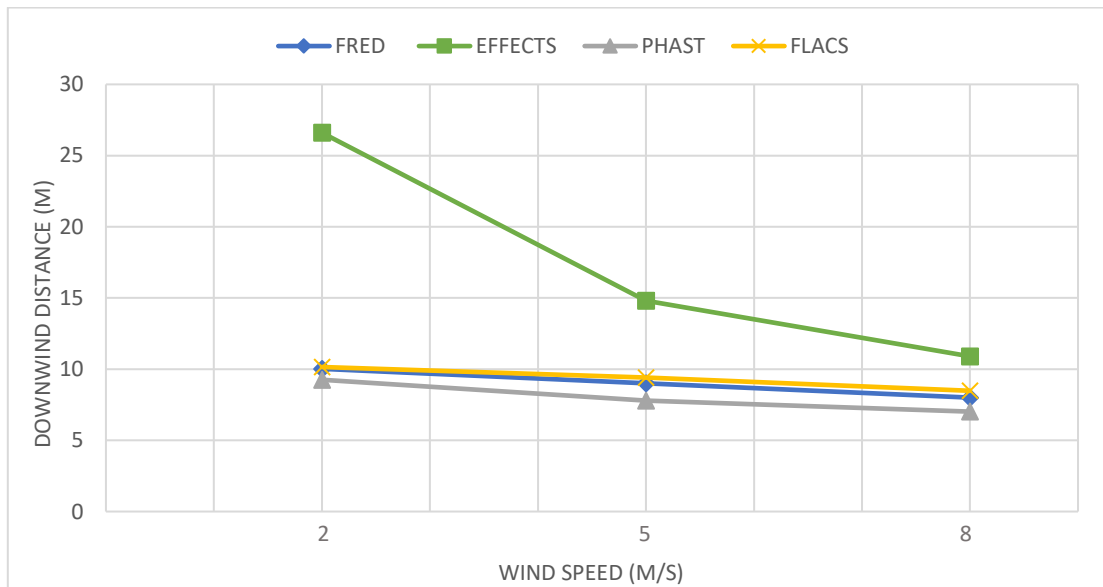


Figure C.12: Case 1 – effect of wind speed on downwind distance to 1/2 LFL.

C.1.5 Effect of stability class

FRED, EFFECTS, PHAST and FLACS were used to study the effect of atmospheric stability class on the downwind distances to LFL and ½ LFL. Atmospheric stability classes D and F were used. The remaining parameters were kept the same as the base case release scenario.

The results are given in tables and graphs:

- Tables C.13 and C.14 give the downwind distances to LFL and ½ LFL for stability classes D and F, respectively.
- Figures C.13 and C.14 give, respectively, the downwind distance to LFL and the downwind distance to ½ LFL for both stability classes.

Table C.13: Case 1 - distances to LFL and ½ LFL for stability class D.

Downwind distance (m)	FRED	EFFECTS	PHAST	FLACS
LFL (40% vol.)	6.01	19.20	5.21	5.75
1/2 LFL (20% vol.)	10.02	26.60	9.25	10.15

Table C.14: Case 1 - distances to LFL and ½ LFL for stability class F.

* *EFFECTS failed to track the rise of the plume and "No Result" could be found.*

Downwind distance (m)	FRED	EFFECTS	PHAST	FLACS
LFL (40% vol.)	6.51	No Result *	4.90	5.80
1/2 LFL (20% vol.)	11.02	No Result *	8.51	10.30

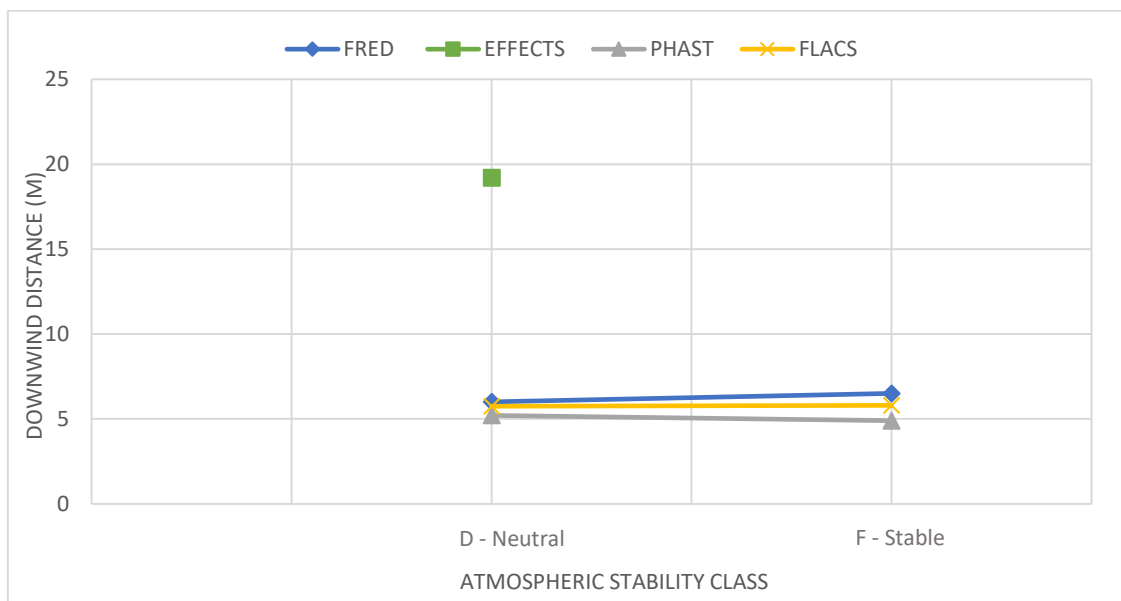


Figure C.13: Case 1 – effect of atmospheric stability class on downwind distance to LFL.

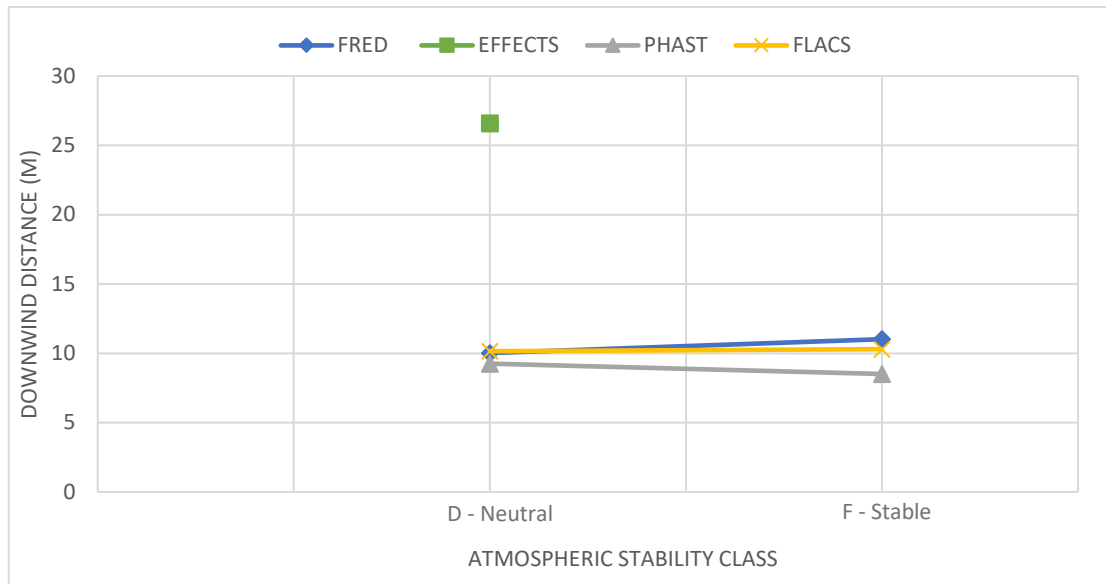


Figure C.14: Case 1 – effect of atmospheric stability class on downwind distance to ½ LFL.

C.1.6 Effect of surface roughness

FRED, EFFECTS, PHAST and FLACS were used to study the effect of the surface roughness length on the downwind distances to LFL and ½ LFL. Three surface roughness lengths were used: 0.005 m, 0.03 m and 0.1 m. The remaining parameters were kept the same as the base case release scenario.

The results are given in tables and graphs:

- Tables C.15, C.16 and C.17 give the downwind distances to LFL and ½ LFL for surface roughness lengths of 0.005 m, 0.03 m and 0.1 m, respectively.
- Figures C.15 and C.16 give, respectively, the downwind distance to LFL and the downwind distance to ½ LFL for the various surface roughness lengths.

Table C.15: Case 1 - distances to LFL and ½ LFL for surface roughness of 0.005 m.

Downwind distance (m)	FRED	EFFECTS	PHAST	FLACS
LFL (40% vol.)	6.51	20.80	5.43	5.75
1/2 LFL (20% vol.)	11.01	29.40	9.95	10.25

Table C.16: Case 1 - distances to LFL and ½ LFL for surface roughness of 0.03 m.

Downwind distance (m)	FRED	EFFECTS	PHAST	FLACS
LFL (40% vol.)	6.01	19.20	5.21	5.75
1/2 LFL (20% vol.)	10.02	26.60	9.25	10.15

Table C.17: Case 1 - distances to LFL and 1/2 LFL for surface roughness of 0.1 m.

Downwind distance (m)	FRED	EFFECTS	PHAST	FLACS
LFL (40% vol.)	6.00	18.20	4.99	5.72
1/2 LFL (20% vol.)	9.51	25.20	8.62	10.05

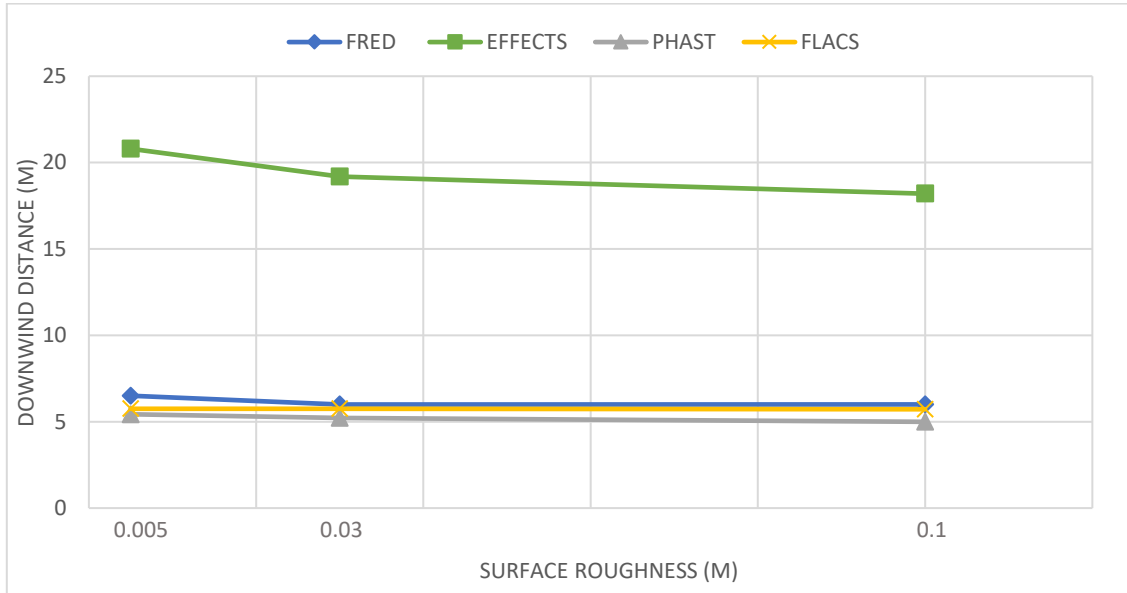


Figure C.15: Case 1 – effect of surface roughness on downwind distance to LFL.

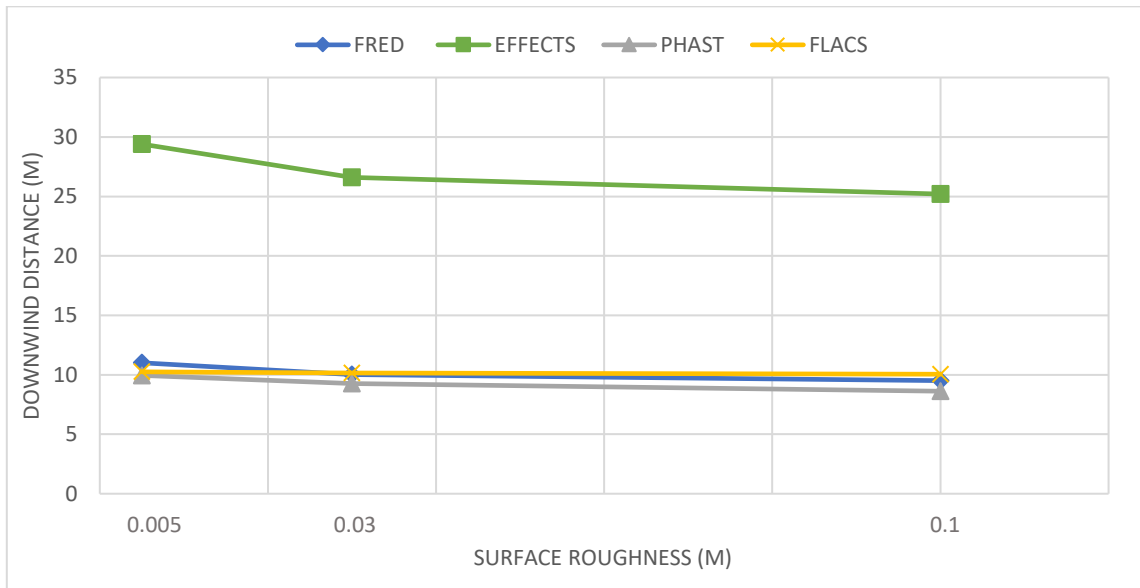


Figure C.16: Case 1 – effect of surface roughness on downwind distance to 1/2 LFL.

C.2 Case 2 – hydrogen gas release from storage tank at 25 bar

C.2.1 Base Case 2

Hydrogen gas is hypothetically released from a pressurized storage tank through an orifice on its side. The storage pressure is 25 bar at a temperature of 20 °C. The size of the orifice is 10 mm in diameter with the leak positioned at a height of 2 m above the ground in the positive x-axis direction. For boundary conditions, Pasquill atmospheric stability class D and wind speed of 2 m/s are used. Wind direction is at 270°, in the same direction as that of the leak. The ground is assumed to be an open flat terrain with few obstacles, with roughness length of 0.03 m.

The results are given in tables, graphs and concentration contours:

- Table C.18 gives the mass flow rate.
- Table C.19 gives the downwind distances to LFL and ½ LFL.
- Figure C.17 gives the downwind distance to LFL and ½ LFL.
- Figures C.18, C.19, C.20 and C.21 give the concentration contours plots predicted by FRED, EFFECTS, PHAST and FLACS, respectively.

Table C.18: Base case 2 – mass flow rate results.

	FRED	EFFECTS	PHAST	FLACS
Mass flow rate (kg/s)	0.097670	0.097255	0.097768	0.098137

Table C.19: Base case 2 – distances to LFL and ½ LFL results.

Downwind distance (m)	FRED	EFFECTS	PHAST	FLACS
LFL (40% vol.)	12.01	46.10	10.59	11.55
1/2 LFL (20% vol.)	19.99	65.20	18.47	23.00

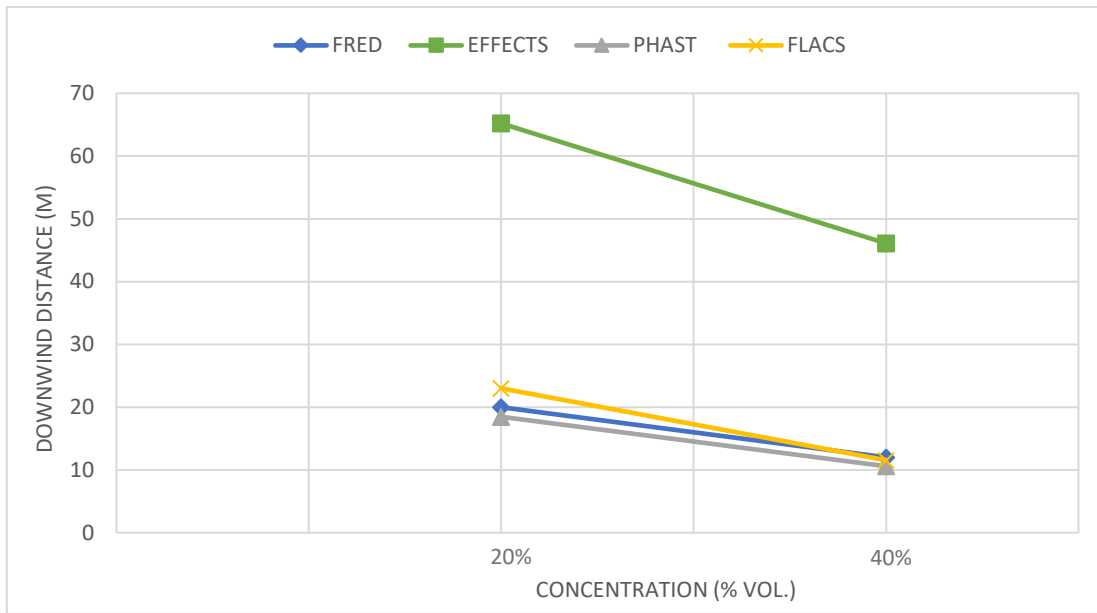


Figure C.17: Base case 2 – distances to LFL and 1/2 LFL for the different tools.

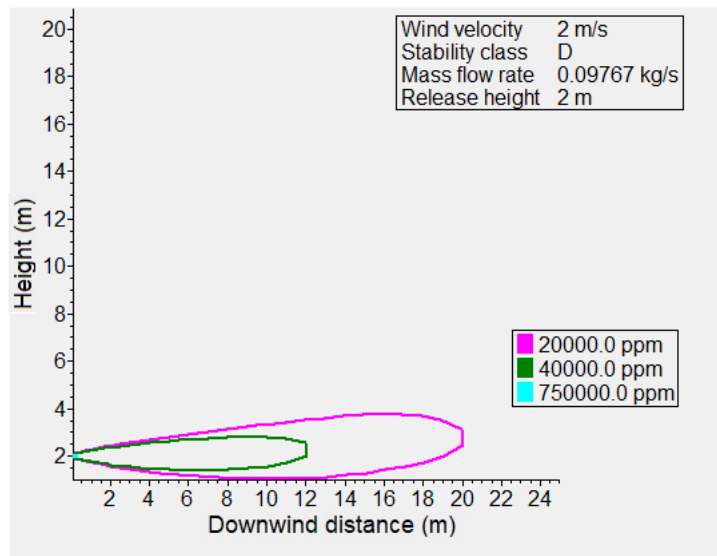


Figure C.18: Base case 2 - concentration contours plot predicted by FRED.

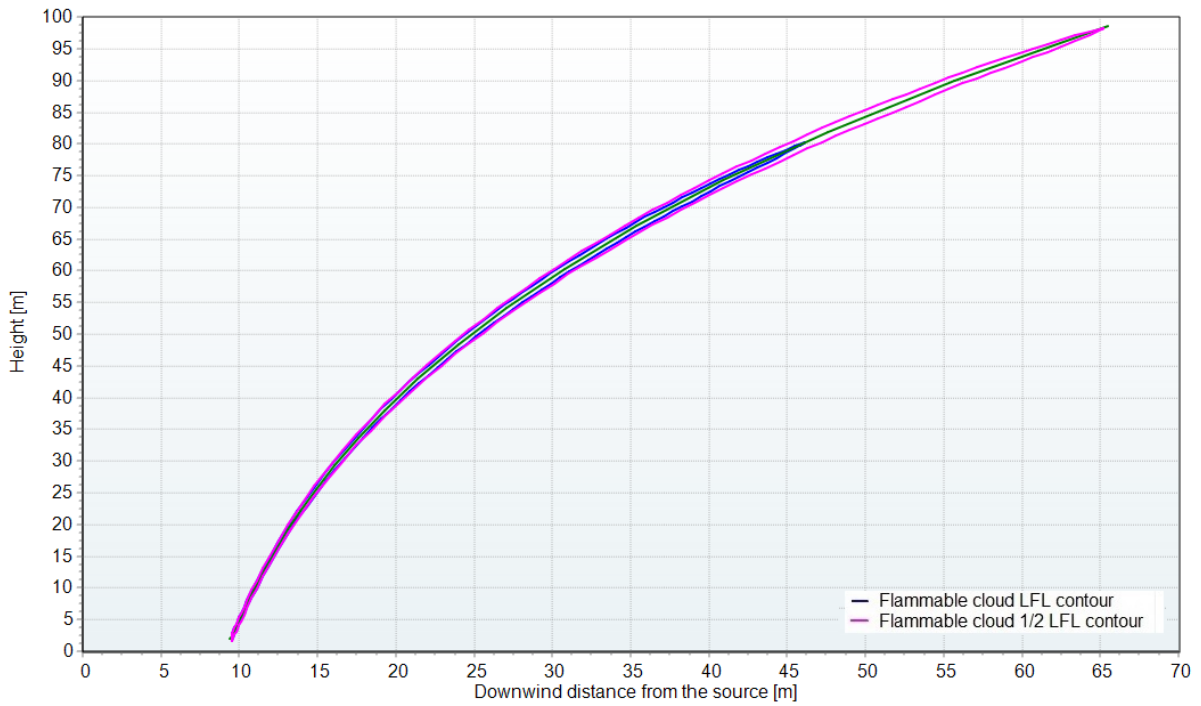


Figure C.19: Base case 2 - concentration contours plot predicted by EFFECTS.

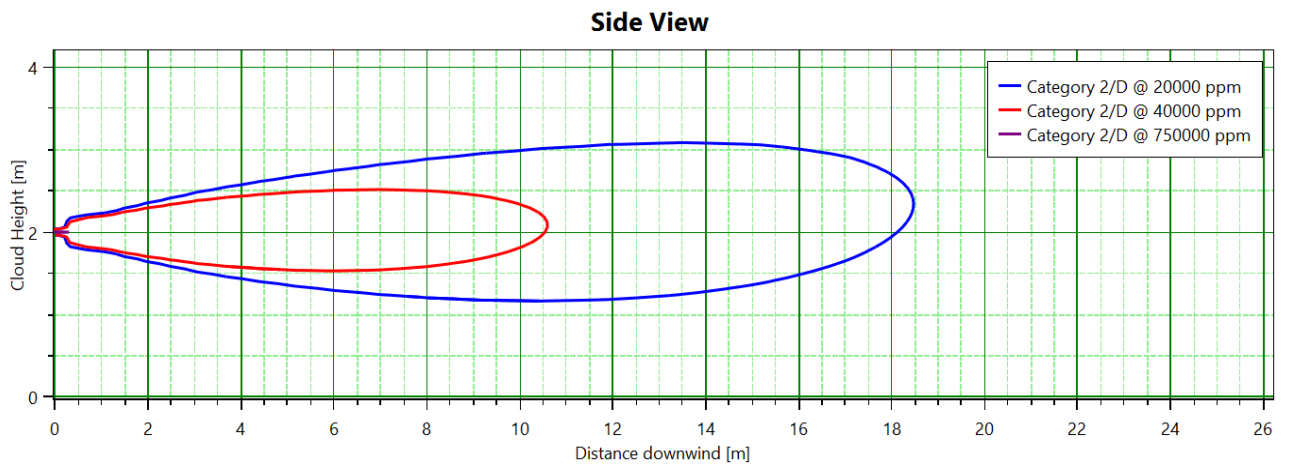


Figure C.20: Base case 2 - concentration contours plot predicted by PHAST.

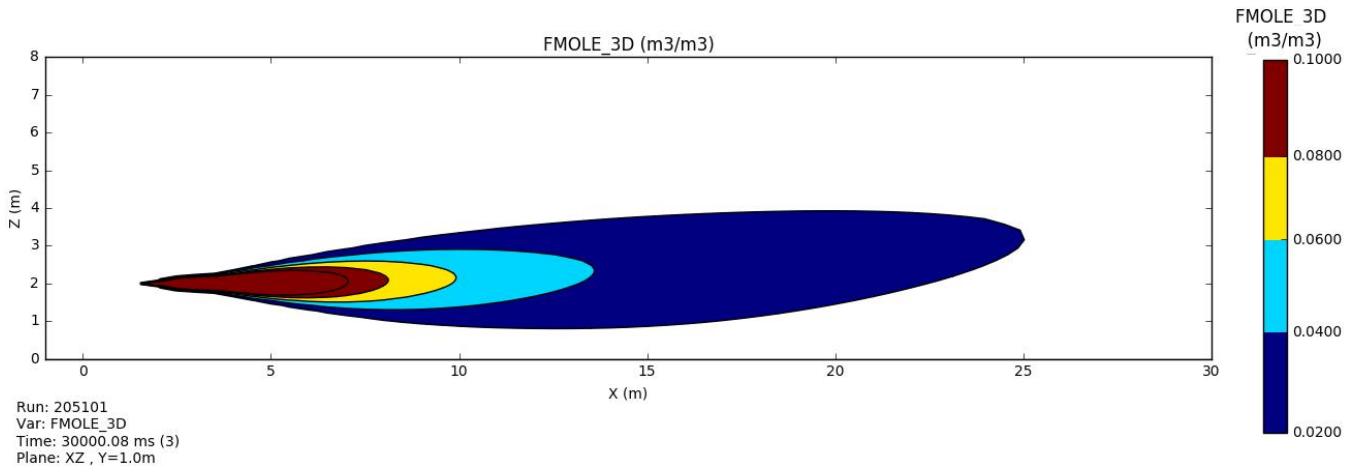


Figure C.21: Base case 2 - concentration contours plot predicted by FLACS.

C.2.2 Effect of orifice size

FRED, EFFECTS, PHAST and FLACS were used to study the effect of orifice size on both the mass flow rate and downwind distances to LFL and 1/2 LFL. Four leak sizes were used by varying the orifice diameter: 3 mm, 5 mm, 10 mm and 50 mm. The remaining parameters were kept the same as the base case release scenario.

The results are given in tables and graphs:

- Table C.20 gives the mass flow rate for the various orifice sizes.
- Tables C.21, C.22, C.23 and C.24 give the downwind distances to LFL and 1/2 LFL for orifice sizes of 3 mm, 5 mm, 10 mm and 50 mm, respectively.
- Figure C.22 gives the mass flow rate for the various orifice sizes.
- Figures C.23 and C.24 give, respectively, the downwind distance to LFL and the downwind distance to 1/2 LFL for the various orifice sizes.

Table C.20: Case 2 - mass flow rate for the various orifice diameters.

Orifice diameter (mm)	Mass flow rate (kg/s)			
	FRED	EFFECTS	PHAST	FLACS
3	0.008790	0.008753	0.008791	0.008832
5	0.024420	0.024314	0.024442	0.024534
10	0.097670	0.097255	0.097768	0.098137
50	2.442000	2.431400	2.444200	2.453410

Table C.21: Case 2 - distances to LFL and 1/2 LFL for orifice diameter of 3 mm.

Downwind distance (m)	FRED	EFFECTS	PHAST	FLACS
LFL (40% vol.)	4.00	10.20	3.38	4.30
1/2 LFL (20% vol.)	7.01	13.30	6.23	7.20

Table C.22: Case 2 - distances to LFL and 1/2 LFL for orifice diameter of 5 mm.

Downwind distance (m)	FRED	EFFECTS	PHAST	FLACS
LFL (40% vol.)	6.50	20.70	5.50	6.10
1/2 LFL (20% vol.)	11.01	28.30	9.91	11.10

Table C.23: Case 2- distances to LFL and 1/2 LFL for orifice diameter of 10 mm.

Downwind distance (m)	FRED	EFFECTS	PHAST	FLACS
LFL (40% vol.)	12.01	46.10	10.59	11.55
1/2 LFL (20% vol.)	19.99	65.20	18.47	23.00

Table C.24: Case 2 - distances to LFL and 1/2 LFL for orifice diameter of 50 mm.

Downwind distance (m)	FRED	EFFECTS	PHAST	FLACS
LFL (40% vol.)	33.98	114.40	49.31	70.30
1/2 LFL (20% vol.)	59.42	163.70	56.66	106.50

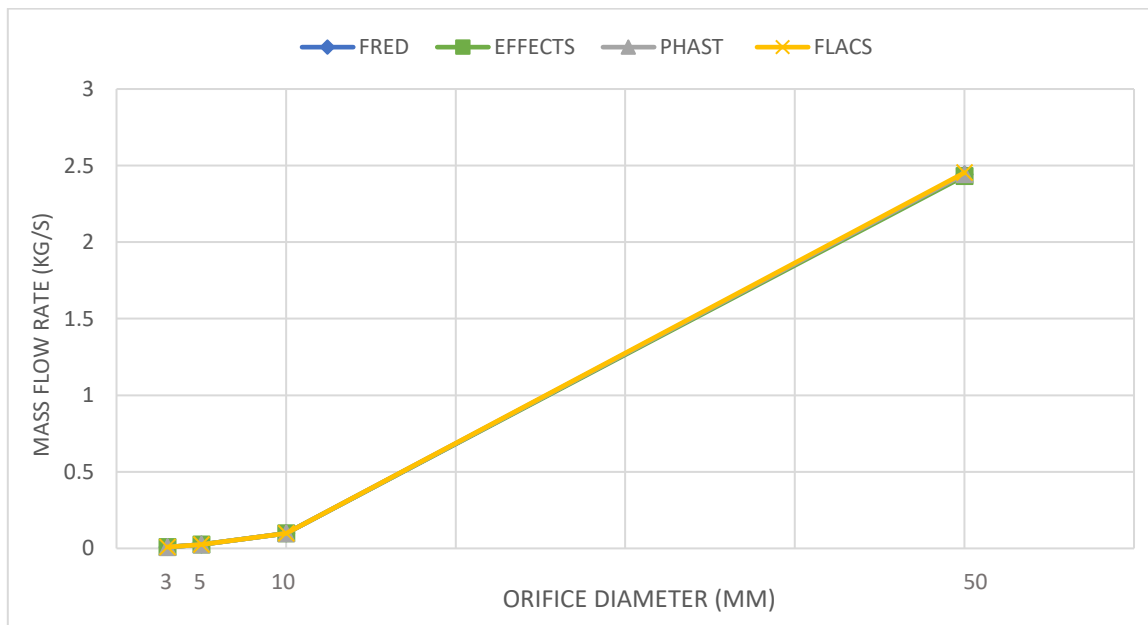


Figure C.22: Case 2 - mass flow rate for the various orifice diameters.

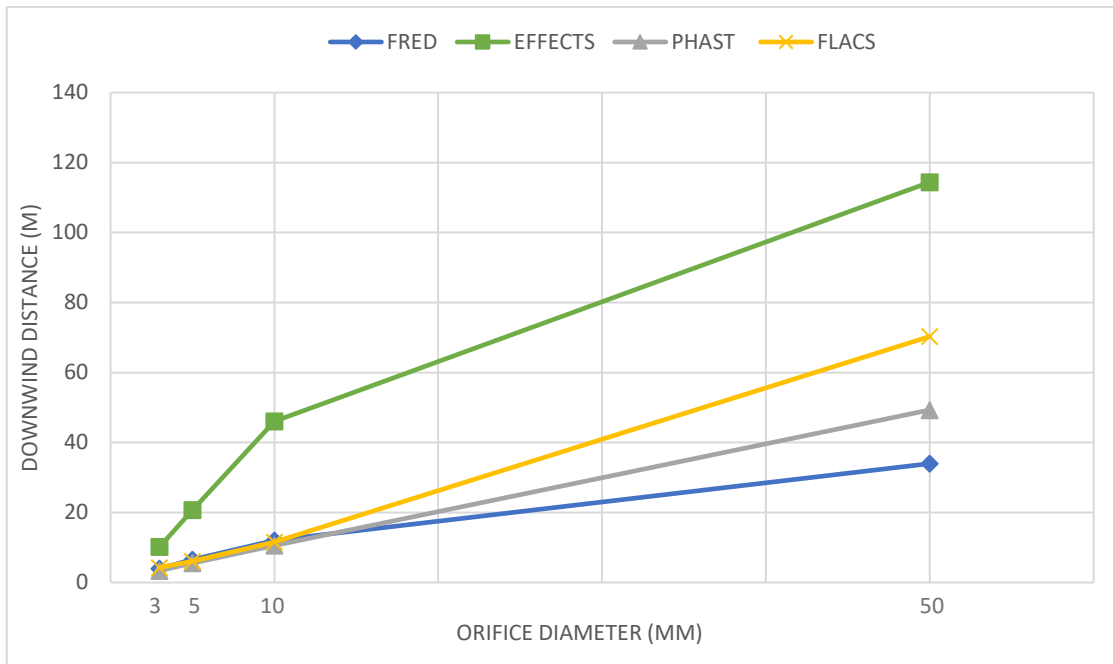


Figure C.23: Case 2 - effect of orifice size on downwind distance to LFL.

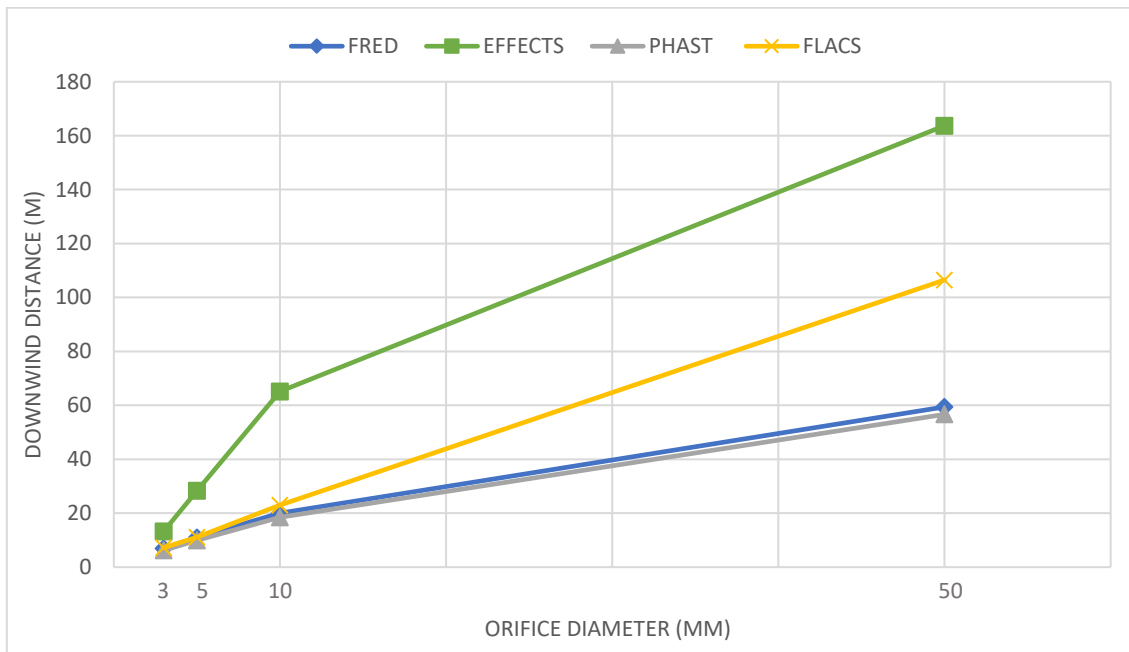


Figure C.24: Case 2 - effect of orifice size on downwind distance to 1/2 LFL.

C.2.3 Effect of release direction

FRED, EFFECTS, PHAST and FLACS were used to study the effect of the release direction of the jet on the downwind distances to LFL and ½ LFL. Both horizontal (+ x-axis direction) and vertical (+z-axis direction) releases were used. The remaining parameters were kept the same as the base case release scenario.

The results are given in tables and graphs:

- Tables C.25 and C.26 give the downwind distances to LFL and ½ LFL for horizontal and vertical jet releases, respectively.
- Figures C.25 and C.26 give, respectively, the downwind distance to LFL and the downwind distance to ½ LFL for both release directions.

Table C.25: Case 2 - distances to LFL and ½ LFL for horizontal jet release.

Downwind distance (m)	FRED	EFFECTS	PHAST	FLACS
LFL (40% vol.)	12.01	46.10	10.59	11.55
1/2 LFL (20% vol.)	19.99	65.20	18.47	23.00

Table C.26: Case 2 - distances to LFL and ½ LFL for vertical jet release.

Downwind distance (m)	FRED	EFFECTS	PHAST	FLACS
LFL (40% vol.)	1.77	43.90	1.00	1.90
1/2 LFL (20% vol.)	3.71	64.50	2.37	5.38

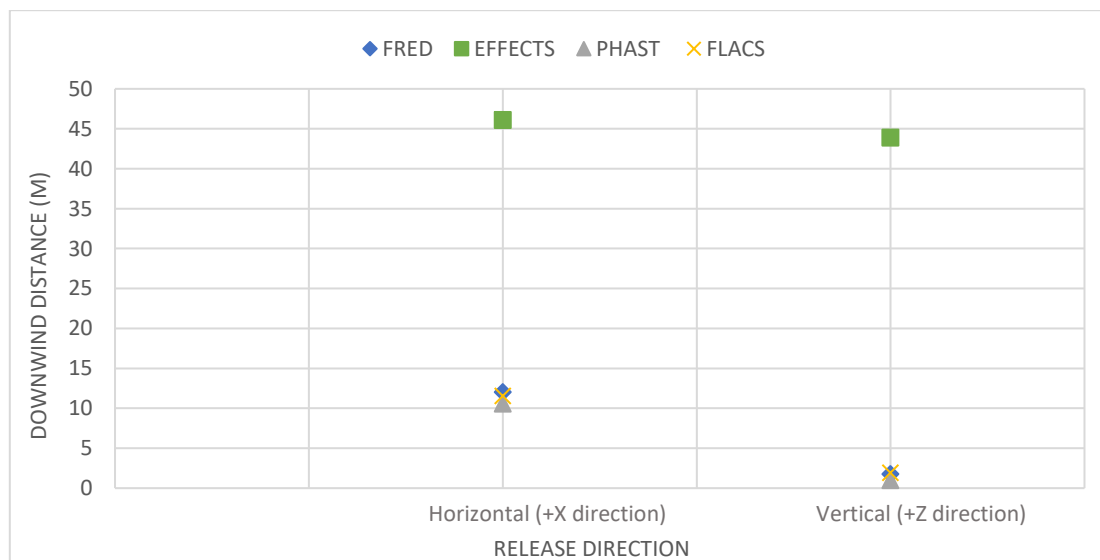


Figure C.25: Case 2 – effect of release direction on downwind distance to LFL.



Figure C.26: Case 2 – effect of release direction on downwind distance to 1/2 LFL.

C.2.4 Effect of wind speed

FRED, EFFECTS, PHAST and FLACS were used to study the effect of the wind speed on the downwind distances to LFL and 1/2 LFL. Three wind speeds were used: 2 m/s, 5 m/s and 8 m/s. The other parameters were kept the same as the base case release scenario.

The results are given in tables and graphs:

- Tables C.27, C.28 and C.29 give the downwind distances to LFL and 1/2 LFL for wind speed of 2 m/s, 5 m/s and 8 m/s, respectively.
- Figures C.27 and C.28 give, respectively, the downwind distance to LFL and the downwind distance to 1/2 LFL for the various wind speeds.

Table C.27: Case 2 - distances to LFL and 1/2 LFL for wind speed of 2 m/s.

Downwind distance (m)	FRED	EFFECTS	PHAST	FLACS
LFL (40% vol.)	12.01	46.10	10.59	11.55
1/2 LFL (20% vol.)	19.99	65.20	18.47	23.00

Table C.28: Case 2 - distances to LFL and 1/2 LFL for wind speed of 5 m/s.

Downwind distance (m)	FRED	EFFECTS	PHAST	FLACS
LFL (40% vol.)	10.01	26.10	9.25	11.10
1/2 LFL (20% vol.)	16.02	36.30	15.06	20.45

Table C.29: Case 2 - distances to LFL and ½ LFL for wind speed of 8 m/s.

Downwind distance (m)	FRED	EFFECTS	PHAST	FLACS
LFL (40% vol.)	9.50	19.50	8.45	10.70
1/2 LFL (20% vol.)	15.00	26.70	13.38	18.80

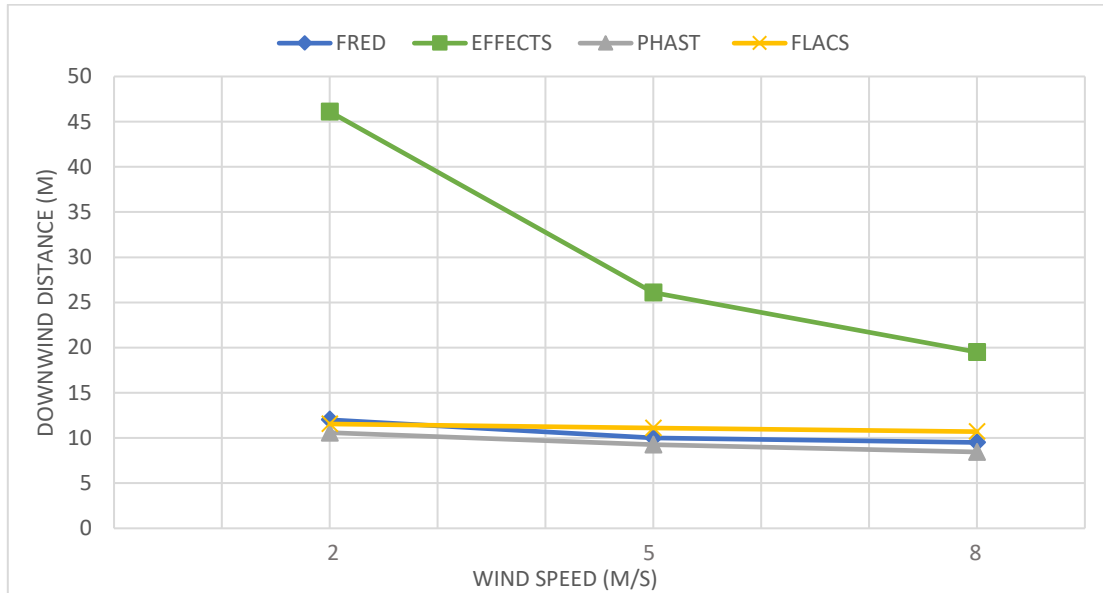


Figure C.27: Case 2 – effect of wind speed on downwind distance to LFL.

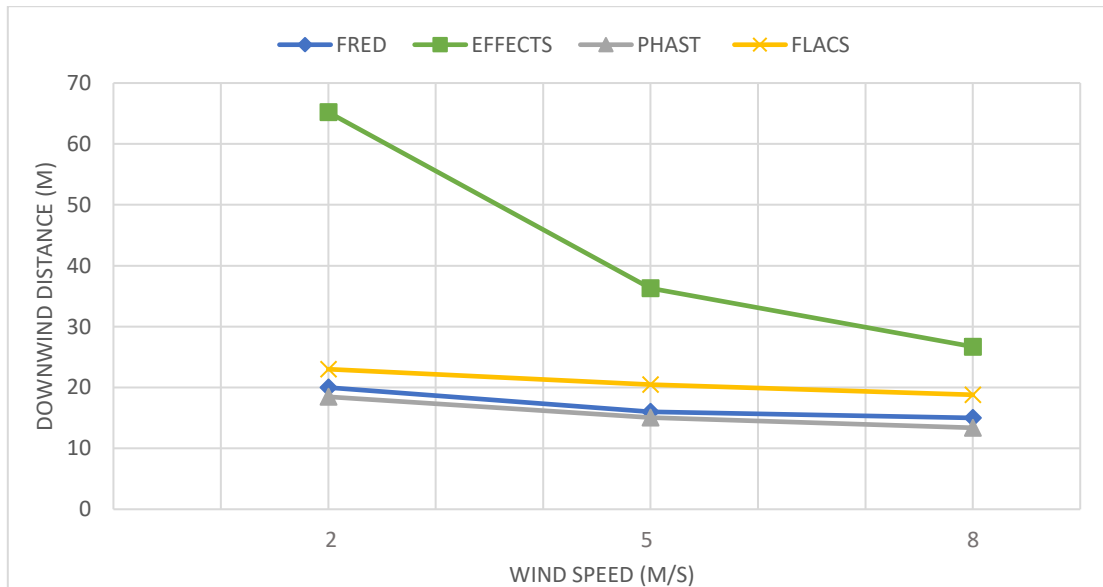


Figure C.28: Case 2 – effect of wind speed on downwind distance to ½ LFL.

C.2.5 Effect of stability class

FRED, EFFECTS, PHAST and FLACS were used to study the effect of atmospheric stability class on the downwind distances to LFL and ½ LFL. Atmospheric stability classes D and F were used. The remaining parameters were kept the same as the base case release scenario.

The results are given in tables and graphs:

- Tables C.30 and C.31 give the downwind distances to LFL and ½ LFL for stability classes D and F, respectively.
- Figures C.29 and C.30 give, respectively, the downwind distance to LFL and the downwind distance to ½ LFL for both stability classes.

Table C.30: Case 2 - distances to LFL and ½ LFL for stability class D.

Downwind distance (m)	FRED	EFFECTS	PHAST	FLACS
LFL (40% vol.)	12.01	46.10	10.59	11.55
1/2 LFL (20% vol.)	19.99	65.20	18.47	23.00

Table C.31: Case 2 - distances to LFL and ½ LFL for stability class F.

* *EFFECTS failed to track the rise of the plume and "No Result" could be found.*

Downwind distance (m)	FRED	EFFECTS	PHAST	FLACS
LFL (40% vol.)	13.01	No Result *	10.06	11.70
1/2 LFL (20% vol.)	22.98	No Result *	17.66	23.50

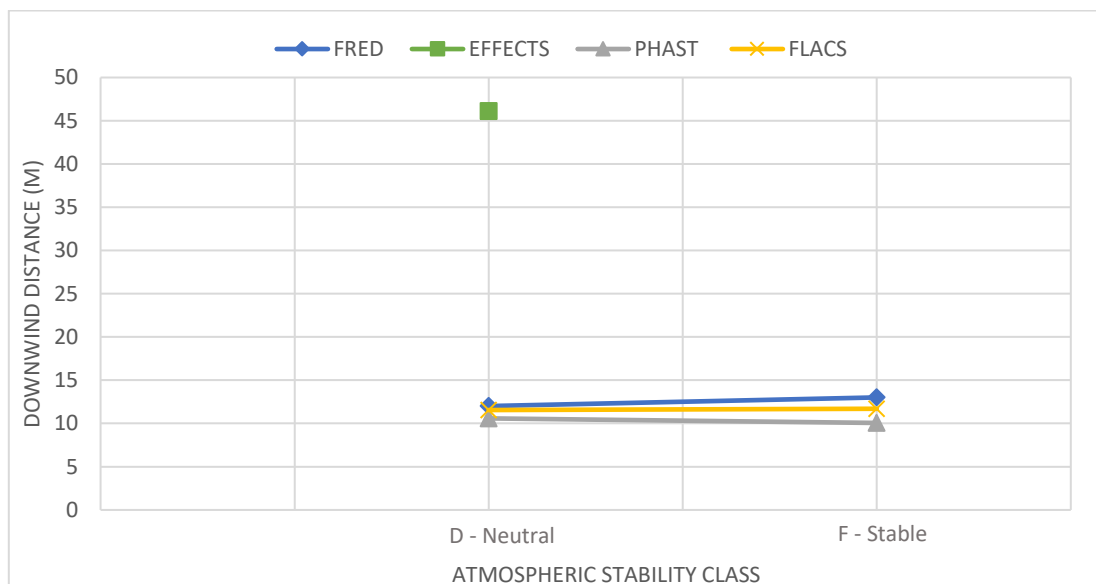


Figure C.29: Case 2 – effect of atmospheric stability class on downwind distance to LFL.

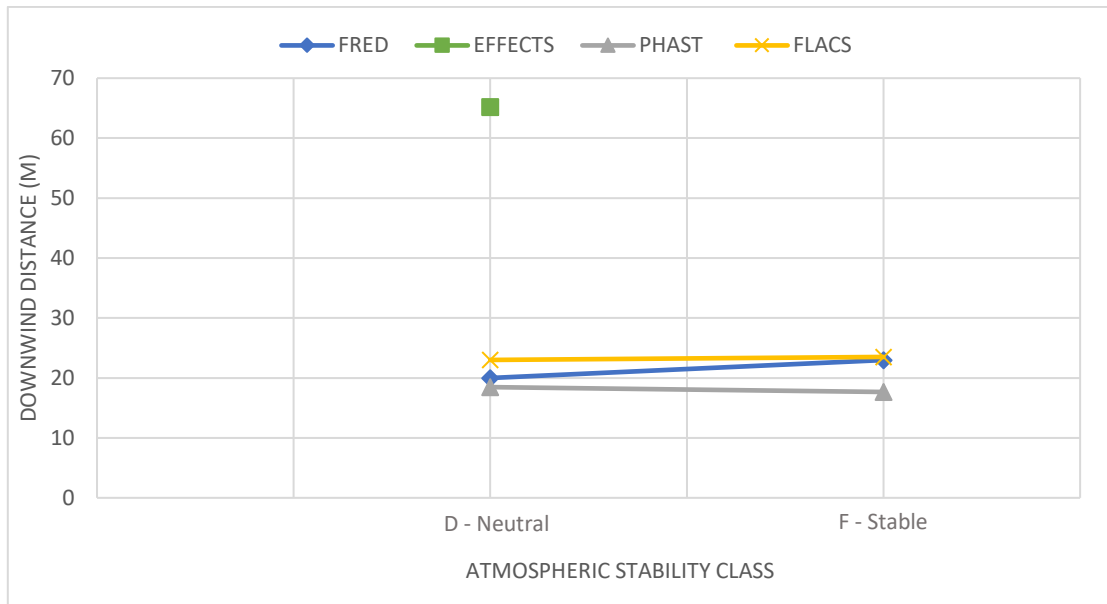


Figure C.30: Case 2 – effect of atmospheric stability class on downwind distance to ½ LFL.

C.2.6 Effect of surface roughness

FRED, EFFECTS, PHAST and FLACS were used to study the effect of the surface roughness length on the downwind distances to LFL and ½ LFL. Three surface roughness lengths were used: 0.005 m, 0.03 m and 0.1 m. The remaining parameters were kept the same as the base case release scenario.

The results are given in tables and graphs:

- Tables C.32, C.33 and C.34 give the downwind distances to LFL and ½ LFL for surface roughness lengths of 0.005 m, 0.03 m and 0.1 m, respectively.
- Figures C.31 and C.32 give, respectively, the downwind distance to LFL and the downwind distance to ½ LFL for the various surface roughness lengths.

Table C.32: Case 2 - distances to LFL and ½ LFL for surface roughness of 0.005 m.

Downwind distance (m)	FRED	EFFECTS	PHAST	FLACS
LFL (40% vol.)	13.00	49.50	11.05	11.60
1/2 LFL (20% vol.)	21.98	71.90	19.81	23.25

Table C.33: Case 2 - distances to LFL and ½ LFL for surface roughness of 0.03 m.

Downwind distance (m)	FRED	EFFECTS	PHAST	FLACS
LFL (40% vol.)	12.01	46.10	10.59	11.55
1/2 LFL (20% vol.)	19.99	65.20	18.47	23.00

Table C.34: Case 2 - distances to LFL and 1/2 LFL for surface roughness of 0.1 m.

Downwind distance (m)	FRED	EFFECTS	PHAST	FLACS
LFL (40% vol.)	11.02	43.70	10.12	11.50
1/2 LFL (20% vol.)	18.02	62.50	17.22	22.70

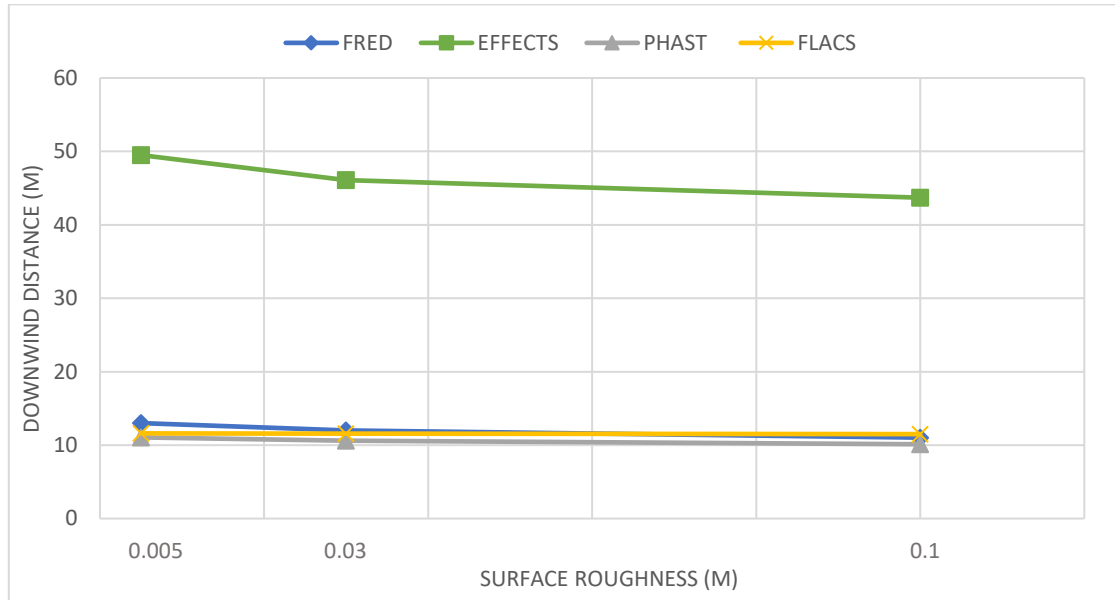


Figure C.31: Case 2 – effect of surface roughness on downwind distance to LFL

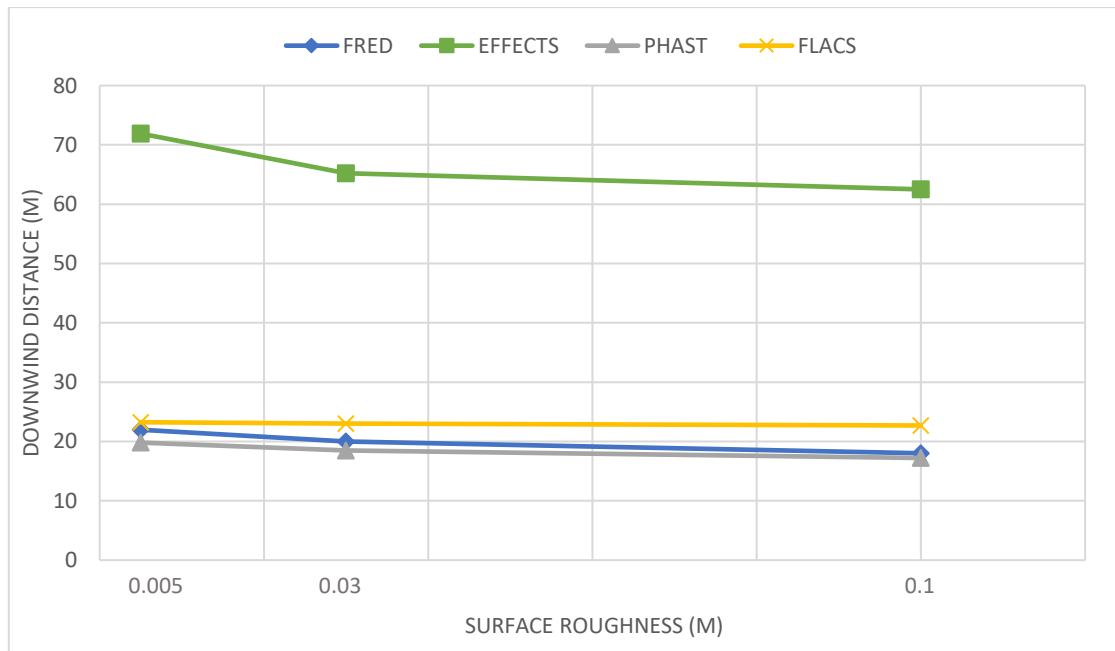


Figure C.32: Case 2 – effect of surface roughness on downwind distance to 1/2 LFL.

C.3 Case 3 – hydrogen gas release from storage tank at 350 bar

C.3.1 Base Case 3

Hydrogen gas is hypothetically released from a pressurized storage tank through an orifice on its side. The storage pressure is 350 bar at a temperature of 20 °C. The size of the orifice is 5 mm in diameter with the leak positioned at a height of 2 m above the ground in the positive x-axis direction. For boundary conditions, Pasquill atmospheric stability class D and wind speed of 2 m/s are used. Wind direction is at 270°, in the same direction as that of the leak. The ground is assumed to be an open flat terrain with few obstacles, with roughness length of 0.03 m.

The results are given in tables, graphs and concentration contours:

- Table C.35 gives the mass flow rate.
- Table C.36 gives the downwind distances to LFL and ½ LFL.
- Figure C.33 gives the downwind distance to LFL and ½ LFL.
- Figures C.34, C.35, C.36 and C.37 give the concentration contours plots predicted by FRED, EFFECTS, PHAST and FLACS, respectively.

Table C.35: Base case 3 - mass flow rate results.

	FRED	EFFECTS	PHAST	FLACS
Mass flow rate (kg/s)	0.315500	0.311660	0.326179	0.344180

Table C.36: Base case 3 - distances to LFL and ½ LFL results.

Downwind distance (m)	FRED	EFFECTS	PHAST	FLACS
LFL (40% vol.)	17.99	85.10	18.13	23.75
1/2 LFL (20% vol.)	29.06	123.80	35.11	47.25

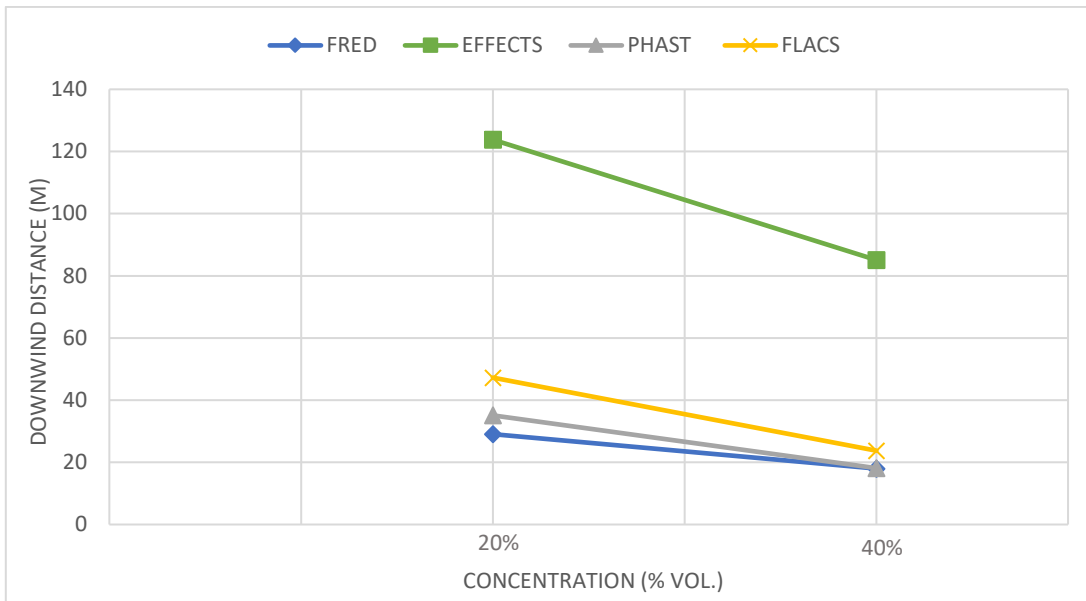


Figure C.33: Base case 3 - distances to LFL and 1/2 LFL for the different tools.

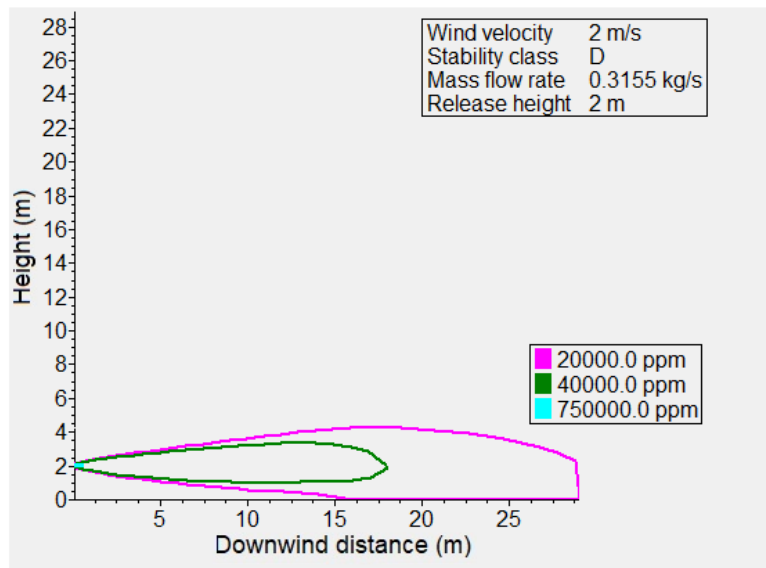


Figure C.34: Base case 3 - concentration contours plot predicted by FRED.

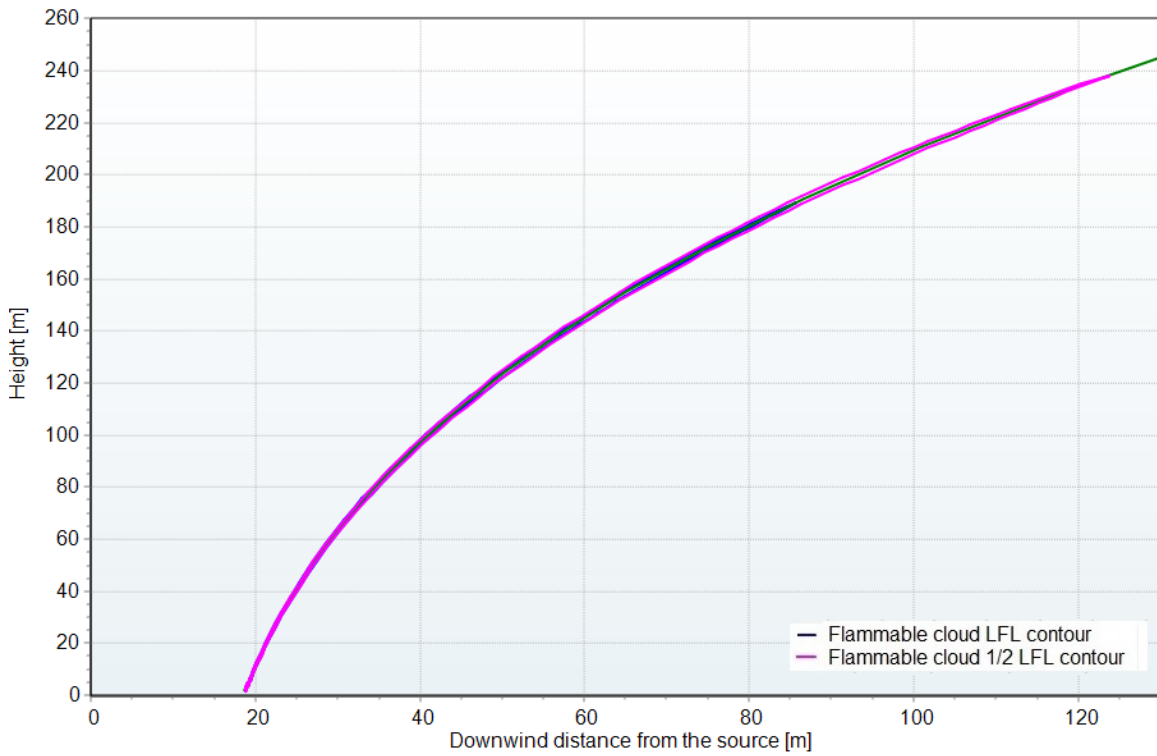


Figure C.35: Base case 3 - concentration contours plot predicted by EFFECTS.



Figure C.36: Base case 3 - concentration contours plot predicted by PHAST.

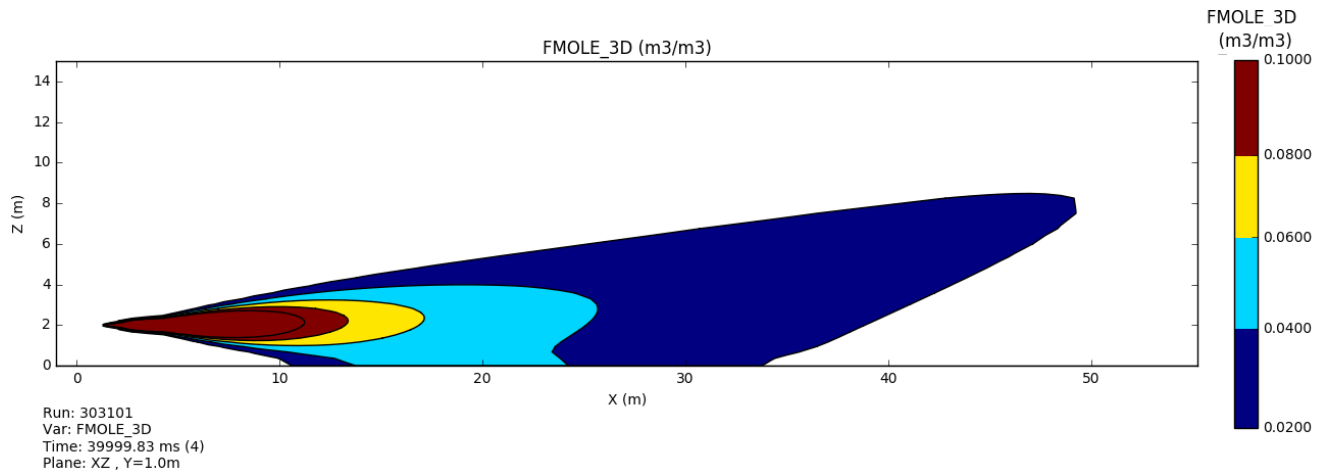


Figure C.37: Base case 3 - concentration contours plot predicted by FLACS.

C.3.2 Effect of orifice size

FRED, EFFECTS, PHAST and FLACS were used to study the effect of orifice size on both the mass flow rate and downwind distances to LFL and ½ LFL. Four leak sizes were used by varying the orifice diameter: 1 mm, 3 mm, 5 mm and 10 mm. The remaining parameters were kept the same as the base case release scenario.

The results are given in tables and graphs:

- Table C.37 gives the mass flow rate for the various orifice sizes.
- Tables C.38, C.39, C.40 and C.41 give the downwind distances to LFL and ½ LFL for orifice sizes of 1 mm, 3 mm, 5 mm and 10 mm, respectively.
- Figure C.38 gives the mass flow rate for the various orifice sizes.
- Figures C.39 and C.40 give, respectively, the downwind distance to LFL and the downwind distance to ½ LFL for the various orifice sizes.

Table C.37: Case 3 - mass flow rate for the various orifice diameters.

Orifice diameter (mm)	Mass flow rate (kg/s)			
	FRED	EFFECTS	PHAST	FLACS
1	0.012620	0.012467	0.013047	0.013767
3	0.113600	0.112200	0.117424	0.123910
5	0.315500	0.311660	0.326179	0.344180
10	1.262000	1.246700	1.304710	1.376700

Table C.38: Case 3 - distances to LFL and ½ LFL for orifice diameter of 1 mm.

Downwind distance	FRED	EFFECTS	PHAST	FLACS
LFL (40% vol.)	4.50	14.40	3.94	4.82
1/2 LFL (20% vol.)	8.00	18.80	7.28	8.15

Table C.39: Case 3 - distances to LFL and 1/2 LFL for orifice diameter of 3 mm.

Downwind distance	FRED	EFFECTS	PHAST	FLACS
LFL (40% vol.)	12.02	44.70	11.18	13.25
1/2 LFL (20% vol.)	20.02	60.80	19.80	26.65

Table C.40: Case 3 - distances to LFL and 1/2 LFL for orifice diameter of 5 mm.

Downwind distance	FRED	EFFECTS	PHAST	FLACS
LFL (40% vol.)	17.99	85.10	18.13	23.75
1/2 LFL (20% vol.)	29.06	123.80	35.11	47.25

Table C.41: Case 3- distances to LFL and 1/2 LFL for orifice diameter of 10 mm.

Downwind distance (m)	FRED	EFFECTS	PHAST	FLACS
LFL (40% vol.)	27.09	115.20	39.63	56.50
1/2 LFL (20% vol.)	46.75	172.40	71.81	88.40

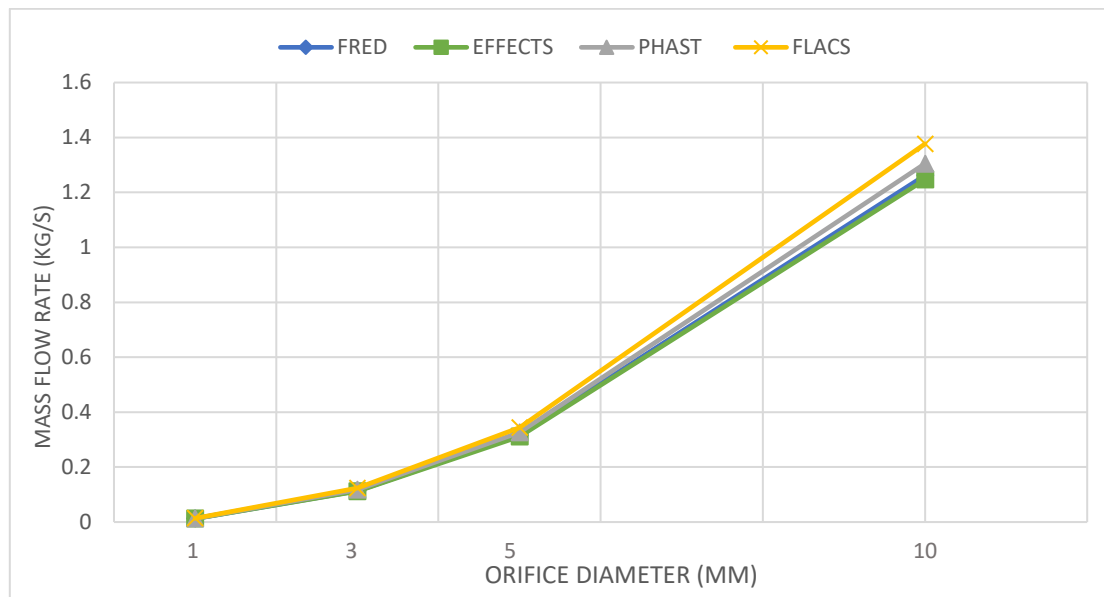


Figure C.38: Case 3 - mass flow rate for the various orifice diameters.

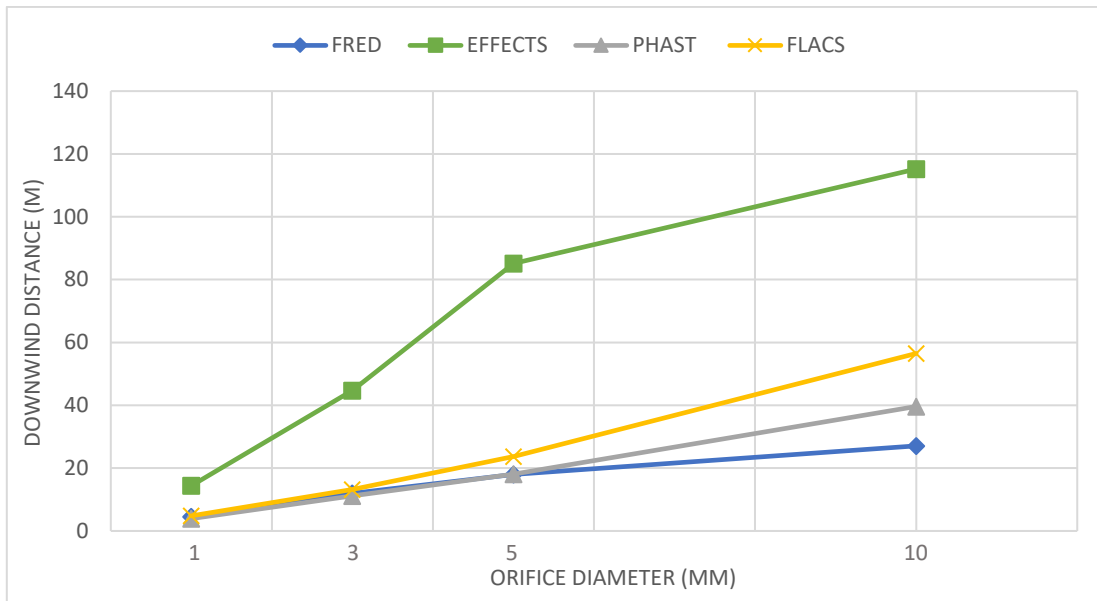


Figure C.39: Case 3 - effect of orifice size on downwind distance to LFL.

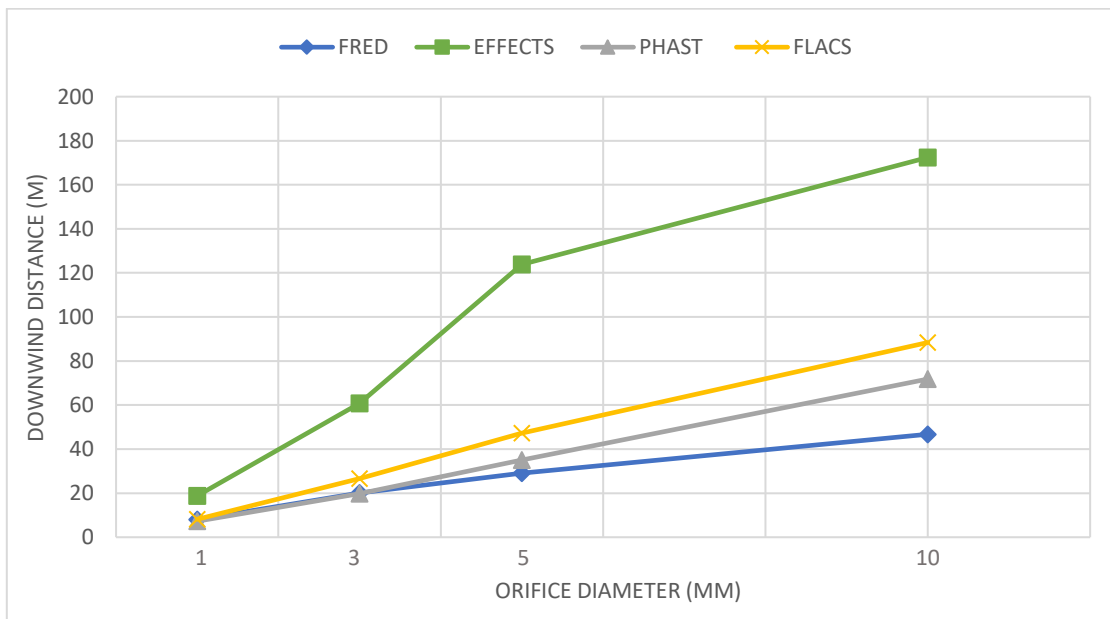


Figure C.40: Case 3 - effect of orifice size on downwind distance to 1/2 LFL.

C.3.3 Effect of release direction

FRED, EFFECTS, PHAST and FLACS were used to study the effect of the release direction of the jet on the downwind distances to LFL and 1/2 LFL. Both horizontal (+ x-axis direction) and vertical (+z-axis direction) releases were used. The remaining parameters were kept the same as the base case release scenario.

The results are given in tables and graphs:

- Tables C.42 and C.43 give the downwind distances to LFL and 1/2 LFL for horizontal and vertical jet releases, respectively.
- Figures C.41 and C.42 give, respectively, the downwind distance to LFL and the downwind distance to 1/2 LFL for both release directions.

Table C.42: Case 3 - distances to LFL and 1/2 LFL for horizontal jet release.

Downwind distance (m)	FRED	EFFECTS	PHAST	FLACS
LFL (40% vol.)	17.99	85.10	18.13	23.75
1/2 LFL (20% vol.)	29.06	123.80	35.11	47.25

Table C.43: Case 3 - distances to LFL and 1/2 LFL for vertical jet release.

Downwind distance (m)	FRED	EFFECTS	PHAST	FLACS
LFL (40% vol.)	2.88	86.10	1.71	4.60
1/2 LFL (20% vol.)	6.01	126.40	4.05	12.90

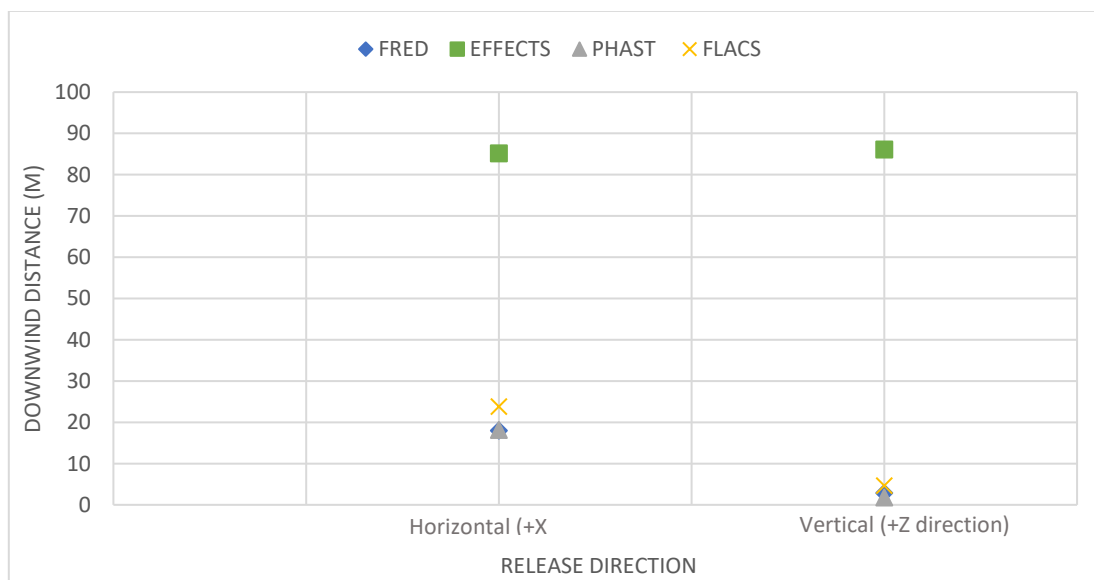


Figure C.41: Case 3 – effect of release direction on downwind distance to LFL.



Figure C.42: Case 3– effect of release direction on downwind distance to 1/2 LFL.

C.3.4 Effect of wind speed

FRED, EFFECTS, PHAST and FLACS were used to study the effect of the wind speed on the downwind distances to LFL and 1/2 LFL. Three wind speeds were used: 2 m/s, 5 m/s and 8 m/s. The other parameters were kept the same as the base case release scenario.

The results are given in tables and graphs:

- Tables C.44, C.45 and C.46 give the downwind distances to LFL and 1/2 LFL for wind speed of 2 m/s, 5 m/s and 8 m/s, respectively.
- Figures C.43 and C.44 give, respectively, the downwind distance to LFL and the downwind distance to 1/2 LFL for the various wind speeds.

Table C.44: Case 3 - distances to LFL and 1/2 LFL for wind speed of 2 m/s.

Downwind distance (m)	FRED	EFFECTS	PHAST	FLACS
LFL (40% vol.)	17.99	85.10	18.13	23.75
1/2 LFL (20% vol.)	29.06	123.80	35.11	47.25

Table C.45: Case 3 - distances to LFL and 1/2 LFL for wind speed of 5 m/s.

Downwind distance (m)	FRED	EFFECTS	PHAST	FLACS
LFL (40% vol.)	16.02	49.20	15.52	22.70
1/2 LFL (20% vol.)	30.99	67.40	29.05	49.00

Table C.46: Case 3 - distances to LFL and 1/2 LFL for wind speed of 8 m/s.

Downwind distance (m)	FRED	EFFECTS	PHAST	FLACS
LFL (40% vol.)	15.01	37.20	14.01	20.75
1/2 LFL (20% vol.)	27.01	50.20	24.48	68.00

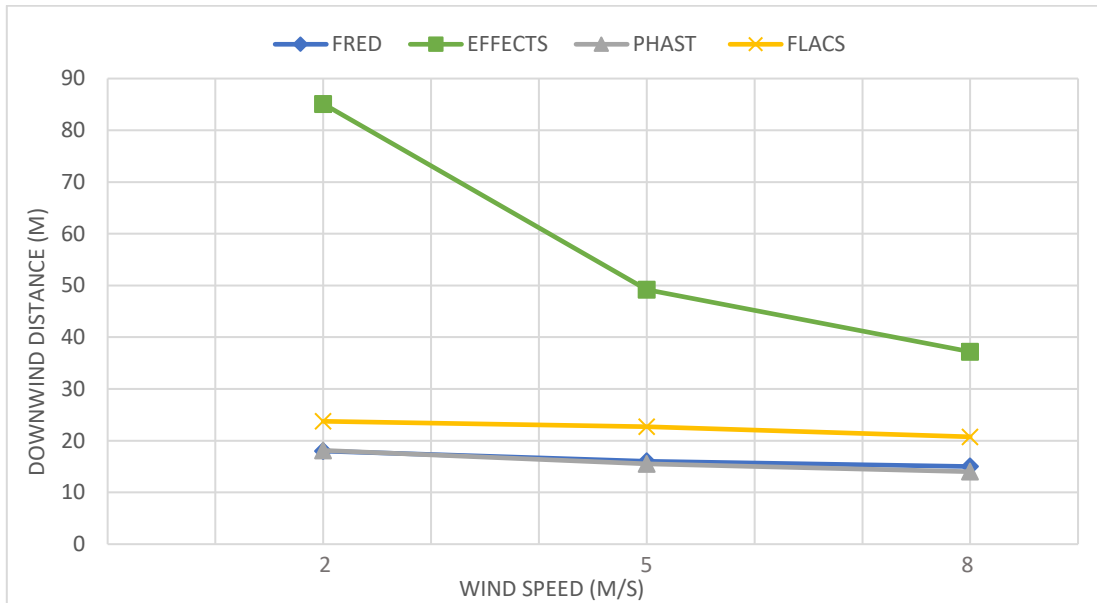


Figure C.43: Case 3 – effect of wind speed on downwind distance to LFL.

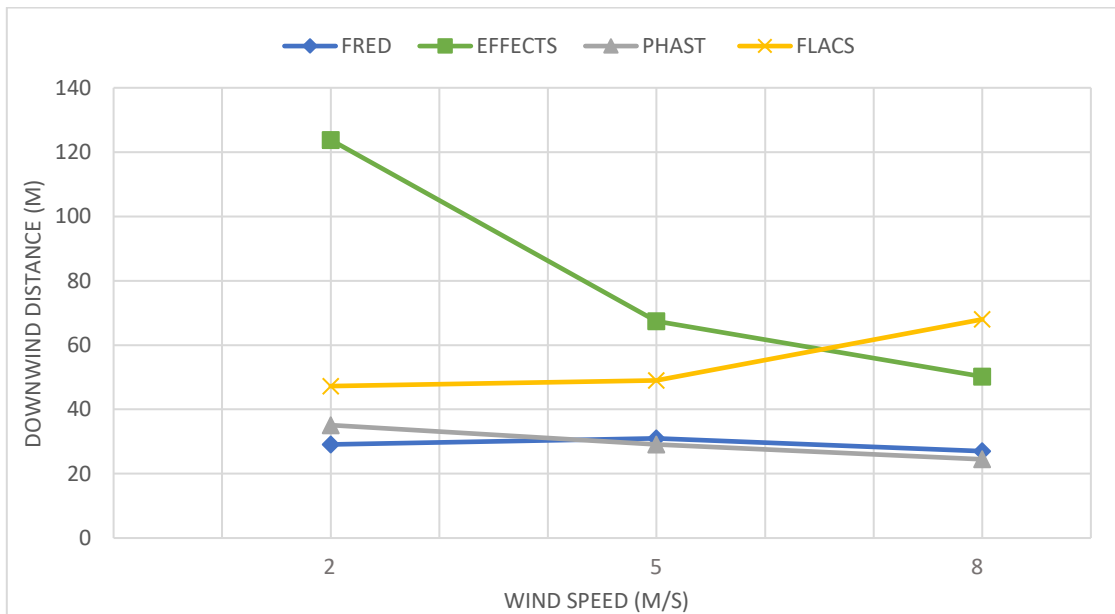


Figure C.44: Case 3 – effect of wind speed on downwind distance to 1/2 LFL.

C.3.5 Effect of stability class

FRED, EFFECTS, PHAST and FLACS were used to study the effect of atmospheric stability class on the downwind distances to LFL and ½ LFL. Atmospheric stability classes D and F were used. The remaining parameters were kept the same as the base case release scenario.

The results are given in tables and graphs:

- Tables C.47 and C.48 give the downwind distances to LFL and ½ LFL for stability classes D and F, respectively.
- Figures C.45 and C.46 give, respectively, the downwind distance to LFL and the downwind distance to ½ LFL for both stability classes.

Table C.47: Case 3 - distances to LFL and ½ LFL for stability class D.

Downwind distance (m)	FRED	EFFECTS	PHAST	FLACS
LFL (40% vol.)	17.99	85.10	18.13	23.75
1/2 LFL (20% vol.)	29.06	123.80	35.11	47.25

Table C.48: Case 3 - distances to LFL and ½ LFL for stability class F.

* *EFFECTS failed to track the rise of the plume and "No Result" could be found.*

Downwind distance (m)	FRED	EFFECTS	PHAST	FLACS
LFL (40% vol.)	18.03	No Result *	17.70	25.10
1/2 LFL (20% vol.)	28.92	No Result *	32.42	47.40

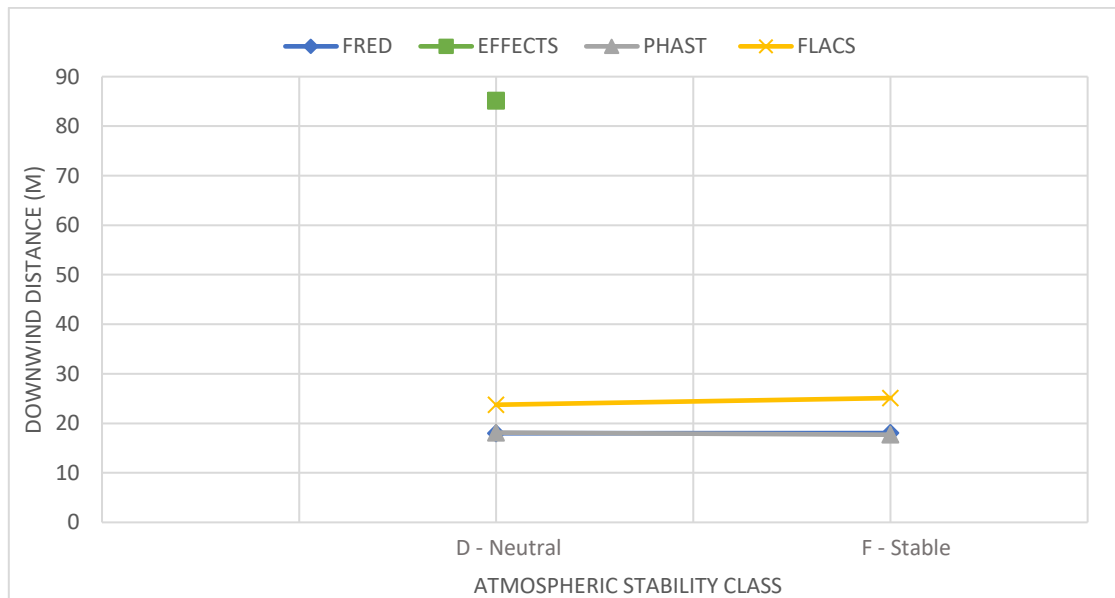


Figure C.45: Case 3 – effect of atmospheric stability class on downwind distance to LFL.

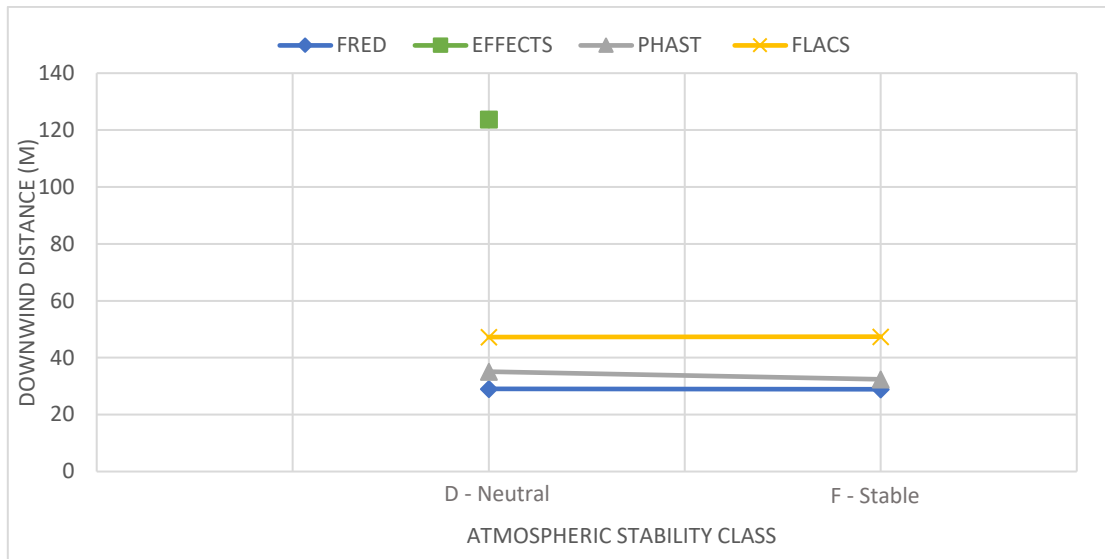


Figure C.46: Case 3 – effect of atmospheric stability class on downwind distance to ½ LFL.

C.3.6 Effect of surface roughness

FRED, EFFECTS, PHAST and FLACS were used to study the effect of the surface roughness length on the downwind distances to LFL and ½ LFL. Three surface roughness lengths were used: 0.005 m, 0.03 m and 0.1 m. The remaining parameters were kept the same as the base case release scenario.

The results are given in tables and graphs:

- Tables C.49, C.50 and C.51 give the downwind distances to LFL and ½ LFL for surface roughness lengths of 0.005 m, 0.03 m and 0.1 m, respectively.
- Figures C.47 and C.48 give, respectively, the downwind distance to LFL and the downwind distance to ½ LFL for the various surface roughness lengths.

Table C.49: Case 3 - distances to LFL and ½ LFL for surface roughness of 0.005 m.

Downwind distance (m)	FRED	EFFECTS	PHAST	FLACS
LFL (40% vol.)	19.01	93.80	18.97	24.70
1/2 LFL (20% vol.)	31.03	135.00	36.79	48.40

Table C.50: Case 3 - distances to LFL and ½ LFL for surface roughness of 0.03 m.

Downwind distance (m)	FRED	EFFECTS	PHAST	FLACS
LFL (40% vol.)	17.99	85.10	18.13	23.75
1/2 LFL (20% vol.)	29.06	123.80	35.11	47.25

Table C.51: Case 3 - distances to LFL and 1/2 LFL for surface roughness of 0.1 m.

Downwind distance (m)	FRED	EFFECTS	PHAST	FLACS
LFL (40% vol.)	16.05	82.20	17.34	24.00
1/2 LFL (20% vol.)	27.97	116.50	33.47	47.00

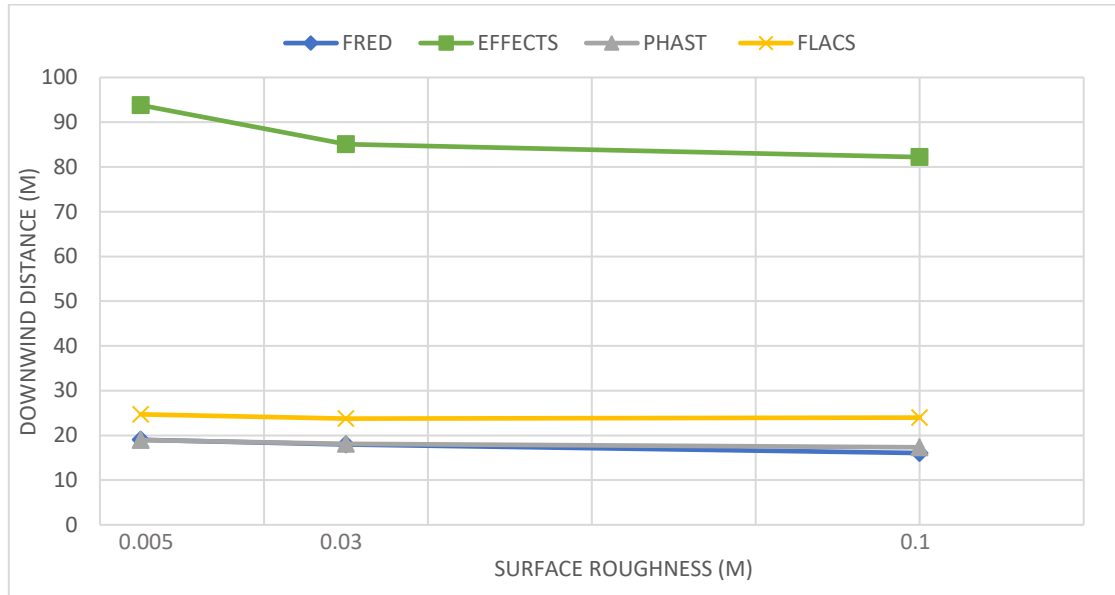


Figure C.47: Case 3 – effect of surface roughness on downwind distance to LFL.

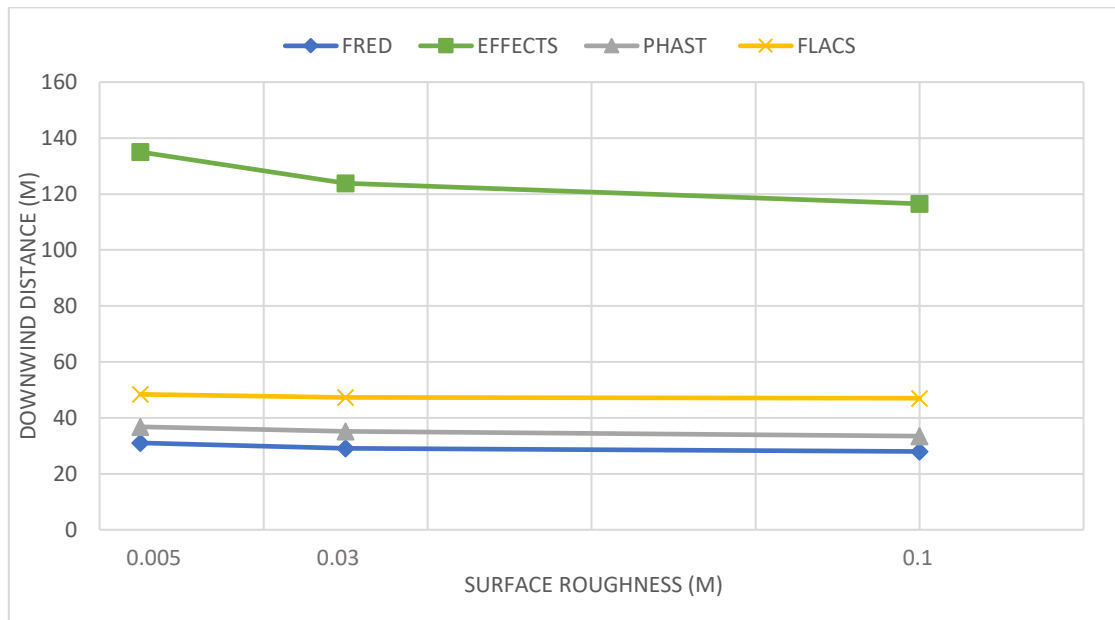


Figure C.48: Case 3 – effect of surface roughness on downwind distance to 1/2 LFL.

Appendix D Simulation Results of Hydrogen Refuelling Gas Station

D.1 Release scenario

Hydrogen gas is hypothetically released from the dispenser through an orifice at an initial pressure of 350 bar and a temperature of 20 °C. The size of the orifice is 3 mm in diameter with the leak in the positive x-axis direction. The release conditions give a mass flow rate of 1.2391 g/s. The release is positioned at a height of 0.9 m above the ground. For boundary conditions, Pasquill atmospheric stability class D and wind speed of 2 m/s and surface roughness length of 0.03 m are used. Wind direction is at 270°, in the same direction as that of the leak.

FLACS was used to study the impact of geometry on the dispersion of the flammable gas cloud. Obstructed release scenario, represented by refuelling gas station, was compared with its corresponding release scenario in an open flat terrain.

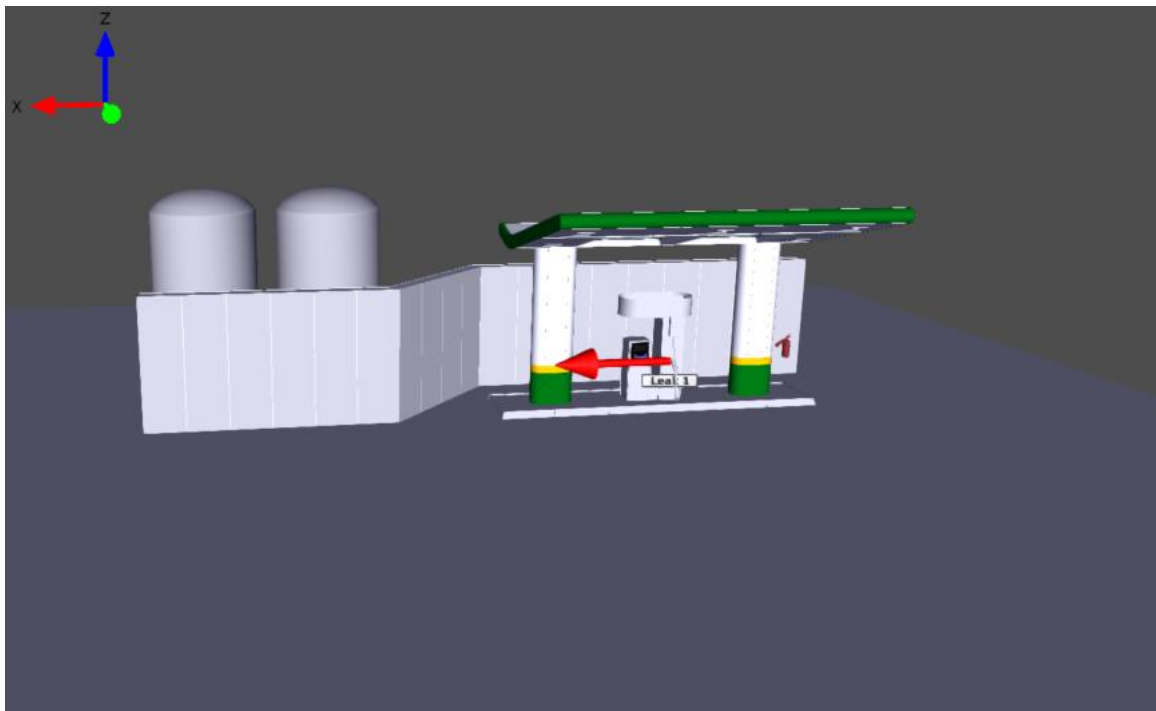


Figure D.1: Hydrogen refuelling gas station.

D.2 Results of dispersion simulations

The results are given in tables, graphs and concentration contours:

- Table D.1 gives the downwind distances to LFL and ½ LFL, and the amount of flammable mass between UFL and LFL.
- Figure D.2 gives the downwind distances to LFL and ½ LFL.
- Figure D.3 and D.4 give the flammable gas concentration contours the refuelling gas station release scenario.
- Figure D.5 gives the flammable gas concentration contours for the release scenario in open flat terrain.

Table D.1: Downwind distances to LFL and ½ LFL.

	Without geometry (open flat terrain)	With geometry (refuelling gas station)
Downwind distance to LFL (m)	30.2	15.6
Downwind distance to 1/2 LFL (m)	44.2	19.95
Amount of flammable mass between UFL and LFL (kg)	0.15292	0.40587

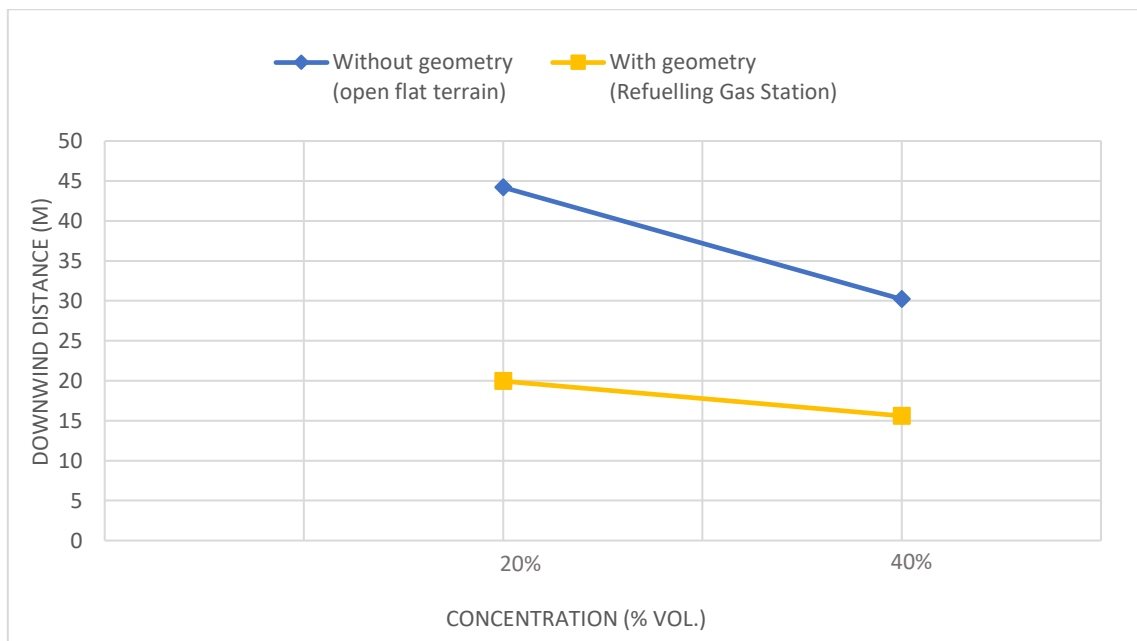


Figure D.2: Effect of geometry on downwind distances to LFL and ½ LFL.

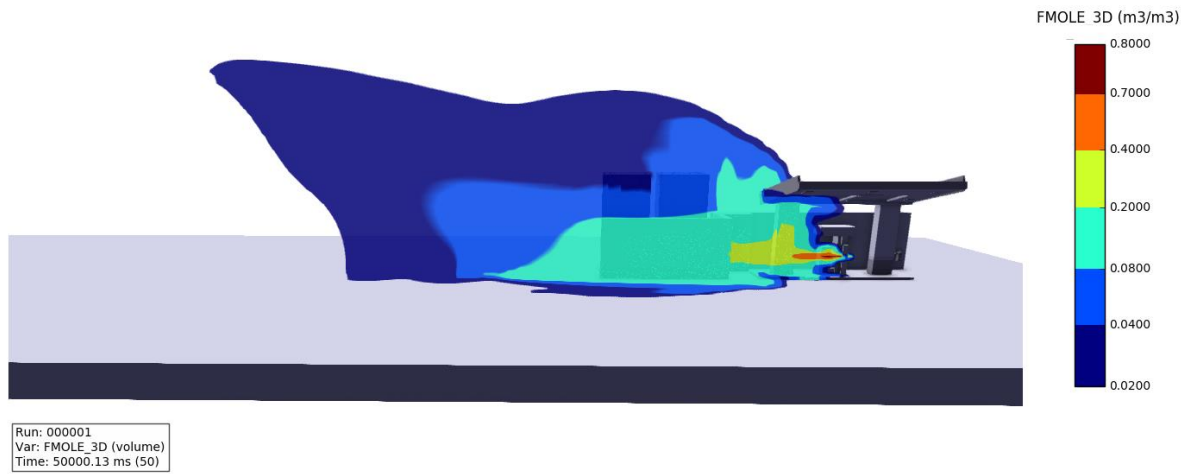


Figure D.3: 3D plot showing the concentration contours for hydrogen release in a refuelling gas station.

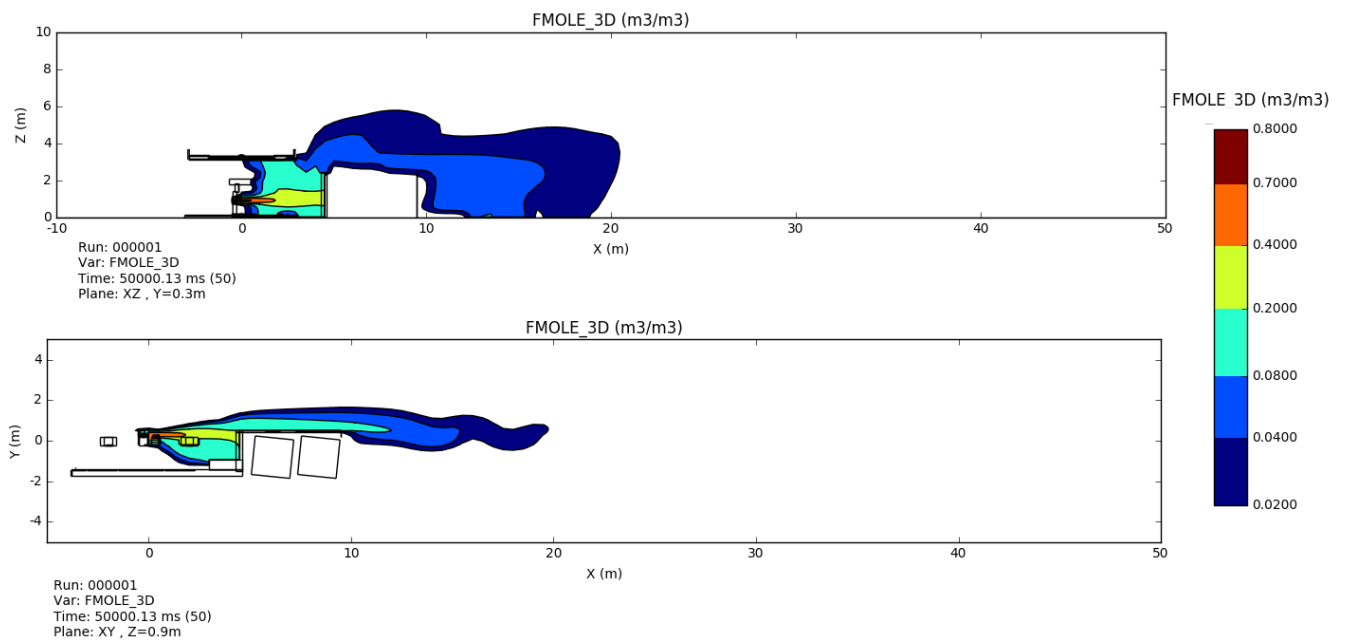


Figure D.4: 2D plot showing the concentration contours for hydrogen release in a refuelling gas station – in XZ and XY planes.

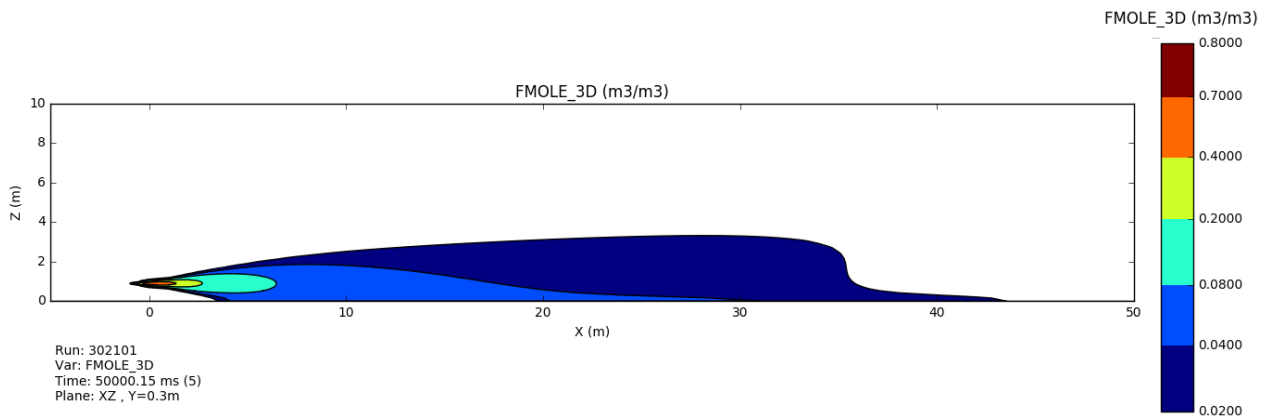


Figure D.5: 2D plot showing the concentration contours for hydrogen release in an open flat terrain.

Appendix E Reference List for Liquid Hydrogen Safety

[1]	Baraldi, D., Kotchourko, A., Lelyakin, A., Yanez, J., Middha, P., Hansen, O.R., Gavrikov, A., Efimenko, A., Verbecke, F., Makarov, D. and Molkov, V. (2009) An inter-comparison exercise on CFD model capabilities to simulate hydrogen deflagrations in a tunnel. <i>Intl J. Hyd. Ener.</i> , 34(18), 7862-7872.
[2]	Breitung, W. et al. (2005) Integral large-scale experiments on hydrogen combustion for severe accident code validation-HYCOM. <i>Nuc. Engg. Des.</i> 235, 253-270.
[3]	Chaîneaux, J. (1999) Leak of hydrogen from a pressurized vessel. Workshop on dissemination of goals, preliminary results and validation of methodology. Brussels, March 11, 1999.
[4]	Dagba, Y., Perette, L. & Venetsanos, A.G. (2005) Description of INERIS-test-6 experiment and requirements for corresponding blind SBEP in the framework of the InsHyde internal project. HYSAFE report, 24 October 2005.
[5]	Davis, S., Hansen, O.R. & Ichard, M. (2009) Validation of FLACS for vapour dispersion from LNG spills: Model Evaluation Protocol. In: Mary Kay O'Connor Process Safety Symposium, College Station, TX, USA, October 27-28, 2009.
[6]	Dorofeev, S.B., Bezmelnitsin, A.V. & Sidorov, V.P. (1995) Transition to detonation in vented H ₂ -air explosions. <i>Comb. Flame</i> , 103, 243-246.
[7]	Dorofeev, S.B., Sidorov, V.P., Breitung, W. & Kotchourko, A. (1997) Large scale combustion tests in the RUT facility: Experimental study, numerical simulations and analysis on turbulent deflagration and DDT. Trans. Of the 14 th Int. Conf. on Structural Mechanics in Reactor Technology, Lyon, France, August 17-22, 1997.
[8]	Friedrich, A., Grune, J., Kotchourko, N., Kotchourko, A., Sempert, K., Stern, G. & Kuznetsov, M. (2007) Experimental study of jet-formed hydrogen-air mixtures and pressure loads from their deflagrations in low confined surroundings. In: Proceedings of 2 nd International Conference on Hydrogen Safety, San Sebastian, Spain.
[9]	Groethe, M., Colton, J. & Chiba, S. (2002) Hydrogen deflagration safety studies in a confined tube. In: Proceedings of the 14 th World Hydrogen Energy Conference, Montreal, Quebec, Canada.

[10]	Groethe, M., Merilo, E., Colton, J., Chiba, S., Sato, Y., and Iwabuchi, H. (2007) Large scale hydrogen deflagrations and detonations, <i>Int. J. Hydrogen Energy</i> , 32(13), 2125-2133.
[11]	Gupta, S., Brinster, J., Studer, E. & Tkatschenko, I. (2007) Hydrogen related risks within a private garage: Concentration measurements in a realistic full scale experimental facility. In: Proceedings of the 2 nd International Conference on Hydrogen Safety, San Sebastian, Spain.
[12]	Hansen, O.R. & Middha, P. (2007) Gexcon blind simulations compared to FZK experiments. Gexcon technical note Ref. Nr. GexCon-07-F46207-TN-1.
[13]	Hansen, O.R., Melheim, J.A. & Storvik, I.E. (2008) Validating the data, LNG industry Magazine, Spring 2008.
[14]	Hansen, O.R., Storvik, I.E. & Renoult, J. (2005) Hydrogen R&D at Gexcon, experiments and simulations, Fire Bridge Second International Conference. Belfast, Northern Ireland, UK, May 2005.
[15]	Jordan, T., Xiao, J., Middha, P., Travis, J., Garcia, J., Hansen, O.R., Molkov, V., Verbecke, F. and Venetsanos, A.G. (2007) Results of the HySafe CFD validation Benchmark SBEP-V5, In: 2nd International Conference of Hydrogen Safety, San Sebastian, Spain, September 11-13, 2007.
[16]	Kuznetsov, M., Alekseev, V., Matsukov, I., & Dorofeev, S. (2005). DDT in a smooth tube filled with a hydrogen-air mixture. <i>Shock Waves</i> , 14, 205-215.
[17]	Lacome, J.M., Dagba, Y., Jamois, D., Perette, L., & Proust, C. (2007) Large-scale hydrogen release in an isothermal confined area. In: 2 nd International Conference on hydrogen safety, 11-13 September 2007, San Sebastian, Spain.
[18]	Marinescu-Pasoi, L. & Sturm, B. (1994) Messung der Ausbreitung einer «Wasserstoff-und Propanwolke in bebautem Gelaende» und «Gasspezifische Ausbreitungsversuche», Battelle Ingenieurtechnik reports R-68202 and R-68264.
[19]	Middha, P. & Hansen, O.R. (2005) FZK Combustion experiments: FLACS calculations of H2 release and subsequent ignition in low confinement situations. GexCon Technical Note Ref. Nr. GexCon-05-F46207-TN-1.

[20]	Middha, P. & Hansen, O.R. (2008) Predicting deflagration to detonation transition in hydrogen explosions, <i>Proc. Safety Prog.</i> , 27(3), 192-204; In: Proceedings of the AIChE Spring National Meeting and 4In: Proceedings of the AIChE Spring National Meeting and 41 st Annual Loss Prevention Symposium, Houston, USA, April 22-26, 2007.
[21]	Middha, P. & Hansen, O.R. (2009) Using Computational Fluid Dynamics as a tool for hydrogen safety studies, <i>J. Loss Prevent. Proc. Ind.</i> , 22(3), 295-302.
[22]	Middha, P. & Hansen, O.R. (2009b) CFD simulation study to investigate the risk from hydrogen vehicles in tunnels, <i>Intl. J. Hyd. Ener.</i> , 34(14), 5875-5886.
[23]	Middha, P. (2008a) HySafe SBEP V11: Dispersion simulations with hydrogen bus in an underpass below a highway. Gexcon Technical Note Ref. Nr. GexCon-08-F46207-TN-4.
[24]	Middha, P. (2008b) HySafe SBEP V15: Explosion simulations with hydrogen bus in an underpass below a highway. Gexcon Technical Note Ref. Nr. GexCon-08-F46207-TN-6.
[25]	Middha, P., Engel, D., & Hansen, O.R. (2009) Can the addition of hydrogen to natural gas reduce the explosion risk? 3 rd International Conference of Hydrogen Safety, Ajaccio, Corsica, France, September 16-18, 2009. <i>Int. J. Hyd. Ener.</i>
[26]	Middha, P., Hansen, O.R. & Schneider, H. (2007) Deflagration to Detonation transition (DDT) in jet ignited Hydrogen-Air mixtures: Large Scale Experiments and FLACS CFD predictions. In: 12 th International Loss Prevention Symposium, Edinburgh, UK, May 22-24, 2007.
[27]	Middha, P., Hansen, O.R., Grune, J. & Kotchourko, A. (2007) Validation of CFD calculations against impinging jet experiments. In: Proceedings of 2 nd International Conference on Hydrogen Safety, San Sebastian, Spain.
[28]	Peraldi, O., Knystautas, R. & Lee, J.H.S. (1986) Criteria for transition to detonation in tubes. <i>Proc. Comb. Inst.</i> , 21, 1629-1637.
[29]	Pfortner, H. & Schneider, H. (1984) Tests with jet ignition of partially confined hydrogen air mixtures in view of the scaling of the transition from deflagration to detonation, Final report for Interatom GmbH, Bergisch Gladbach, Germany, Oct. 1984, Fraunhofer ICT Internal report.
[30]	Roberts, P.T., Shirvill, L.C., Roberts, T.A., Butler, C.J. & Royle, M. (2006) Dispersion of hydrogen from high-pressure sources. In: Proceedings of the XIX Hazards Conference, 27-30 March 2006, Manchester, UK.

[31]	Royle, M., Shirvill, L.C. & Roberts, T.A. (2007) Vapour Cloud Explosions from the ignition of methane/hydrogen/air mixtures in a congested region. In: Proceedings of 2 nd International Conference on Hydrogen Safety, San Sebastian, Spain.
[32]	Sato, Y., Iwabuchi, H., Groethe, M., Merilo, E. and Chiba, S. (2006) Experiments on hydrogen deflagration. <i>Journal of Power Sources</i> , Vol. 159(1), 144-148.
[33]	Sato, Y., Merilo, E., Groethe, M., Colton, J., Chiba, S., & Iwabuchi, H. (2006) Homogeneous hydrogen deflagrations in a sub-scale vehicle tunnel. In: Proceedings of 15 th World Hydrogen Energy Conference, Lyon, France.
[34]	Sherman, M.P., Tieszen, S.R. & Benedick, W.B. (1989) FLAME Facility, the effect of Obstacles and Transverse Venting on Flame acceleration and Transition to Detonation for hydrogen-air mixtures at Large scale, Sandia National Laboratories, Albuquerque, NM 87185, USA, NUREG/CR-5275, SAND85-1264, R3.
[35]	Shirvill, L.C., Royle, M. & Roberts, T.A. (2007) Hydrogen releases ignited in a simulated vehicle refuelling environment. In: Proceedings of 2 nd International Conference on Hydrogen Safety, San Sebastian, Spain.
[36]	Statharas, J.C., Venetsanos, A.G., Bartzis, J.G., Wurtz, J. & Schmidtchen, U. (2000) Analysis of data from spilling experiments performed with liquid hydrogen, <i>J. Haz. Mat.</i> , 7, 57-75.
[37]	Swain, M.R., Filoso, P.A. & Swain, M.N. (2007) An experimental investigation into the ignition of leaking hydrogen. <i>Int. J. Hydrogen Energy</i> , 32(2), 287-295.
[38]	Swain, M.R., Grilliot, E.S. & Swain, M.N. (1998) Phase 2: Risks in indoor vehicle storage, in Addendum to Hydrogen Vehicle Safety Report: Residential Garage Safety Assessment, U.S. Department of Energy, Office of transportation Technologies, Contract DE-AC02-94CE50389.
[39]	Venetsanos, A.G., Baraldi, D., Adams, P., Heggem, P.S. and Wilkening, H. (2008) CFD modelling of hydrogen release, dispersion and combustion for automotive scenarios, <i>J. Loss Prevent. Proc. Ind.</i> , 21(2), 162-184.
[40]	Witcofski, R.D. (1981) Dispersion of flammable clouds resulting from large spills of liquid hydrogen, NASA Technical Memorandum 83131.
[41]	Witcofski, R.D. and Chirivella, J.E. (1984) Experimental and analytical analysis of the mechanisms governing the dispersion of flammable clouds formed by liquid hydrogen spills, <i>Int. J. Hydrogen Energy</i> , 9(5), 425-435.